PHOTOCHEMICAL PROBES FOR
INTRAMOLECULAR ELECTRON TRANSFER

BY

YINGSHENG WANG

A DISSERTATION PRESENTED TO THE GRADUATE SCHOOL
OF THE UNIVERSITY OF FLORIDA IN PARTIAL FULFILLMENT
OF THE REQUIREMENTS FOR THE DEGREE OF
DOCTOR OF PHILOSOPHY

UNIVERSITY OF FLORIDA

1994

Dedicated to my parents for their love and support

ACKNOWLEDGEMENTS

TABLE OF CONTENTS

LIST OF TABLES

LIST OF FIGURES

PHOTOCHEMICAL PROBES FOR
INTRAMOLECULAR ELECTRON TRANSFER

By

Yingsheng Wang

August, 1994

The photophysics and photochemistry of charge-separated excited states generated by intramolecular photoinduced electron transfer in three chromophore-quencher (C-Q) systems are examined. For each system the mechanism and kinetics of photochemical reactions are established using luminescence lifetime measurements, steady-state photochemical quantum yields determinations, and nanosecond transient absorption spectroscopy.

The first C-Q system contains a fac-(bpy)$Re^I(CO)_3$ chromophore (where bpy = 2,2'-bipyridine) which is coordinatively bonded to a 1,2-amino alcohol (1,2-AA) reactive electron donor ligand. The 1,2-AA ligands include a 2° aliphatic amine donor, *erythro*-2[N-4-(Pyridyl)methyl]amino-1,2-diphenylethanol (AA1), and a 2° aromatic amine donor, *erythro*-N-(1,2-Diphenyl-2-hydroxyethyl)-*p*-[4-(Pyridyl)methyl]aniline (AA2). Photoexcitation of Re-AA complexes into the dπ (Re) -> π* (bpy) metal-to-ligand charge transfer (MLCT) manifold is followed by

intramolecular donor ligand-to-metal forward electron transfer to produce ligand-to-ligand charge-transfer (LLCT) state (bpy⁻·)Re^I(CO)₃(1,2-AA⁺·). The formation of the radical cation (1,2-AA⁺·) in the LLCT state triggers a C-C bond fragmentation (C-C BF) reaction within the 1,2-AA ligand to compete weakly with back electron transfer. The rates of BF are found to be > 10^5 s^{-1}, and strongly depend on the structure of the 1,2-AA donors.

The second C-Q system includes three 1,2-diamine (1,2-DA) molecules: *erythro*-1-N-[4-(Pyridyl)]anilino-2-piperidino-1,2-diphenylethane (*e*-DA3), *erythro*-1-N-(4-Cyanophenyl)amino-2-piperidino-1,2-diphenylethane (*e*-DA4), and *threo*-1-N-(4-Cyanophenyl)amino-2-piperidino-1,2-diphenylethane (*t*-DA4). Photoexcitation into the singlet charge-transfer (CT) band of these molecules triggers a rapid C-C BF reaction which competes with back electron transfer. The BF reaction generates substituted benzyl radical pairs which decay by radical recombination and by O₂ quenching. The rates of BF are found to be ≥ 10^8 s^{-1}.

The third C-Q system contains a fac-(bpy)Re^I(CO)₃ chromophore which is coordinatively bonded to a 1,2-DA reactive electron donor ligand. The 1,2-DA ligands include *erythro*-1-[N-4-(Pyridyl)methyl]amino-2-piperidino)-1,2-diphenylethane (*e*-DA1), *erythro*-1-N-[p-[4-(Pyridyl)methyl]anilino-2-piperidino)-1,2-diphenylethane (*e*-DA2), and *erythro*-1-N-[4-(Pyridyl)]anilino-2-piperidino-1,2-diphenylethane (*e*-DA3). Photoexcitation of Re-DA complexes into the MLCT state is followed by intramolecular forward electron transfer to produce LLCT state (bpy⁻·)Re^I(CO)₃(1,2-DA⁺·). A rapid C-C bond fragmentation reaction within the 1,2-DA⁺· of the LLCT state produces a diradical metal complex and an iminium ion. The rates of BF are found to be ≥ 10^8 s^{-1}, show no donor structure dependence. The BF reaction clocks back electron transfer effectively.

<u>Photoinduced Electron Transfer</u>

One of the remarkable achievements of photochemistry has been the recognition that certain molecules on photoexcitation become powerful electron donors (D) or acceptors (A) (Figure 1-1). The phenomenon known as photoinduced electron transfer (PET) has attracted the interest of chemists from many fields[1-4]. For example, inorganic chemists have applied PET to development of solar energy storage and conversion systems by utilizing transition metal complexes;[5,6] molecular biologists are investigating photosynthesis and electron-transport in biological systems on the basis of simple models of PET.[7-9]

The feasibility of forward electron transfer (FET) between an excited-state sensitizer and a quencher is dictated by the change in free energy, ΔG_{FET}. In the gas phase, ΔG_{FET} can be examined in terms of the simplified molecular orbital diagrams (Figure 1-1) and expressed as equation 1-1, where IP = ionization potential of the donor, EA = electron affinity of the acceptor and E_{0-0} = the energy difference between the ground state and excited state of the light-absorbing component. In solution, ΔG_{FET} can be estimated from the Rehm-Weller equation (equation 1-2),[10-12] where E°_D and E°_A are the redox potentials of the donor and acceptor, ΔG_S represents Coulombic stabilization and solvation of the charge-transfer intermediates formed by FET. Back electron transfer (BET) within the
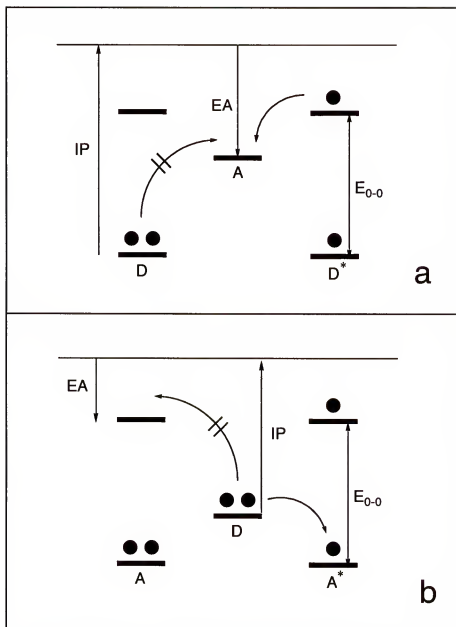
Figure 1-1

Energetics of PET in gas phase when (a) the sensitizer is the electron donor (D) and (b) the sensitizer is the electron acceptor (A).

(IP = ionization potential of donor, EA = electron affinity of acceptor, E_{0-0} = the energy difference between the ground state and the excited state of the light-absorbing component.)

charge-transfer intermediates competes with the charge separation of the redox components. The change in free energy for BET, ΔG_{BET}, can be estimated from equation 1-3, where E°_D and E°_A are the redox potentials of the donor and acceptor.

$$\Delta G^{\circ}_{FET} \text{ (gas phase)} = IP - EA - E_{0\text{-}0} \tag{1-1}$$

$$\Delta G^{\circ}_{FET} \text{ (solution)} = E^{\circ}_D - E^{\circ}_A - \Delta G_S \tag{1-2}$$

$$\Delta G^{\circ}_{BET} \text{ (solution)} \approx E^{\circ}_A - E^{\circ}_D \tag{1-3}$$

PET is an essential component of most systems designed for storage of solar energy. Absorption of light is the energy input step that triggers the PET process. The absorbed light is stored as chemical energy in the excited state. Light energy conversion occurs through ET, while the energy storage process usually utilizes the PET products in subsequent redox processes. The electron transfer rate constants (k_{FET} and k_{BET}), therefore, have a direct impact on the primary charge-separated products in terms of yield, lifetime, and reactivities for the subsequent chemical reactions. During the last three decades, enormous research efforts, experimental and theoretical, have been directed toward understanding the energetics and kinetics related to the charge-separated states in a large number of PET systems.[2,3,4]

Electron transfer is a simple, weak-interaction chemical process in which no bond breaking or forming is involved. The reactivity and the effects of structure and environment on the rates of electron transfer have been widely treated by a classical model first developed by Marcus, and elaborated on by Hush, Sutin and others.[13-26] According to Marcus Theory, the rate of electron transfer can be expressed in equation 1-4 to 1-8:

$$k_{ET} = A \, \kappa_n \tag{1-4a}$$

$$A = \nu_n \, \kappa_{el} \tag{1-5}$$

$$\kappa_n = \exp(-\Delta G^{\neq}/RT) \tag{1-6}$$

$$\Delta G^{\neq} = (\lambda/4)(1 + \Delta G^{\circ}/\lambda)^2 \tag{1-7}$$

$$\lambda = \lambda_{in} + \lambda_{out} \tag{1-8}$$

$$k_{ET} = A \, \exp[-(\lambda/4RT)(1 + \Delta G^{\circ}/\lambda)^2] \tag{1-4b}$$

The term A in equation 1-4a depends on the nature of the electron transfer reaction (e.g., bimolecular or intramolecular), and κ_n in equation 1-4a is called the nuclear factor. The term A can be expressed as the product of ν_n (the effective nuclear vibrational frequency) and κ_{el} (the electronic factor which ranges from 0 to 1) by equation 1-5.

Electron transfer consists of electron movement between orbitals. An electron may flow from a singly or doubly occupied molecular orbital of the donor to a fully vacant or half-vacant orbital of the acceptor. The orbital overlap between the occupied and unoccupied orbitals must play an important role in electron transfer. The orbitals act like "conductors" of the electron, structural and environmental factors which influence their mutual separation, orientation, and symmetry, or restrict their freedom of movement to find the most favorable spatial orientation, can profoundly influence the rate of electron transfer. When $\kappa_{el} = 1$ (the reaction is adiabatic) the term A is equal to ν_n; whereas when $\kappa_{el} \ll 1$ (the reaction is nonadiabatic) the term A is given by $A = \nu_{el}$, where ν_{el} is the electron-hopping frequency which is directly related to the nature and the overlap of the occupied and unoccupied orbitals involved in electron transfer.[22-24]

According to Marcus Theory, the initial thermally equilibrated nuclear geometry of the reactants and surrounding solvent molecules undergoes reorganization in the stages preceeding electron transfer, which brings the

reactants and surrounding solvent molecules into the high energy, distorted, and nonequilibrium geometry of the transition state. At the transition state, electron transfer takes place rapidly. During this brief moment, the nuclear geometry of the transition state remains fixed (the Franck-Condon principle). Following electron transfer, nuclear relaxation rapidly establishes the thermally equilibrated product state. The nuclear factor κ_n in equation 1-4a, also ranging from 0 to 1, is related to the activation energy $\Delta G^{\neq}$ by equation 1-6 to 1-8, where ΔG° is the standard free energy of reaction, λ is the total reorganizational energy composed of vibrational (λ_{in} for the inner-sphere barrier) and solvational (λ_{out} for the outer-sphere barrier) components. λ_{in} is the free energy change associated with the nuclear bond length changes within the reactant molecules, and it can be estimated from a classical model[20,21,23] provided the knowledge of bond-lengths and force constants in the reacting molecules before and after electron transfer is available. λ_{out} is the free energy change associated with the slow changes in the polarization of the surrounding solvent molecules prior to electron transfer, and is generally calculated from a classical model developed by Marcus and Hush.[21] λ_{out} depends on solvent polarity, on the separation of the redox sites, and (for a given separation) on the shape of the reacting molecules.

Inspection of equation 1-4b shows that k_{ET} will increase as $-\Delta G^{\circ}$ increases, reaching a maximum value when $-\Delta G^{\circ} = \lambda$. When $-\Delta G^{\circ}$ becomes larger than λ, k_{ET} will decrease. Thus a plot of $\log(k_{ET})$ vs. $-\Delta G^{\circ}$ should have the shape of an inverted parabola. The portion of the parabola where k_{ET} is increasing with increasing driving force is known as the "normal" region, and the part where k_{ET} is decreasing with increasing driving force is known as the "inverted" region.

Intermolecular and Intramolecular PET

Many studies have focused on PET involving bimolecular encounter of an excited donor (or acceptor) with a ground-state acceptor (or donor), viz., $*D + A \rightarrow D^+ + A^-$. There are several intrinsic features that are associated with intermolecular PET: (1) Intermolecular PET is essentially a diffusional process. Many experiments reveal that k_{FET} between donors and acceptors increases with increasing driving force, but levels off at the diffusional limit.[10,11,27,18] The diffusional limit obscures PET rates in excess of $\approx 10^{10}$ s^{-1}. (2) The lifetimes of singlet excited states are usually not much longer than a few nanoseconds. Even with the diffusion limited rate, the concentration of the quencher must be large (e.g., ≥ 0.1 M) to give 90% quenching. (3) The dynamics of quenching by ET must take into account the positions and motions of the reactants in a given solvent environment (Figure 1-2).[29] Depending upon the driving force of these reactions, FET may take place within the encounter complex and/or within the collision complex. In some cases FET can also be accomplished by irradiation of a charge-transfer band of a ground state donor-acceptor charge-transfer (CT) complexes. Such ground-state charge-transfer complexes form when the energy gap between the HOMO of the donor and the LUMO of the acceptor is sufficiently small and the orbitals have adequate overlap. In this case FET and BET take place between the same set of orbitals: the HOMO of the donor and the LUMO of the acceptor that are engaged in the CT interaction. (4) Regardless of the method of generation, the primary products of FET are radical ion pairs with a certain solvation status. Depending on the solvation status, these radical ion pairs can be divided into (i) contact radical ion pair (CRIP) wherein the ions are in direct contact without any solvent penetration; (ii) solvent-separated radical ion pair (SSRIP) wherein a solvent molecule or two are shared between the ions;
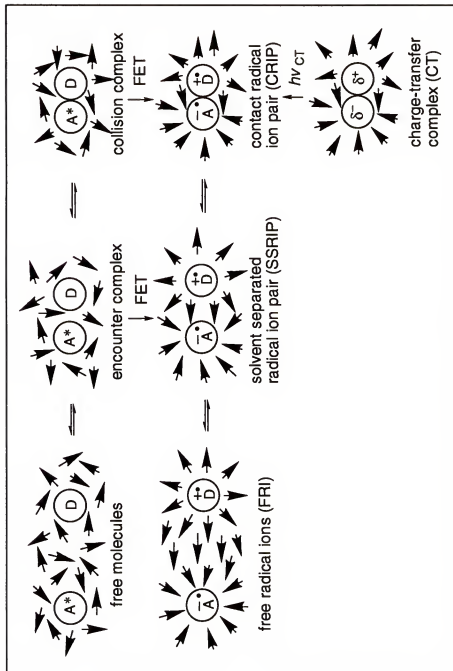
Figure 1-2

Schematic representation of donor and acceptor partners in solution at various separation distances before and after electron transfer. The arrows represent solvent molecules.

and (iii) free radical ion (FRI) with no Coulombic interactions between ions of opposite charge. The dynamic behavior of these ion pairs depends on the electronic coupling, the solvent reorganization energy as well as the solvent polarity. For example, for the case of CRIP, since the ion separation is small, the electronic coupling is relatively large and the reorganization energy is small. BET within CRIP is therefore expected to be very efficient. In competition with BET, in polar solvents, these pairs may undergo solvation into SSRIP with a rate constant comparable to BET.

Rigidly linked acceptor-donor compounds allow the dependence of k_{ET} on fundamental parameters to be studied without obfuscation by diffusional limitations. These fundamental parameters include the ET driving force, distance, structures of donor and acceptor, and solvent polarity. Flexibly linked acceptor-donor compounds may permit the intramolecular formation of encounter complexes or CT complexes. Under these circumstances, the fate of charge-transfer intermediates formed by FET reflects the structure and dynamic conformations of the molecular link. However, a chemical link will always present a synthetic challenge and may hamper optimal orbital overlap for FET.

In intermolecular PET, an excited molecule and a ground state molecule are visualized as diffusing into an encounter complex and/or a collision complex, in which the donor/acceptor orbitals are assumed to overlap to a certain extent. ET is a one-electron reaction in which an electron jumps from an occupied orbital of the donor to an vacant or half-vacant orbital of the acceptor within encounter complexes or collision complexes. In rigid environments or in intramolecular systems where the donor and acceptor are linked by a rigid or flexible molecular bridge, the separation distance between the two redox sites may exceed the encounter distance (~ 7 Å). It is generally assumed that an electron may tunnel through the bonds of the molecular bridge separating the donor and acceptor.

Two possible tunneling pathways have been proposed.[30] In the first, the electron travels from the donor to the acceptor through the LUMO's of the molecular bridge. In the second pathway, the electron transfer occurs via a hole mechanism wherein a positive charge travels from the acceptor to the donor via the HOMO's of the molecular bridge.

<u>Examples of Intermolecular PET</u>

In a series of publications, Gould, Farid, and coworkers reported their investigations of BET in laser flash generated radical ion pairs in acetonitrile solution.[31-35] Shown in Figure 1-3 is part of their work in which 2,6,9,10-tetracyanoanthracene (TCA) was used as the elctron acceptor and a series of methylated benzenes were used as electron donors.

Quenching of free $^1TCA^*$ by the alkylbenzene donors that have low oxidation potentials, such as pentamethylbenzene and hexamethylbenzene, in acetonitrile solution leads to the direct formation of solvent-separated radical ion pairs (SSRIP). Rates of BET in the SSRIP, k_{BET}^{SSRIP}, were determined from quantum yields for formation of free radical ions (FRI), Φ_{FRI}^{SSRIP}, which were monitored with a cation radical trap such as dimethoxystilbene (DMS). Assuming a constant k_{SEP} from earlier studies,[35 b-d] they obtained k_{BET}^{SSRIP} according to equation 1-9:

$$\Phi_{FRI}^{SSRIP} = k_{SEP} / (k_{SEP} + k_{BET}^{SSRIP}) \qquad (1-9)$$

They also found that TCA forms ground-state charge-transfer complexes (CT) within the same set of methylated benzenes. The CT complexes are characterized by a new absorption band which is red-shifted as compared to TCA local excitation band. The equilibrium constants, K_{CT} (Figure 1-3), were found to
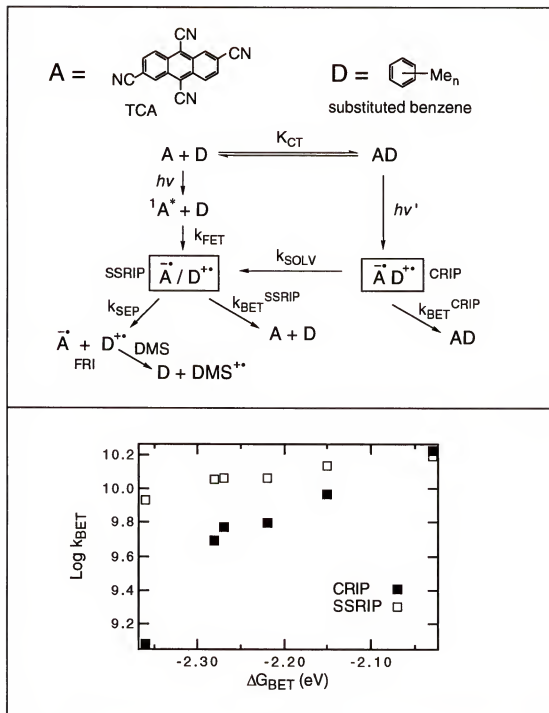
Figure 1-3

BET of contact radical ion pairs (CRIP) and solvent separated radical ion pairs (SSRIP) for PET between TCA and a series of substituted alkyl benzenes.[34,35]

increase as the oxidation potential of the donor decreases. Excitation of the ground-state CT complexes into the charge-transfer band leads to contact radical ion pair (CRIP) formation directly with formation efficiency near unity. Rates of BET from CRIP, k_{BET}^{CRIP}, were determined from quantum yields for formation of FRI, Φ_{FRI}^{CRIP}, together with the CRIP fluorescence decay lifetimes according to equation 1-9, 1-10 and 1-11:

$$\Phi_{FRI}^{CRIP} = \Phi_{SOLV}^{CRIP} \times \Phi_{FRI}^{SSRIP} \tag{1-10}$$

$$\Phi_{SOLV}^{CRIP} = k_{SOLV} / (k_{SOLV} + k_{BET}^{CRIP}) = k_{SOLV} \times \tau^{CRIP} \tag{1-11}$$

Comparing k_{BET}^{SSRIP} and k_{BET}^{CRIP} (Figure 1-3) revealed that k_{BET}^{CRIP} is much more dependent on the reaction exothermicity. This can be ascribed to the electronic coupling which is recognizably higher in the CRIP compared to the SSRIP due to the shorter distance of the charged species. The solvent reorganization energy also depends on the separation distance, and for CRIP the solvent reorganization energy is ca. 1 eV lower than that of SSRIP.

Mataga and coworkers investigated rates of BET by laser flash spectroscopy in a bimolecular system in which $Ru^{II}(bpy)_3^{2+}$ was used as the electron acceptor and a series of aromatic amines were used as electron donors.[36] A mixed solvent of acetonitrile and water was used as the solvent in their experiments. Photoexcitation of the $d\pi$ (Ru) -> π^* (bpy) metal-to-ligand charge-transfer excited state (MLCT) in the presence of donors initiated FET from amine donors to the MLCT excited state, $Ru^{III}(bpy^-\cdot)(bpy)_2^{2+}$, to generate geminate radical ion pairs (Figure 1-4). Ratios of k_{BET} over k_{SEP} from geminate radical ion pairs were determined from quantum yields of $Ru^{II}(bpy^-\cdot)(bpy)_2^+$ production in solvent bulk, Φ_{FRI}, according to equation 1-12. A decrease in k_{BET} with an increase in exothermicity ($-\Delta G_{BET}$) was observed.

$$k_{BET} / k_{SEP} = (1 / \Phi_{FRI} - 1) \tag{1-12}$$
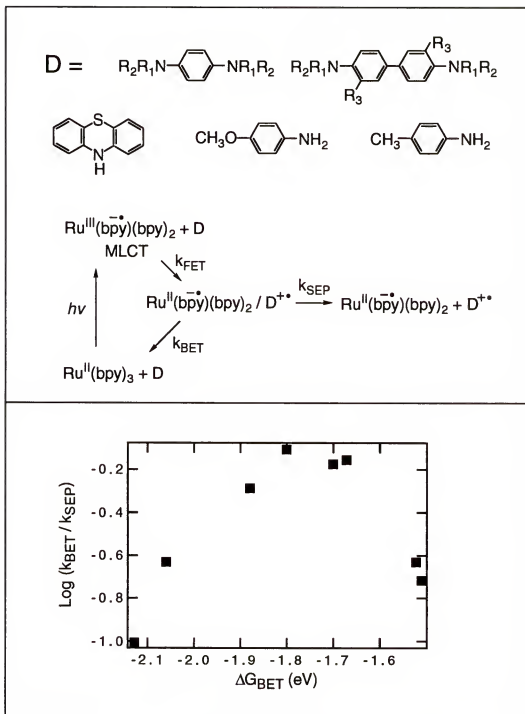
Figure 1-4

BET and cage escape of geminate radical ion pairs for PET between $Ru(bpy)_3^{2+}$ and a series of aromatic amines.[36]

Examples of Intramolecular PET

Covalently linked porphyrin-quinone compounds are important models of PET in the photosynthetic reaction center.[8] In these donor-acceptor molecules, the porphyrin functions as the donor chromophore and a covalently linked quinone as the electron acceptor. Strategies used for linking the donor and acceptor include rigid and flexible spacers in order to study the distance, conformational and solvent effects on electron transfer rates.[37-39] Shown in Figure 1-5 is a tetraarylporphyrin linked through a single amide bridge to methyl-p-benzoquinone (P-Q) which has been investigated in detail by Bolton and coworkers.[37] In benzonitrile, excitation of the porphyrin chromophore initiated the sequence of events shown in Figure 1-5. The mechanism was established from the photophysical properties of P-Q and its reduced hydroquinone as a model compound. The fluorescence lifetime of P-Q was quenched strongly and picosecond transient absorption studies demonstrated that quenching of the excited singlet state, $^1{}^*$P-Q, is due to intramolecular FET to form the singlet radical ion pair ^{1}(P$\cdot$+ - Q$\cdot$-) with $k_{FET} = 4 \times 10^8$ s^{-1} and ^{1}(P$\cdot$+ - Q$\cdot$-) subsquently decays by BET with $k_{BET} = 1.6 \times 10^8$ s^{-1}. The ET quenching of $^1{}^*$P-Q is efficient ($\Phi_{FET} = 0.83$), but intersystem crossing takes place to a sufficient extent ($\Phi_{ISC} = 0.11$) that ET quenching of $^3{}^*$P-Q can also be observed. The k_{FET} from $^1{}^*$P-Q depend markedly on solvent, going from 4.8×10^7 s^{-1} in acetonitrile to 2.2×10^9 s^{-1} in chloroform.[38]

Schanze and coworkers investigated a series of Re-based acceptor-donor complexes with emphasis on understanding driving force and solvent dependence of k_{FET} and k_{BET}.[40,41] In these complexes the chromophore, (diimine)Re^I(CO)$_3$, is linked to an N,N-dimethylaniline (DMA) donor through a short amide linkage as shown in Figure 1-6. The driving force, ΔG_{FET} and
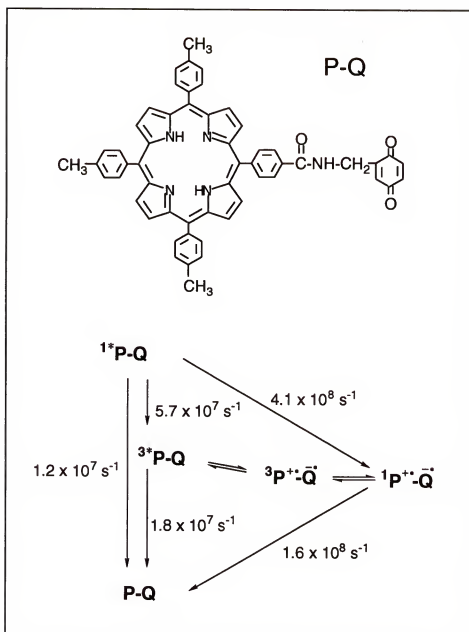
Figure 1-5
Mechanism and kinetics of a porphyrin-quinone
intramolecular PET system.[37]
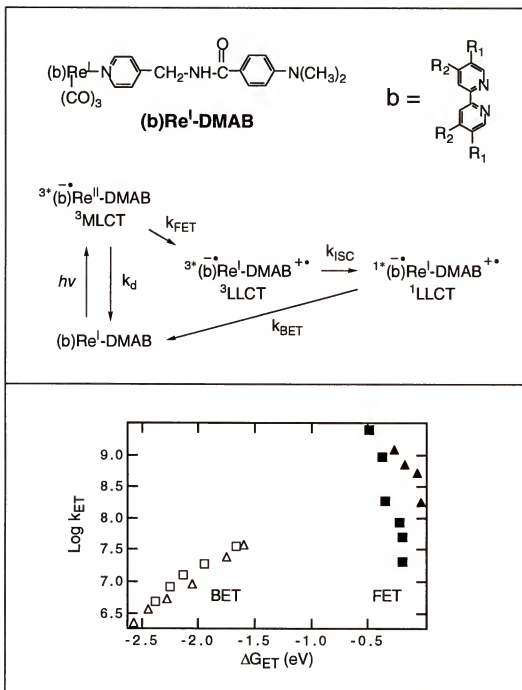
Figure 1-6
FET and BET in a series Re-based acceptor-donor complexes.[40,41]

(filled and open squares): in acetonitrile solutions;

(filled and open triangles): in methylene chloride.

ΔG_{BET}, was varied by changing the electron demand of the diimine ligand. The system was studied in three solvents: CH_2Cl_2, DMF, and CH_3CN. Photoexcitation of the $d\pi$ (Re) -> π^* (diimine) metal-to-ligand charge-transfer excited state (^3MLCT) initiated FET from DMA to the MLCT excited state to generate a ligand-to-ligand charge-transfer excited state (^3LLCT) which decays by BET, presumably through the ^1LLCT state. The mechanism and kinetics were established using fluorescence lifetime measurements and nanosecond transient absorption spectroscopy. Interestingly, k_{FET} is strongly dependent on ΔG_{FET} and solvent polarity with k_{FET} ranging from 10^7 s^{-1} to > 10^9 s^{-1}, whereas k_{BET} displays a weak inverted dependence on ΔG_{BET} with k_{BET} ranging from 10^7 to 5 x 10^8 s^{-1}, and shows no solvent dependence.

Bond Fragmentations Initiated by PET

Much of the experimental work on the PET systems discussed above has been carried out using spectroscopic techniques such as fluorescence, laser flash photolysis, and time-resolved electron spin resonance. These methods have provided a wealth of information about the rates of primary processes and the identity of reaction intermediates. Concurrently, a keen interest has developed in the manifold of chemical reactions initiated by PET. The primary product of PET is a pair of high-energy intermediates, usually a pair of radical ions. A conceptually simple reaction that often follows is a cleavage of a single bond within one of the intermediates to yield two fragments.[42-44] The overall process utilizes light energy to carry out a chemical reaction and may serve as a simple model for energy conversion as well as a means to generate reactive intermediates for meaningful use.[45]

$(A-B)^{+\bullet} \xrightarrow{\text{BDE}(AB^{+\bullet})} A\bullet + B^+$

$E^o(AB^{+\bullet}/AB)$ ⇌ ... ⇌ $E^o(B^+/\bullet B)$

$A-B \xrightarrow{\text{BDE}(AB)} A\bullet + \bullet B$

$\text{BDE}(AB^{+\bullet}) = \text{BDE}(AB) + F[E^o(B^+/\bullet B) - E^o(AB^{+\bullet}/AB)]$

$= \text{BDE}(AB) + \Delta E$

(1-13)
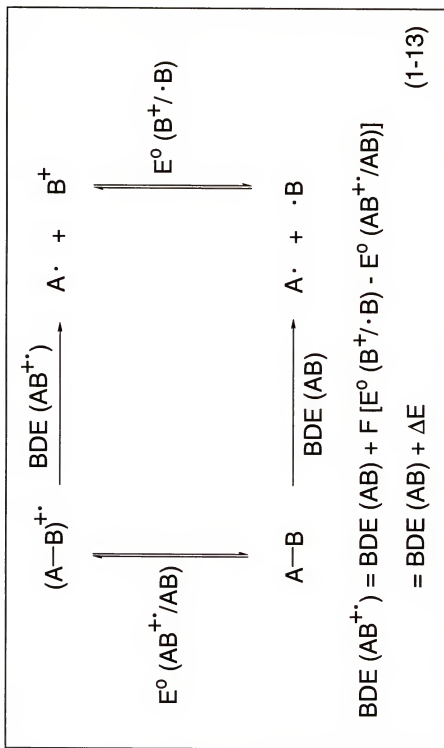
Figure 1-7

Thermodynamics of bond fragmentation in cation radical ($AB^{+\bullet}$).

Similar to the rate of BET, the bond fragmentation (BF) rate, k_{BF}, is primarily controlled by thermodynamic factors. The free energy of radical ion cleavage may be conveniently estimated from simple thermodynamic cycles.[46-48] Shown in Figure 1-7 is the thermodynamics of BF in a cation radical, $AB^{+\cdot}$, where BDE represents bond dissociation energy and E° represents the redox potential for the corresponding redox pair. The BDE of $AB^{+\cdot}$ can be expressed in terms of the BDE of the corresponding neutral compound, AB, and related redox properties according to equation 1-13 ($F = 23.06$ kcal $\cdot$ mol^{-1} $\cdot$ V^{-1}). The homolytic bond strengths in organic compounds vary in general from ca. 5 eV to just under 1.5 eV. In PET systems high energy radical ions with redox potentials ranging from -2.5 eV to +2.5 eV vs SCE can be easily produced. If the ionic fragment is particularly stable (for example, B^+ in Figure 1-7), the value of ΔE may be negative enough to make BDE($AB^{+\cdot}$) low, even negative. On the other hand, the BF competes with BET within the photogenerated radical ion pairs, therefore, the overall efficiency of the PET initiated BF is controlled by the dynamics of the photogenerated radical ion pairs. When the quantum efficiency of the BF, Φ_{BF}, is accessible experimentally, it provides information reflecting the competition between BET and BF.

Examples of Bond Fragmentations Initiated by PET

In a series of publications Whitten and coworkers reported their investigations on oxidative C-C BF of a number of 1,2-amino alcohols initiated by bimolecular PET in several solvents such as benzene, CH_2Cl_2, and CH_3CN.[49-53] A variety of acceptors such as thioindigo (TI), 2,6,9,10-tetracyanoanthracene (TCA), 9,10-dicyanoanthracene (DCA) and 1,4-dicyanonaphthalene (DCN) served as the excited-state component of the PET systems. In all solvents and

for all acceptor/donor combinations, the driving force for FET ranged from moderately to strongly exothermic (-1.1 eV < ΔG_{FET} < -0.3 eV) with k_{FET} being near or equal to diffusion controlled rates.

It was recognized that the PET initiated C-C bond cleavage within an amino alcohol cation radical occurs in three distinct solvation states of radical ion pairs, depending chiefly upon solvent polarity as shown in Figure 1-8.[53] In solvents of low polarity, PET gives rise primarily to a CRIP wherein the rate for separation, k_{SEP}, is low and the BF competes only with BET. In solvents of moderate polarity, PET involves direct formation of SSRIP wherein the BF competes with both BET and rapid radical ion separation by polar solvents. Cosensitized by TCA (or DCA) with biphenyl in acetonitrile, PET leads to formation of free ions with an efficiency of 0.83 for DCA and of 0.25 for TCA.[31] In this case the C-C BF within an amino alcohol cation radical from free ions should show first-order kinetics in competition with the second-order bimolecular BET.

Among the diverse 1,2-amino alcohols studied, two diastereomers, *erythro*-AA (*e*-AA) and *threo*-AA (*t*-AA) as shown in Figure 1-9 have been extensively studied. Two features of C-C BF reactions in non-polar solvents (where CRIP is expected to dominate) are significant: (1) Strongly basic radical anions enhance the BF efficiency. For example, in benzene solution, Φ_{BF} = 0.04 for TI/*e*-AA and Φ_{BF} = 0.00007 for DCN/*e*-AA. The isotope effect, $\Phi_{BF}^H / \Phi_{BF}^D$ of *e*-AA or *t*-AA, increases in the order of TI < DCA < TCA < DCN. (2) A stereochemical preference of BF for *e*-AA compared to *t*-AA is sensitive to the basicity of radical anions, being lowest for the relatively basic radical anion of TI and highest for nonbasic radical anion of DCN. The stereochemical preference disappears in acetonitrile if DCA and biphenyl are used as co-sensitizers, where FRI is expected to dominate. These observations are accounted for by radical anion (base) assisted BF, where anti stereochemistry is favored. The
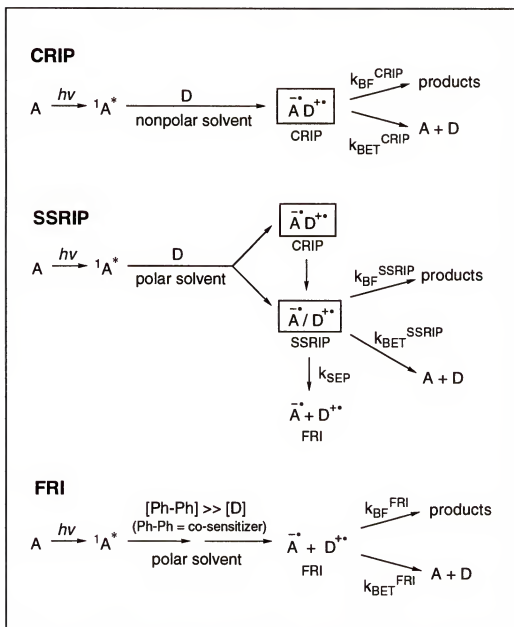
Figure 1-8
BF and BET in CRIP, SSRIP and FRI.[53]
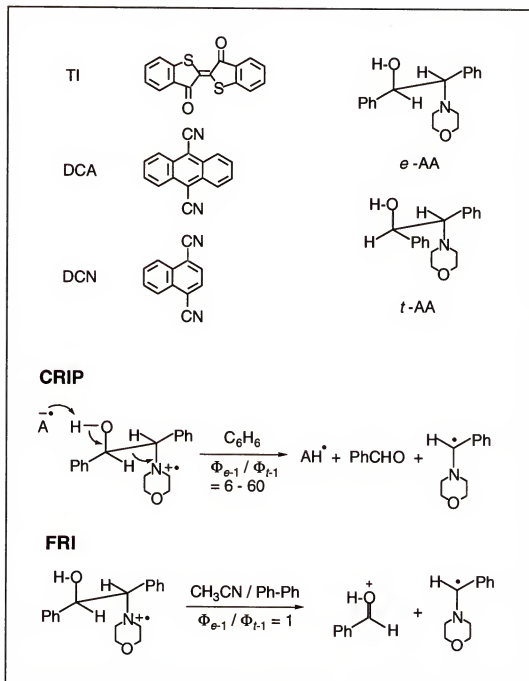
Figure 1-9
Intermolecular C-C BF of 1,2-amino alcohols by PET.[53]

intramolecular hydrogen bonding in t-AA leads to gauche arrangement of the corresponding cation radical, diminishing the rate of assisted BF. In more polar solvents and under circumstances where the free ions are produced (biphenyl co-sensensitization), the unassisted process is observed (Figure 1-9).

Another general feature of C-C BF reactions is that for a given acceptor/donor combination, the overall PET initiated BF efficiency is in the order of $\Phi_{BF}^{SSRIP} \ll \Phi_{BF}^{CRIP} < \Phi_{BF}^{FRI}$. For example, for Tl/$e$-AA system, $\Phi_{BF} = 0.04$ in benzene and $\Phi_{BF} = 0.00003$ in acetonitrile. Since the driving force for BET is strongly exothermic (-2.6 eV < ΔG_{BET} < -1.3 eV) in all solvents, k_{BET} is expected to be very rapid in both SSRIP and CRIP. Part of the reason that Φ_{BF}^{CRIP} are significantly higher than Φ_{BF}^{SSRIP} is attributed to the assisted BF rate constant, k_{BF}^{CRIP}, which can be several orders higher than the unassisted rate constant, k_{BF}^{FRI}, which is estimated to be $\geq 10^5$ s^{-1} for e-AA from biphenyl co-sensensitized PET reactions in acetonitrile. The activation energy for C-C BF of Tl/e-AA and Tl/t-AA are estimated to be 2.8 and 4.9 kcal / mole from temperature dependent experiments in toluene.

The same group also investigated PET initiated C-C BF of a number of 1,2-diamines.[54,55] Figure 1-10 shows a systematic study of $meso$-DA, which is structurally analogous to e-AA, in both bimolecular and intramolecular systems. The acceptors are the singlet excited state of DCA and the triplet excited state of anthraquinone (AQ). For the bimolecular DCA/$meso$-DA system, k_{BF} is estimated to be more than an order of magnitude faster than that of DCA/e-AA in both benzene and acetonitrile. As to the intramolecular DCA-$meso$-DA system, the overall Φ_{BF} is an order of magnitude lower than that of the bimolecular DCA/$meso$-DA system in acetonitrile, in agreement with the poor competition of k_{BF} with k_{BET} due to the lack of the possibility of cage escape. In contrast both bimolecular AQ/$meso$-DA and intramolecular AQ-$meso$-DA, which should be
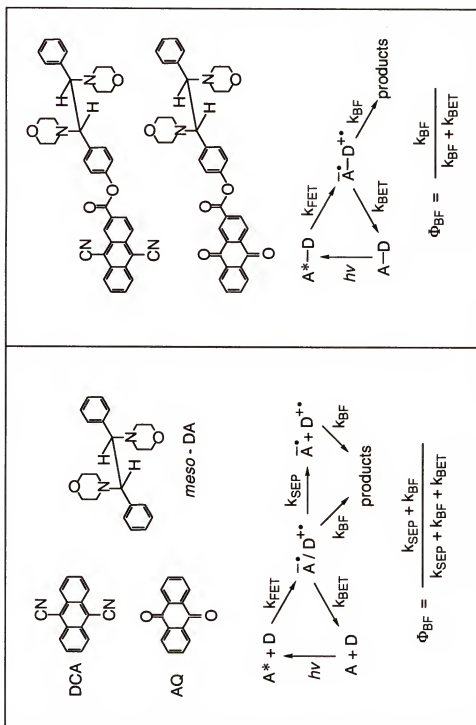
Figure 1-10

Intermolecular and intramolecular C-C BF in 1,2-diamine by PET.[55]

reactive from the acceptor triplet, show fairly higher Φ_{BF} and little sensitivity to solvent polarity. For example, for AQ/*meso*-DA: Φ_{BF} = 1.0 in acetonitrile and Φ_{BF} = 0.8 in methylene chloride.

Alkyltriphenylborate salts of cyanine dyes have been observed by Schuster and coworkers to undergo rapid carbon-boron (C-B) bond cleavage in benzene solution after PET.[45,56,57] Figure 1-11 shows one system they studied in which the cyanine cation used is N,N'-dimethyldimethylindocarbocyanine (Cy+). In PET reaction of such systems, the excited singlet of cyanine (^{1*}Cy+) serves as an electron acceptor, and alkyltriphenylborate as an electron donor. The cyanine borates in bezene solution exist essentially as tight ion pairs over the concentration used.

The PET mechanism was established from the photophysical properties of (Cy+)(R-BPh$_3^-$) with Cy+PF$_6^-$ as a model which has a fluorescence decay rate constant of 4 x 10^9 s^{-1} in benzene. The fluorescence lifetime of (Cy+)(R-BPh$_3^-$) is quenched strongly, and picosecond transient absorption study demonstrates that quenching of the excited singlet state, ^{1*}Cy+, is due to FET from R-BPh$_3^-$ to ^{1*}Cy+ to generate the singlet radical pair (Cy·)(R-BPh$_3$·). The neutral cyanine radical has a characteristic absorption band centered at 430 nm, which has been observed for all borate salts but not for the PF$_6^-$ salt. Unlike the model compound, Cy+PF$_6^-$, for all (Cy+)(R-BPh$_3^-$) salts no photoisomerization of Cy+ from the all-*trans* geometry to the mono-*cis* geometry has been observed in benzene solution by laser flash photolysis. The rates of FET strongly depend on the driving force, ranging from 4 x 10^{10} s^{-1} to 4 x 10^{11} s^{-1}.

The neutral boranyl radical undergoes C-B bond cleavage to generate the free alkyl radical and triphenylborane. Certain neutral R radicals that are formed by C-B BF can also be observed by transient absorption spectroscopy. Additional evidence for free radical formation from the irradiation of cyanine borates comes
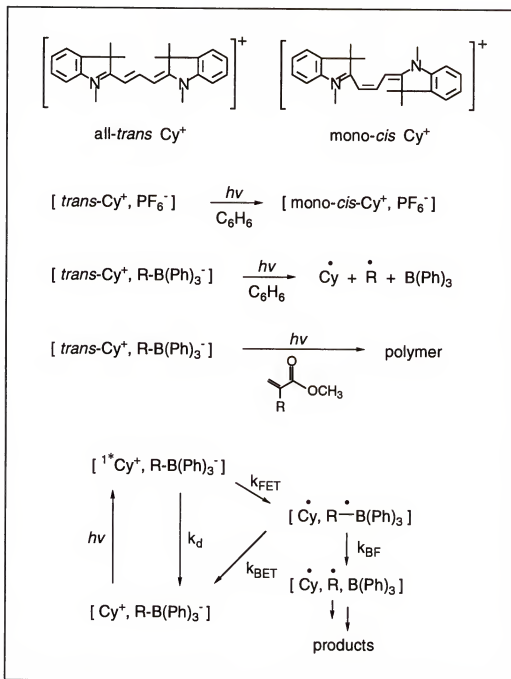
Figure 1-11
Carbon-Boron BF in alkyltriphenylborates by PET.[45,56,57]

from the observation that upon irradiation in butyl acrylate with visible light leads to polymerization of the acrylate.

On the other hand, the C-B BF competes with BET in the same solvent cage. The rate of BF, k_{BF}, depends directly on the stability of the alkyl radical formed. When a stablized alkyl radical is formed, k_{BF} is faster than k_{BET}. For example, the naphthylmethyl radical, as a BF product, is formed instantaneously after the laser pulse, and k_{BF} is estimated to be $> 10^{11}$ s^{-1}.

There are many examples of PET bond cleavage in other systems, such as in group 4a organometallic compounds (organotins, organosilanes) and in hydrocarbon (olefins, arenes, bibenzyl derivatives), which have been studied and well characterized.[42,58-64]

Brief Description of The Present Study

Charge-separated excited states generated by intramolecular PET in three chromophore-quencher systems have been studied in the present work. Figure 1-12 presents (1) general structural features of each system studied, and (2) the kinetic processes involved in the corresponding PET generated charge-separated excited state.

The objectives of this work are, for each system, (1) to establish the mechanism for the formation and decay pathways of the charge-separated excited state, (2) to quantify the kinetic processes involved in the charge-separated excited state based on the mechanism established, (3) to quantify thermodynamic parameters controlling those kinetic processes.

These efforts are directed toward (1) to study factors that control electron transfer rates, (2) to understand factors that influence stability and reactivity of electron deficient species, (3) to develop a general method that utilizes BF to effectively clock BET rates.
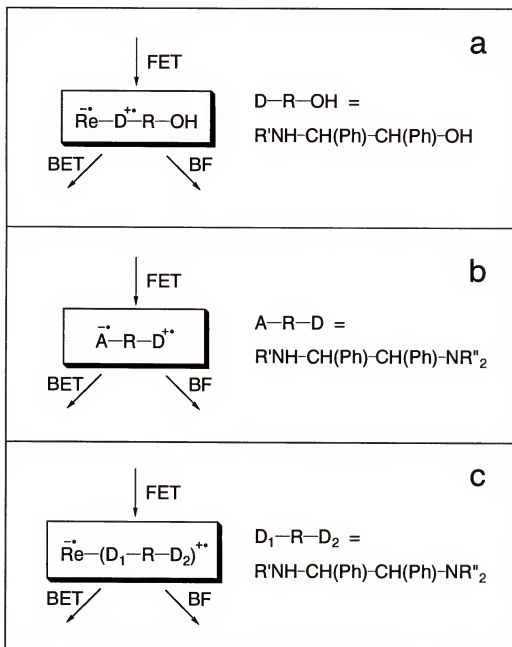
Figure 1-12

Photochemical probes of intramolecular electron transfer studied in present work: (a) in Chapter 2, (b) in Chapter 3, (c) in Chapter 4. (Re stands for (bpy)Re(CO)$_3$- chromophore)

CHAPTER 2

CHARGE TRANSFER PHOTOCHEMISTRY OF RE-AA COMPLEXES

Introduction

The central focus of this work is to investigate Re^I metal complexes containing electron acceptor (A) and electron donor (D) ligands that undergo photochemistry which originates in the ligand-to-ligand charge transfer state (LLCT). In many $A-M(d^6)-D$ complexes, although the LLCT state is the lowest energy configuration, due to poor electronic coupling between the donor and acceptor ligands the LLCT state is formed indirectly via initial metal-to-ligand charge transfer (MLCT) excitation followed by rapid donor ligand-to-metal forward electron transfer (FET).[40,41,65-71] In some cases efficient charge separation can be achieved, but the energy-wasting non-radiative back electron transfer (BET) is the dominant decay path (Scheme 2-1). Since the LLCT state is often non-luminescent, its involvement in the photophysics of a complex must be inferred either indirectly from its effect on the properties of the MLCT state or in favorable cases by transient absorption studies.[40,65,66,68,69]

The objective of this study is accomplished by using "reactive donor ligands" (D-R) which undergo rapid carbon-carbon bond-fragmentation (C-C BF) that originates in the LLCT state. In complexes which feature reactive donor ligands, $A-Re^L-(D-R)$, the formation and dynamics of the LLCT state can, in principle, be deduced by examining the efficiency for formation of products which result from C-C BF in the LLCT state (Scheme 2-2).

Scheme 2-1

MLCT

$\overline{\overset{\bullet}{A}}\text{-M}(d^5)\text{-}\overset{\bullet\bullet}{D}$

k_{FET}

LLCT

$\overline{\overset{\bullet}{A}}\text{-M}(d^6)\text{-}D^{+\bullet}$

hv k_d

k_{BET}

$A\text{-M}(d^6)\text{-}\overset{\bullet\bullet}{D}$

Scheme 2-2

MLCT

$\overline{\overset{\bullet}{A}}\text{-Re}^{II}\text{-}(\overset{\bullet\bullet}{D}\text{-R})$

k_{FET}

LLCT

$\overrightarrow{\overset{\bullet}{A}}\text{-Re}^{I}\text{-}(\overset{+\bullet}{D}\text{-R})$

hv k_d

k_{BET}

k_{BF}

$A\text{-Re}^{I}\text{-}(\overset{\bullet\bullet}{D}\text{-R})$

$\overrightarrow{\overset{\bullet}{A}}\text{-Re}^{I}\text{-}\overset{\bullet}{D} + R^+$

Products
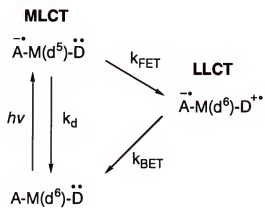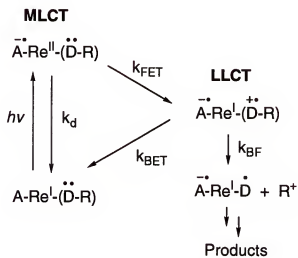
The studies presented in this chapter focus on Re-AA1 and Re-AA2 (Figure 2-1), that feature 1,2-amino alcohol (1,2-AA) reactive donor ligands. The choice of the 1,2-AA ligand was guided by studies in which a structurally diverse set of 1,2-AA donor molecules undergo rapid heterolytic C-C BF following photoinduced bimolecular ET oxidation (Scheme 2-3).[43,53] C-C BF in cation radical 1,2-AA^{+}· produces an α-amino radical (α-A·) and a stable carbonyl compound; further oxidation of α-A· results in formation of an iminium ion which is susceptible to hydrolysis to form a de-alkylated amine and a second carbonyl compound.

It is important to point out the rationale behind the design of each of the structures shown in Figure 2-1. Re-AA1 and Re-AA2 contain the reactive donor 1,2-amino alcohol ligand. These complexes are expected to form and subsequently undergo photochemistry from the LLCT state. Complexes Re-2 and Re-6 serve as non-donor substituted models for Re-AA1 and Re-AA2, respectively. Since these complexes do not have an amine donor, they cannot form the LLCT state; they are examined to allow characterization of the MLCT state. Complexes Re-1 and Re-5 serve as "non-reactive" donor substituted models for Re-AA1 and Re-AA2, respectively. These complexes contain similar aliphatic or aromatic amine donors compared to Re-AA1 and Re-AA2, and therefore should form the LLCT state with similar rates compared to their reactive counterparts; however, they are not expected to be photochemically reactive.

The goal of the studies in this Chapter includes: (1) to survey the photochemistry of 1,2-AA substituted complexes to establish that reactivity characteristic of 1,2-AA^{+}· indeed occurs under conditions where the LLCT state is formed; (2) to quantify the kinetic parameters for the Re-AA complexes and to "clock" the rates for BET in the LLCT state.
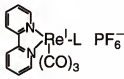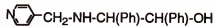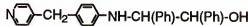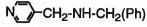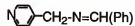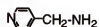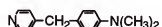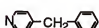
Figure 2-1
The metal complexes and ligands in Chapter 2.

Scheme 2-3

Results

Electrochemistry

Cyclic voltammetry was carried out on several of the complexes to (1) allow estimation of the free energy for FET (ΔG_{FET}) and, (2) examine the reversibility of the anodic waves for the D–R ligands. Relevant potentials for complexes Re-AA1, Re-AA2, Re-5, and Re-6 are listed in Table 2-1. All of the complexes display a characteristic, reversible cathodic wave at $E_{1/2} \approx -1.17$ V which is due to reduction of the coordinated bpy acceptor ligand.[41] In addition, each donor-substituted complex displays an anodic wave with a potential and degree of reversibility that depends upon the structure of the ligand (Figure 2-2). Complex Re-5, in which the donor is an N,N-dimethylaniline (DMA) unit, displays a quasi-reversible wave, which is consistent with the moderate chemical stability of the cation radical, DMA$^{+\cdot}$. By contrast, the anodic wave for Re-AA1 and Re-AA2 is irreversible, which suggests that in each case the amine radical cation formed by electrochemical oxidation is chemically unstable. Presumably the irreversibility of the anodic process is due to rapid C-C BF which occurs after anodic oxidation.

Photophysics

Figure 2-3 shows a comparison of the UV-visible absorption spectra of Re-AA1, Re-AA2 and Re-6. Each complex displays a moderately intense absorption in the near-UV region ($\lambda \approx 355$ nm, $\varepsilon \approx 4000$ M^{-1}cm^{-1}) which is assigned to the lowest $d\pi$ (Re) -> π^* (bpy) MLCT transition.[72-74,41] The intensity of the MLCT absorption is identical for Re-AA1 and Re-6, indicating that there is negligible intraligand (π,π^*) absorption in the 360 - 400 nm wavelength range for these complexes. Complex Re-AA2 exhibits slightly stronger absorption in

Table 2-1 Electrochemical Potentials of Re-L Complexes[a]

Compound	$E_{1/2}$ ($D^{+\cdot}$ / D) /V	$E_{1/2}$ (bpy / bpy$^{-\cdot}$) /V
Re-AA1	$\approx 1.20 \pm 0.2$[b]	-1.13
Re-AA2	+ 0.94[c]	-1.17
Re-5	+ 0.82[d]	-1.17
Re-6		-1.16

a: All the measurements in acetonitrile / 0.1 M [(C$_4$H$_9$)$_4$N$^+$][PF$_6^-$] relative to SSCE reference electrode.

b: E_p value for poorly defined irreversible wave.

c: E_p value for well-defined irreversible wave.

d: $E_{1/2}$ value for quasi-reversible wave.
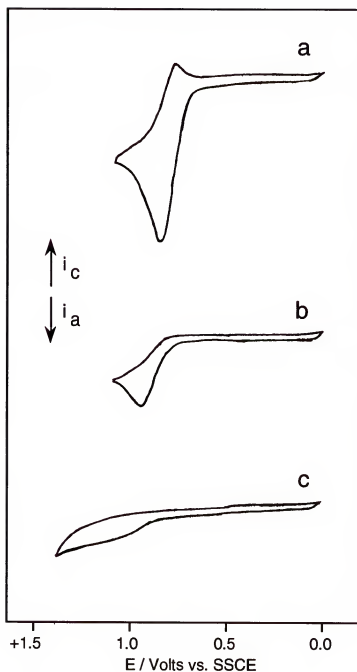
Figure 2-2
Oxidative cyclic voltammographs for Re-L complexes.
(a) Re-5; (b) Re-AA2; (c) Re-AA1.
Sweeps were obtained on 2 mM solutions in CH_3CN / 0.1 M tetrabutyl-ammonium hexafluorophosphate with a Pt disk working electrod, SCE reference, and at a sweep rate of 100 mV/s.
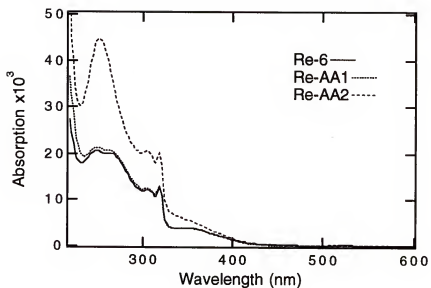
Figure 2-3
Absorption spectra of Re-L complexes in acetonitrile.
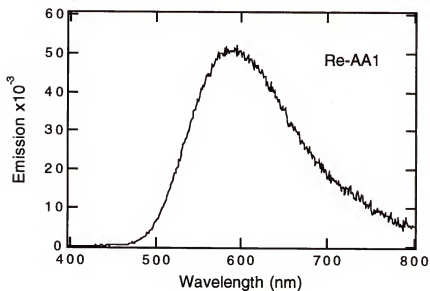
Figure 2-4
Emission spectrum of Re-AA1 in Ar-degassed acetonitrile.

MLCT region (the near UV) and substantially stronger absorption in the far UV range compared to Re-AA1 and Re-6. Examination of the absorption spectrum of AA2 ligand reveals that the increased UV absorptivity of Re-AA2 is due to π,π^* (CT) absorption of the AA2 ligand.

Steady-state and time-resolved emission studies were carried out on each of the Re complexes; a summary of the emission data is presented in Table 2-2. Excitation of Re-AA1, Re-1, Re-2 and Re-6 at 350 nm produces a moderately intense emission at $\lambda_{max} \approx 595$ nm (Figure 2-4). This emission is clearly due to the $d\pi$ (Re) -> π^* (bpy) MLCT excited state.[41] The MLCT emission of each complex was characterized by determining the quantum yield and lifetime (Φ_{em} and τ_{em}, respectively). The non-donor substituted complexes Re-2 and Re-6 exhibit remarkably similar Φ_{em} and τ_{em} values which indicates that the natural decay rate for the MLCT excited state (k_d, Schemes 2-1 and 2-2) is not sensitive to the composition of the organic group which is attached to the pyridyl ligand, as long as this group does not contain an electron donor. The Φ_{em} and τ_{em} values for secondary aliphatic amine donor-substituted complexes Re-AA1 and Re-1 are very slightly, but reproducibly, depressed compared to non-donor complexes Re-2 and Re-6. The slight depression in Φ_{em} and τ_{em} suggests that an additional, non-radiative decay path is operative in Re-AA1 and Re-1; this pathway is believed to be FET to form the LLCT state (k_{FET} path, Schemes 2-1 and 2-2).

By contrast, MLCT emission from aromatic amine donor-substituted complexes Re-AA2 and Re-5 is almost completely quenched. Virtually no steady-state emission is observed upon excitation of these complexes at 350 nm; however, a short-lived emission is detected from Re-AA2 by using time-correlated single photon counting. The MLCT emission is strongly quenched in these complexes because FET is much faster than normal decay of the MLCT

Table 2-2 Photophysical Data of Re-L Complexes[a]

Compound	λ^{max}_{em} (nm)	$E_{0,0}$[b] (cm^{-1})	Φ_{em}[c]	τ_{em}[d] (ns)	τ_{LLCT}[e] (ns)
Re-AA1	593 ± 2	19200	0.042	201 ± 3	f
Re-1	595 ± 2	19200	0.041	207 ± 4	f
Re-2	593 ± 2	19200	0.045	212 ± 3	g
Re-AA2	h		<0.001	0.5	12
Re-5	h		<0.001		15
Re-6	595 ± 2	19200	0.045	209 ± 2	g

a: All the measurements in argon-degassed acetonitrile solutions with λ_{exc}=350nm.

b: $E_{0,0}$ values estimated from Franck-Condon vibronic analysis of emission spectra.

c: Estimated error $\pm$ 10%.

d: Reported emission lifetimes are average of ≥ 5 independent measurements.

e: τ_{LLCT} determined by laser flash photolysis.

f: Φ_{LLCT} too low to allow determination.

g: Not applicable.

h: Emission too weak for acurate determination.

state ($k_{FET} \gg k_d$, Schemes 2-1 and 2-2). That k_{FET} is faster in complexes Re-AA2 and Re-5 compared to Re-AA1 and Re-1 is consistent with the fact that the free energy for this process (ΔG_{FET}) is more exothermic for the aromatic amine donors.

<u>Laser Flash Photolysis</u>

Nanosecond-transient absorption (ns-TA) experiments were conducted on Re-AA2, Re-5 and Re-6 in order to gain spectroscopic and kinetic information on the MLCT and LLCT excited states. Transient spectra of the complexes obtained at various delay times following 355 nm laser excitation (6 ns fwhm, 10 mj/pulse) are shown in Figure 2-5. Figure 5a shows the spectrum of Re-6 obtained at 20 ns delay after excitation. This spectrum is characteristic of the MLCT excited state in (bpy)Re(CO)$_3$-L complexes; the strong band at 370 nm is likely due to a π^*,π^* transition of the bpy anion radical which is present in the MLCT state e.g., *[(bpy$^-$)Re^{II}(CO)$_3$-L].[40,69,75] Figure 5b shows the transient absorption spectrum of Re-5 at 0 ns delay after 355 nm excitation. This spectrum differs significantly from that which is typical for the MLCT state; in particular, there is a strong absorption in the mid-visible ($\lambda_{max} \approx 480$ nm) in addition to moderate absorption in the near-UV region. This spectrum is attributed to the LLCT state, *[(bpy.$^-$)Re^I(CO)$_3$–(DMA+.)] which is formed from the MLCT state by rapid FET following photoexcitation. The LLCT assignment is supported by the presence of the 480 nm absorption band which coincides with the reported absorption of the N,N-dimethylaniline radical cation (DMA+.).[76] The transient absorption which is assigned to the LLCT state for complex Re-5 decays with a lifetime of 15 ns. Figure 5c shows the transient absorption spectrum of reactive donor-substituted complex Re-AA2 obtained at 0 ns delay after 355 nm excitation. This spectrum is quite similar to the
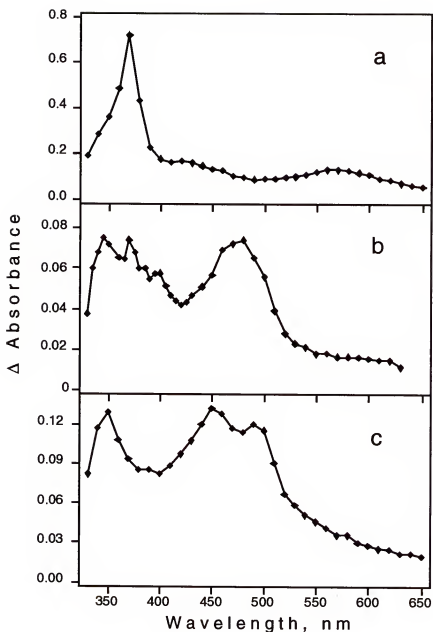
Figure 2-5

Transient absorption spectra of (a) Re-6, 20 ns delay;
(b) Re-5, 0 ns delay; (c) Re-AA2, 0 ns delay.

All the spectra were obtained following 355 nm pulsed excitation from
a Nd:YAG laser (6ns fwhm, 10 mj/pulse); all the spectra were taken in
argon-degassed acetonitrile solution with [Re] ≈ 5 x 10^{-5} M.

spectrum observed for DMA-substituted complex Re-5; in particular, a strong mid visible absorption band is clearly apparent which can be assigned to the N-alkyl anilinium radical cation. The mid-visible band in the spectrum of Re-AA2 exhibits two maxima (450 and 490 nm), which is interesting in view of the fact that the published absorption spectrum of the N-methylanilinium radical cation is dominated by a mid-visible band with two maxima.[76] These facts strongly support the assignment of the transient formed by ns flash photolysis of Re-AA2 to the LLCT state. Analysis of the transient absorption decay shows that the LLCT state in reactive donor complex Re-AA2 has a lifetime of 12 ns.

Steady-State Photochemistry of Re-AA1

Extensive steady-state photochemical studies were carried out on secondary amino alcohol substituted complex Re-AA1. All photochemistry was conducted on argon-degassed acetonitrile solutions using 366 nm monochromatic light from either medium- or high-pressure Hg lamps. This wavelength corresponds to the MLCT absorption band of the $(bpy)Re(CO)_3$- chromophore.

Several product isolation experiments were carried out to determine the overall reaction(s) which occur as a result of photolyis of Re-AA1. A reaction scheme which is consistent with the experimental observations is summarized in Scheme 2-4. First, immediate post-irradiation HPLC analysis indicates that benzaldehyde (PhCHO) is formed in 1:1 stoichiometry with respect to dissappearance of Re-AA1 (Figure 2-6a). Second, semi-preparative scale photolysis of Re-AA1 followed by alumina chromatography led to isolation of the major metal complex product. Spectroscopic characterization (^{1}H and ^{13}C NMR, High-Resolution FAB Mass Spectrometry) indicates that the product is Re-4. Third, semi-preparative photolysis of an argon-degassed acetonitrile solution

Scheme 2-4
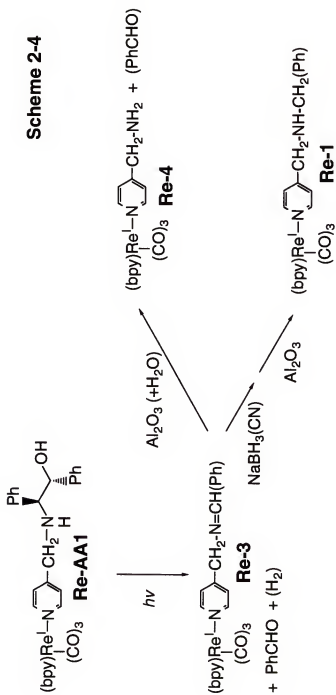
of Re-AA1 followed by overnight incubation with a five-fold excess of $NaBH_3(CN)$ (a selective reducing agent for imines),[77] led to isolation of secondary amine complex Re-1. Compounds which have not been isolated or whose presence has not been directly confirmed by at least two methods are shown in parenthesis in this Scheme. Formation of Re-4 is envisioned to occur via a pathway that involves two-electron oxidation of Re-AA1 to generate imine Re-3 and one equivalent of PhCHO; subsequent hydrolysis of imine Re-3 during semi-preparative chromatography produces Re-4 and a second equivalent of PhCHO. Isolation or independent synthesis of imine Re-3 proved impossible; however, its presence in the acetonitrile reaction mixture was indirectly confirmed by the $NaBH_3(CN)$ reduction which yielded the expected reduction product Re-1.

Since the stoichiometry for formation of PhCHO is important in determining the kinetic parameters, further analytical experiments using HPLC were carried out to establish the time dependence of the stoichoimetry for formation PhCHO relative to dissappearence of Re-AA1 (see Figure 2-6). These experiments indicate that "prompt" analysis (e.g. within 1-2 hours of irradiation) of photoreaction mixtures gives 1:1 stoichiometry for PhCHO relative to dissappearence of Re-AA1 (Figure 2-6a); however, if the photolysis reaction mixture is allowed to stand in the dark in a 1:1 mixture of H_2O / acetonitrile for 4 days the stoichiometry approaches 2:1 for PhCHO relative to dissappearence of Re-AA1 (Figure 2-6b). Presumably the second equivalent of PhCHO is formed by slow thermal hydrolysis of the intermediate metal complex imine, Re-3, which is formed in the primary photochemical step.

Quantum yields for the dissappearence of Re-AA1 (Φ^-_{Re-AA1}) and for prompt formation of PhCHO (Φ^+_{PhCHO}) were determined relative to Aberchrome 540 actinometer and the results are summarized in Table 2-3. As can be seen
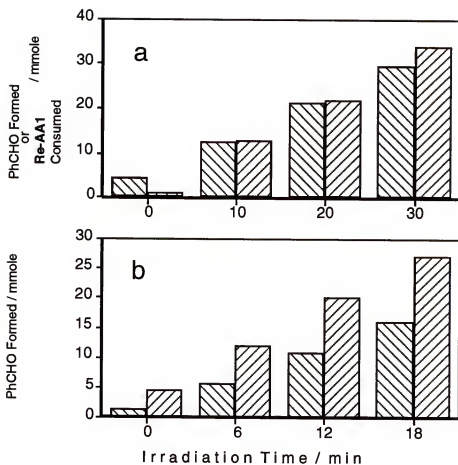
Figure 2-6

Rates of photochemical formation of benzaldehyde and consumption of Re-AA1. (a) left bars: benzaldehyde formed by prompt analysis; right bars: Re-AA1 consumed. (b) left bars: benzaldehyde formed by prompt analysis; right bars: benzaldehyde formed analyzed after hydrolysis of photoproduct solution for 4 days.

Table 2-3 Photochemical Quantum Yield of Re-AA Complexes[a]

Compound	[Re-AA] / M[b]	Φ^+benzaldehyde[c]	Φ^-Re-AA
Re-AA1	1.0×10^{-4}	0.014 ± 0.004	0.016 ± 0.004
Re-AA1	5.0×10^{-4}	0.013 ± 0.002	
Re-AA2	5.0×10^{-4}	0.006 ± 0.001	0.007 ± 0.001

a: All experiments were performed in argon-degassed acetonitrile solutions with λ_{exc}=366 nm; all reactions were driven to < 15% conversion; values represent the average of ≥ 5 individual measurements; errors are standard deviations in the averages. b: Concentration of Re-AA at t=0. c: Quantum yield for "prompt" formation of benzaldehyde. d: Quantum yield for disappearance of starting Re-AA complex.

from this data, Φ^+_{PhCHO} and Φ^-_{Re-AA1} are the same within experimental error (1:1 stoichiometry), and Φ^+_{PhCHO} is the same for $[Re-AA1]_{t=0} = 1 \times 10^{-4}$ M and $[Re-AA1]_{t=0} = 5 \times 10^{-4}$ M. The lack of a concentration dependence on Φ^+_{PhCHO} strongly supports the hypothesis that the photoreaction is unimolecular.

Steady-State Photochemistry of Re-AA2

Less extensive characterization of the photoreaction was carried out for complex Re-AA2. Steady-state experiments were limited to quantitative "prompt" HPLC analysis of reaction mixtures to determine the amount of PhCHO produced and the amount of Re-AA2 consumed by 366 nm irradiation. Quantum yield data for this reaction are summarized in Table 2-3. Several points are of interest with respect to this data. First, it is clear that Φ^+_{PhCHO} and Φ^-_{Re-AA2} are the same within experimental error, indicating that the stoichiometry for prompt formation of PhCHO is 1:1 relative to disappearance of Re-AA2. Second, note that the overall quantum yield for photoreaction of Re-AA2 is lower than for Re-AA1. This is interesting in view of the fact that MLCT quenching (formation of the LLCT state) is substantially more efficient for Re-AA2; the significance of this point will be discussed in more detail below.

Discussion

Excited-State Kinetic Model

In order to relate the photophysical and photochemical results to the rate of the photochemically induced C-C BF reaction which is observed for Re-AA1 and Re-AA2, a kinetic and thermodynamic model must be developed (Scheme 2-5). Using the model presented in this scheme, the photochemical reaction is proposed to occur via the following sequence: (1) initial photoexcitation to the

Scheme 2-5
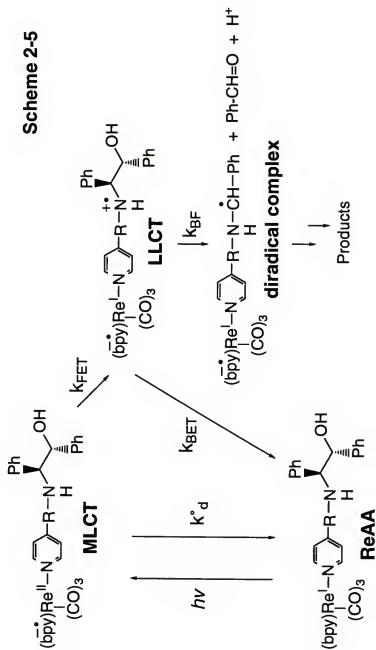
luminescent MLCT excited state; (2) irreversible intramolecular donor ligand to metal ET (with rate k_{FET}) to produce the LLCT state; (3) irreversible C-C BF in the LLCT state to produce an α-amino radical (with rate k_{BF}). Note that FET competes with decay of the MLCT excited state via normal radiative and non-radiative pathways (with rate k_d), and C-C BF competes with decay of the LLCT state via BET (with rate k_{BET}). Under the assumptions implied by the model presented in Scheme 2-5, the relationships between kinetic parameters (k_{FET}, k_{BF} and k_{BET}) and experimentally accessible parameters (Φ^+_{PhCHO}, τ_{em}, τ^*_{em} and τ_{LLCT}) are established in equations 2-1 to 2-6 in Table 2-4.

Thermodynamics and Kinetics for Formation of the LLCT State

The kinetic model presented above indicates that the overall quantum efficiency for the photochemistry depends on both the efficiency for formation of the LLCT state, Φ_{LLCT}, and on the branching ratio for reaction within the LLCT state, β_{BF}. Because of the significance of Φ_{LLCT} in determining the overall reaction efficiency it is important to consider how structural and thermodynamic terms influence this parameter in the two systems which have been examined in the present study.

In previous investigations it has been demonstrated that the free energy for FET (ΔG_{FET}), is given approximately by equation 2-7 in Table 2-4. Using the relevant electrochemical and spectroscopic information collected in Tables 2-1 and 2-2, ΔG_{FET} is estimated for Re-AA1 and Re-AA2 (Table 2-5). Because the D/D$^{+\cdot}$ couples are irreversible, these ΔG_{FET} values are only approximations; however, in spite of this limitation two points are qualitatively clear. (1) ΔG_{FET} is more exothermic for aromatic amine substituted complex Re-AA2 than for complex Re-AA1, which features a 2° aliphatic amine donor. (2) ΔG_{FET} for Re-AA1 is at best only weakly exothermic.

Table 2-4   Kinetic Model of Exited-States in Re-AA Complexes

$$\Phi^+_{PhCHO} = \Phi_{LLCT} \times \beta_{BF} \tag{2-1}$$

$$\Phi_{LLCT} = \frac{k_{FET}}{k_{FET} + k^\circ_d} = 1 - \frac{\tau_{em}}{\tau^\circ_{em}} \tag{2-2}$$

$$\beta_{BF} = \frac{k_{BF}}{k_{BF} + k_{BET}} = k_{BF} \times \tau_{LLCT} \tag{2-3}$$

$$k_{FET} = \frac{1}{\tau_{em}} - \frac{1}{\tau^\circ_{em}} \tag{2-4}$$

$$\beta_{BF} = \frac{\Phi^+_{PhCHO}}{\Phi_{LLCT}} = \frac{\Phi^+_{PhCHO}}{1 - \frac{\tau_{em}}{\tau^\circ_{em}}} \tag{2-5}$$

$$k_{BF} = \frac{\beta_{BF}}{\tau_{LLCT}} \tag{2-6}$$

Φ^+_{PhCHO} : quantum yield for prompt formation of benzaldehyde.

Φ_{LLCT} : quantum yield for formation of the LLCT state.

β_{BF} : the efficiency for C-C BF within the LLCT state.

τ_{em} : the MLCT emission lifetime of the donor-substituted complex.

τ°_{em} : the MLCT emission lifetime of the non-donor substituted model complex.

τ_{LLCT} : lifetime of the LLCT excited state of the donor-substituted complex.

k_{FET} : rate constant for FET.

k_{BET} : rate constant for BET.

k_{BF} : rate constant for C-C BF.

k°_d : rate constant for natural decay from MLCT of the non-donor substituted model.

$$\Delta G_{FET} \approx E_{1/2} (D^{+\cdot} / D) - E_{1/2} (bpy / bpy^-) - E_{0,0} \tag{2-7}$$

ΔG_{FET} : the free energy for FET.

$E_{1/2} (D^{+\cdot} / D)$: electrochemical half-wave potential for oxidation of the donor ligand of the complex.

$E_{1/2} (bpy / bpy^-)$: electrochemical half-wave potential for reduction of the bpy ligand of the complex.

$E_{0,0}$: the 0-0 energy of the relaxed MLCT state obtained from emission spectra.

Values of k_{FET} and Φ_{LLCT} for Re-AA1 and Re-AA2 calculated using emission data and equations 2-2 and 2-4 are collected in Table 2-5. Several comments regarding the accuracy of these parameters are in order. First, for Re-AA2, it is clear that FET from the MLCT state is very fast; the MLCT emission decays with $k \approx 2 \times 10^9$ s^{-1}, which is nearly 10^3 times faster than the normal MLCT decay rate ($k_d \approx 4.8 \times 10^6$ s^{-1}) . Because FET is so rapid in Re-AA2, $\Phi_{LLCT} = 1.0$. On the other hand, the situation regarding k_{FET} and Φ_{LLCT} for Re-AA1 is somewhat less clear. Time-resolved studies indicate that τ_{em} for this complex is depressed only slightly compared to model complexes Re-2 and Re-6. However, based on the fact that model complexes, Re-2 and Re-6, consistently give τ_{em} in the 210 - 212 ns range, we believe that the reproducible, but modest suppression of τ_{em} for complex Re-AA1 is due to formation of the LLCT state via FET. Thus, using emission lifetime data for Re-AA1, Re-2, and Re-6, it is estimated that $k_{FET} \approx 2 \times 10^5$ s^{-1} and $\Phi_{LLCT} \approx 0.05$. It is important to note that the significantly lower k_{FET} observed for Re-AA1 compared to Re-AA2 is in accord with the fact that ΔG_{FET} is less exothermic for Re-AA1 compared to Re-AA2. In addition, the absolute values of k_{FET} and their relationship to ΔG_{FET} for these two complexes are consistent with expectations based on a previous study which examined the dependence of k_{FET} on ΔG_{FET} in a series of non-reactive donor substituted Re(I) complexes.[40]

C-C BF in the LLCT State: Mechanism and Estimated Rates

The primary mechanistic step which is proposed to lead to decomposition of the donor ligand is C-C BF in the LLCT excited state (Scheme 2-5). Although there is no direct spectroscopic evidence on the initial product, the corresponding diradical complex, from both Re-AA1 and Re-AA2, the ns-TA studies on a bimolecular system comprised of Re-6 and an 1,2-AA donor with

Table 2-5 Kinetics of Photofragmentation of Re-AA Complexes

Complex	Re-AA1	Re-AA2
ΔG°_{FET} (eV)	0 ± 0.2	-0.27
k_{FET} (s^{-1})	2.2×10^5	2.0×10^9
Φ_{LLCT}	0.05	1.0
Φ_{RXN}	0.015	0.006
ΔG°_{BET} (eV)	-2.4 ± 0.2	-2.11
k_{BET} (s^{-1})	$\approx 1 \times 10^7$	8.3×10^7
k_{BF} (s^{-1})	$\approx 4 \times 10^6$	5.0×10^5

similar structure to AA2 in argon-degassed acetonitrile does provide direct spectroscopic evidence on the formation of Ph-NH-(Ph)CH·, which absorbs strongly in the near-UV.[78]

A question which is of central interest in this study concerns the rate of this C-C BF reaction. The 1,2-AA reactive donor ligands were selected because previous bimolecular photochemical studies indicated that in 1,2-AA$^{+·}$ the σ-bond between the amine and alcohol carbon atoms undergoes heterolytic fragmentation (Scheme 2-3) with a rate that is sufficiently fast such that the process can compete with annihilation of 1,2-AA$^{+·}$ by bimolecular BET.[43,53] Although studies of this process in bimolecular systems do not allow direct measure of k_{BF}, results suggest that in 1,2-AA molecules which feature 2° or 3° amines $k_{BF} \approx 10^5$ s^{-1}. In addition, comparison of fragmentation efficiencies for 1,2-AA molecules that feature either aromatic or 3° aliphatic amines provides qualitative evidence that k_{BF} is slower in the aromatic 1,2-AA systems.[53]

According to the kinetic model, k_{BF} can be calculated for Re-AA1 and Re-AA2 from the experimental data of Φ^+_{PhCHO}, τ_{em}, τ^*_{em} and τ_{LLCT} using equations 2-5 and 2-6. All of these parameters are available for Re-AA2: Φ^+_{PhCHO}, τ_{em} and τ^*_{em} were obtained from steady-state photochemical measurements and emission studies, and τ_{LLCT} was obtained by laser flash photolysis. Using this data for Re-AA2 we estimate $k_{BF} = 5 \times 10^5$ s^{-1}.

The kinetics are less well-defined for complex Re-AA1. Although Φ^+_{PhCHO} and Φ_{LLCT} are available for this complex, direct measurement of τ_{LLCT} by laser flash photolysis was not possible. Detection of the LLCT state in Re-AA1 by flash photolysis is precluded because (1) Φ_{LLCT} is small, and (2) the 2° aliphatic amine radical cation does not absorb strongly in the near-UV or visible region. Thus, in an effort to provide an estimate for τ_{LLCT} for Re-AA1 a Stern-Volmer (S-V) experiment was carried out in which N,N-dimethylaniline (DMA)

was used to quench the C-C BF by reductive ET from DMA to the LLCT state. Because DMA also quenches the MLCT state, a parallel experiment was conducted to determine the efficiency of S-V quenching of the MLCT emission by DMA. A simplified working mechanism for these two processes is summarized in Scheme 2-6, and the result of this experiment is presented in Figure 2-7, where ($\Phi^{\bullet+}_{PhCHO}/\Phi^+_{PhCHO}$) and ($\tau^\bullet_{em}/\tau_{em}$) are plotted vs [DMA]. This experiment indicates that, as expected, DMA quenches the MLCT state at the diffusion-controlled rate ($k_q^{MLCT} = 1.1 \times 10^{10}$ M^{-1}s^{-1}). However, S-V quenching of Φ^+_{PhCHO} exactly parallels quenching of the MLCT emission. The parallel quenching of τ_{em} (MLCT) and Φ^+_{PhCHO} indicates two important features: (1) quenching of the LLCT state, if it occurs at all, is too inefficient to detect; (2) the MLCT state is clearly a precursor in the mechanism leading to C-C BF, consistent with the proposed mechanism in Scheme 2-5.

Two possible reasons can be suggested to explain the lack of LLCT quenching in the S-V experiment. The first is that the bimolecular rate constant for interception of the LLCT state by DMA is large (e.g., $k_q^{LLCT} \geq 10^9$ M^{-1}s^{-1}), but τ_{LLCT} is short (e.g., $\tau_{LLCT} \leq 100$ ns), so that the overall quenching efficiency is low. The second is that bimolecular quenching is slow (e.g., $k_q^{LLCT} << 10^9$ M^{-1}s^{-1}), and therefore regardless of how long-lived the LLCT state is, the quenching efficiency is low. We favor the former explanation for two reasons. First, the reaction between DMA and the LLCT state is exothermic by ≥ 0.3 eV, thus ET from DMA to the LLCT state should be relatively fast.[79-81] Second, studies of the decay of the LLCT state in non-reactive donor substituted Re(I) complexes lead to the prediction that for Re-AA1, $\tau_{LLCT} \approx 100$ ns.[40] We have used $\tau_{LLCT} = 100$ ns to provide an estimate for k_{BF} in Re-AA1 of 4×10^6 s^{-1}.

An interesting feature now emerges upon comparison of k_{BF} for complexes Re-AA1 and Re-AA2: C-C BF is apparently much faster in the 2°

Scheme 2-6
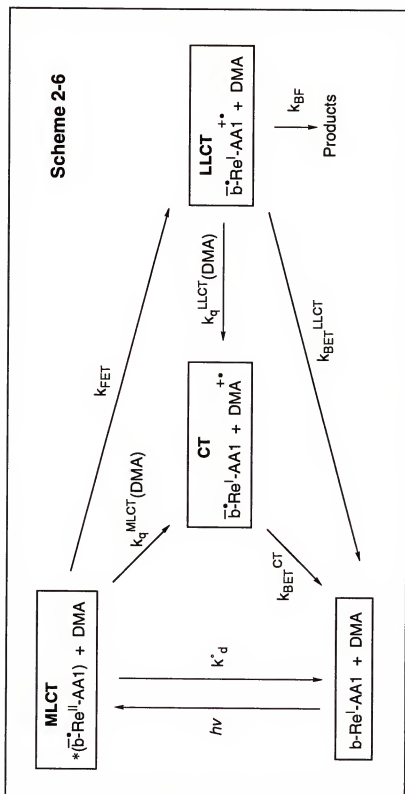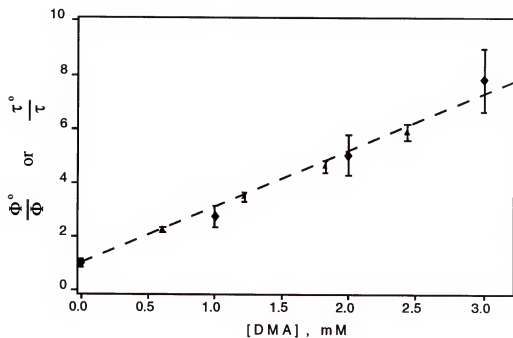
Figure 2-7

Stern-Volmer quenching of Re-AA1 MLCT emission lifetime (τ) and quantum yield for benzaldehyde formation (Φ) by N,N-dimethylaniline (DMA). (triangle) emission lifetime quenching ($\tau° / \tau$); (diamond) quantum yield quenching ($\Phi° / \Phi$).

aliphatic amine donor ligand (Re-AA1) compared to the 2° aromatic amine donor ligand (Re-AA2). This disparity in k_{BF} values provides a rationale for the observation that Φ^+_{PhCHO} is comparable in the two systems, despite the fact that Φ_{LLCT} is significantly larger for Re-AA2 compared to Re-AA1. Apparently the high efficiency of Φ_{LLCT} in complex Re-AA2 is offset by a comparatively lower k_{BF}. Note that the finding that k_{BF} is greater for the aliphatic 1,2-AA$^+$· is consistent with the qualitative results based on bond-fragmentation efficiencies in bimolecular systems.

Dark Reactions of the Diradical Metal Complex Re-7: Concerning the Mechanism for Ultimate Product Formation

To this point the discussion has centered on the mechanism leading to C-C bond fragmentation in the LLCT state. The photophysical and photochemical results are consistent, and indicate that the primary photophysical sequence shown in Scheme 2-5 culminates in formation of reactive intermediate Re-7, which is a Re^I complex that contains a bpy anion radical ligand and an α-amino radical ligand. While no direct experimental information is available concerning the reactivity of Re-7, it is of some interest to speculate on the pathway which is followed during decomposition of this reactive intermediate.

First, it is important to note that α-amino radicals are highly reducing; transient electrochemical experiments indicate that the half-wave potential for the α-amino radical / iminium ion couple is in the range -0.9 to -1.2 V vs SCE. Consistent with the highly reducing nature of the α-amino radical is the fact that the decay pathway expressed in equation 2-8 does not operate for reactive intermediate Re-7. This reaction would involve intramolecular ET from the bpy anion radical to the α-amino radical site. Protonation of the resultant carbanion

would form Re-1; however, Re-1 is not observed in the product mixture following photolysis of Re-AA1.

$$b\text{-}\overset{\bullet}{Re}^I\text{-}N\bigcirc\text{-}(R)\text{-}NH\text{-}\overset{\bullet}{C}H(Ph) + H^+ \xrightarrow{\quad\times\quad} b\text{-}\overset{\bullet}{Re}^I\text{-}N\bigcirc\text{-}(R)\text{-}NH\text{-}CH_2(Ph) \quad (2\text{-}8)$$
$$\quad (CO)_3 \qquad\qquad\qquad\qquad\qquad\qquad (CO)_3$$

Re-7   R = CH₂ : Re-1
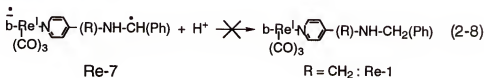
Because the product studies strongly suggest that the final photoproduct of Re-AA1 is imine Re-3, which results from two-electron oxidation of the 1,2-AA ligand, effort was expended to determine the ultimate fate of the reducing equivalents generated during the reaction. Since $(bpy)Re^I(CO)_3L$ complexes undergo one-electron reduction of the coordinated bipyridine ligand at relatively low cathodic potentials (Table 2-1), and the one electron reduction products, $(bpy^{-\cdot})Re^I(CO)_3L$, are typically stable in the absence of O_2, we felt that it was possible that the reducing equivalents could accumulate in the form of one-electron reduced starting Re complex. The reduced complex, $(bpy^{-\cdot})Re^I(CO)_3L$, has a strong absorption band at ≈ 370 nm due to the coordinated bpy anion radical. Therefore, if metal complex reduction occurs during photoreaction under an inert atmosphere, it should be possible to detect the buildup of $bpy^{-\cdot}$ by UV absorption spectrosocopy. However, repeated experiments on samples contained in dry and degassed acetonitrile provided no evidence for the appearance of the UV absorption characteristic of metal complex reduction.

Due to the lack of evidence for the accumulation of $(bpy^{-\cdot})Re^I(CO)_3L$, or for that matter any other reduction products, we reasoned that the only alternative was that H^+ might be reduced to H_2 (H^+ should be produced during the C-C BF process, see Scheme 2-5). Gas chromatograhic analysis of the headspace over a semi-preparative-scale solution (10 mg sample of Re-AA1 in 3 mL of argon-degassed acetonitrile) following exhaustive photolysis provided

evidence that H_2 gas is formed. Insufficient experimental information is available to allow any conclusions to be drawn concerning the mechanism or the species that might catalyze the $2e^-$, $2H^+$ reduction reaction.

Conclusion

This study has examined the efficacy of using reactive 1,2-AA donor ligands to probe the electronic structure and dynamics of the LLCT state in $(bpy)Re^I(CO)_3L$ complexes. The results indicate that the concept works; however, this project defines some limitations which must be overcome if the method is to become generally useful. The most prominent limitation is that the reaction which is triggered by donor ligand oxidation must be sufficiently fast so that it competes effectively with decay of the LLCT state by BET. The 1,2-AA based reactive donor ligands fragment comparatively slowly relative to the rate for BET and, as a result, the overall quantum efficiency for photochemistry in these systems is low.

An interesting finding of the present study is the significantly different fragmentation rates for the radical cations of the 2° aliphatic and the 2° aromatic amino alcohols. The difference in reactivity is qualitatively rationalized by considering factors which stabilize the amine radical cations; however, further studies are clearly warranted to carefully explore the relationship between the thermodynamic stability of the radical cations and the rate for C-C BF.

CHAPTER 3

CHARGE TRANSFER PHOTOCHEMISTRY OF 1,2-DIAMINES

Introduction

The work in Chapter 2 demonstrates the concept of using reactive donor ligands to aid the study of electron transfer (ET) processes in covalently linked A-D compounds.[83] For example, in Re-AA1, photoinduced donor to metal forward ET (FET) is relatively slow and the photophysical information, on its own, is not compelling evidence that photoinduced ET (PET) occurs. However, the fact that photoinduced bond fragmentation (BF) is observed at the donor ligand provides supporting evidence that PET occurs. In Re-AA2, the photophysical properties of the LLCT excited state are clear; the photochemical efficiency provides additional kinetic information allowing the rates for C-C BF and for back ET (BET) to be determined accurately. The results indicate that AA ligands fragment comparatively slowly ($10^5 \sim 10^6$ s^{-1}) relative to the rate of back ET ($10^7 \sim 10^8$ s^{-1}).[83,84,78] As a result, the LLCT decay is dominated by BET in both Re-AA1 and Re-AA2. One goal of this study is to explore reactive donor systems which undergo faster reactions upon single ET activation so that photochemical reactions can compete effectively with the energy wasting BET.

A number of investigations have shown that 1,2-diamines undergo photoinduced selective oxidative cleavage of the C-C bond between the two amino groups.[54,55] The C-C BF was found to be very fast (> 10^8 s^{-1}) and the reaction was very efficient ($\Phi \sim 1$) in a system in which the reaction was believed

to occur via a triplet excited state of the acceptor.[55] On the basis of the previous work we chose 1,2-diamines as reactive donor ligands and developed another Re-based intramolecular A-D system, Re-DA, to further study MLCT and LLCT photochemistry. Figure 3-1 shows the 1,2-diamine ligands and the Re-DA complexes studied in Chapter 3 and Chapter 4. These $(bpy)Re(CO_3)$-DA complexes were designed for several reasons: (1) previous work demonstrated the facile photoinduced C-C BF of 1,2-diamines; (2) the oxidation potentials of aromatic and tertiary amines are usually in the range of $+ 0.7 \sim + 1.0$ V vs SCE, and the excited state reduction potential of $(bpy)Re(CO_3)$-L is $+ 1.22$ V vs SCE, which indicates that the initial photoexcitation to MLCT of the Re-based chromophore will provide sufficient driving force for FET; (3) it is desired to gain spectroscopic information on reactive intermediates because of the lack of such information in previous work; (4) the photochemistry of Re-DA complexes can be directly compared with that of the Re-AA complexes studied in Chapter 2; (5) the syntheses of the diamine ligands and the Re-DA complexes are straight forward.

It can be seen from structures that DA3 and DA4 themselves are intramolecular A-D molecules, and they are also used as donor ligands in Re-DA complexes. In order to survey photochemical reactions of 1,2-diamines in general and to gain understanding of the reactivities of DA3 and DA4, the photophysics and the photochemistry of DA3 and DA4 were fully characterized in this chapter. Table 3-1 shows the compounds and intermediates involved in the study of Chapter 3.
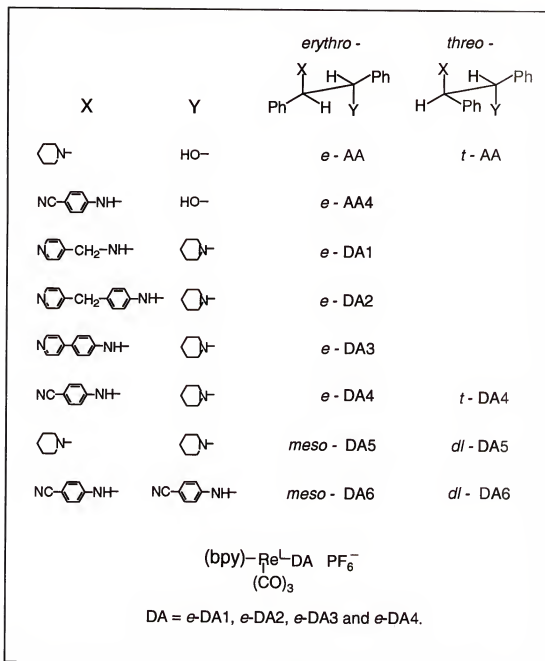
Figure 3-1

1,2-Diamine ligands and Re-DA complexes in Chapters 3 and 4.

Table 3-1   Compounds and Intermediates in Chapter 3

Compound or Intermediate	Acronym
(bpy)Re(CO)$_3$–N◯–CH$_2$◯ PF$_6^-$	Re - 6
4-Aminobenzonitrile	ABN
4-(Benzylamino)-benzonitrile	BZABN
4-(Dimethylamino)-benzonitrile	DMABN
4-(Dibenzylamino)-benzonitrile	DBABN
4-[p-(Amino)phenyl]-pyridine	APP
4-[p-(Dimethylamino)phenyl]pyridine	DMAPP
N-Benzylpiperidine	BZPIP
2,2,6,6-Tetramethyl-1-piperidinyloxy	TEMPO
◯Ṅ=CH(Ph)	iminium 1
◯N–ĊH(Ph)	α-piperidinobenzyl radical
R–ṄH=CH(Ph)	iminium 2
R–NH–ĊH(Ph)	α-aminobenzyl radical
R–N=CH(Ph)	imine

Results

Photophysics

The absorption and fluorescence spectra of *e*-DA3 and *e*-DA4 in acetonitrile at room temperature are shown in Figure 3-2. The photophysical properties of these two compounds and several related compounds are summarized in Table 3-2. Every compound in Table 3-2 exhibits a strong absorption band in near-UV which is due to a π, π^* transition to the singlet charge-transfer excited state (^{1}CT).[85,86] 4-(Benzylamino)-benzonitrile (BZABN) and *e*-DA4 have similar absorption energies with λ_{max} being 284 nm and 286 nm, respectively; the absorption of 4-Aminobenzonitrile (ABN) is blue-shifted slightly compared to BZABN and *e*-DA4. The absorption energies of 4-aminophenylpyridine (APP) and *e*-DA3 are even lower; the λ_{max} of *e*-DA3 is 12 nm red-shifted compared to APP. Every compound shows a single structureless emission band at lower energy relative to the absorption band. The emission is due to radiative relaxation of the first ^{1}CT excited state to the ground state fluorescence.[85,86] BzABN and *e*-DA4 have the same emission maximum ($\lambda_{max} =$ 346 nm) which is 10 nm red-shifted to that of ABN. On the other hand, BzABN and ABN have the same emission lifetime ($\tau_{em} = 3.1$ ns),[87] whereas DA4 has much shorter emission lifetime ($\tau_{em} = 0.4$ ns). The emission data of APP and DA3 show similar features: the emission band of DA3 is a few nm red-shifted relative to that of APP and the emission lifetime of DA3 ($\tau_{em} = 1.2$ ns) is shorter than that of APP ($\tau_{em} = 2.0$ ns).
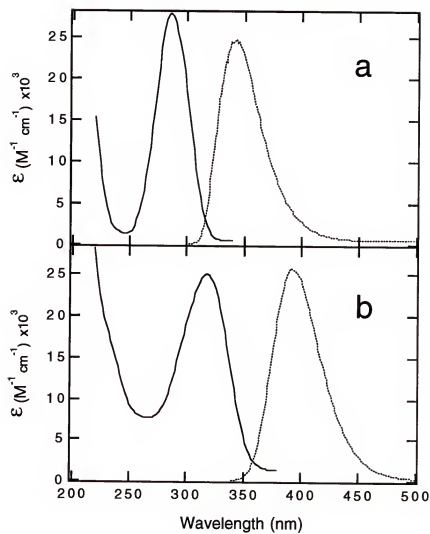
Figure 3-2

Absorption and emission spectra of (a) *e*-DA4, solid line: absorption, dot line: emission x 100,000; (b) *e*-DA3, solid line: absorption, dot line: emission x 25,000. All spectra were for acetonitrile solutions; the solution was argon-degassed for emission measurement.

Table 3-2 Photophysical Properties of DA3, DA4 and Related Compounds.[a]

| Compound | Absorption | | Emission | |
	λ_{max} (nm)	ε ($M^{-1}cm^{-1}$)	λ_{max} (nm)	τ (ns)
ABN	272	23,000	336	3.1
BZABN	284	27,000	346	3.1
e-DA4	286	28,000	346	0.4
t-DA4	286	28,000	346	0.4
APP	306	22,000	386	2.0
e-DA3	318	25,000	392	1.1

a: All the measurements were for acetonitrile solution at room temperature.

<u>Steady-State Photochemistry</u>

Studies have examined the photoreactivity of e-DA3 and e-DA4 resulting from excitation into the long-wavelength ^{1}CT absorption. Initial experimental work involved characterization of photolysis of e-DA4. A preparative photolysis of e-DA4 in argon-degassed acetonitrile solution was carried out and the reaction was monitored by HPLC (Figure 3-3), and a complete photolysis of e-DA4 was performed in air-saturated acetonitrile followed by HPLC analysis (Figure 3-4). Photolysis of e-DA4 in argon-degassed acetonitrile leads to the disappearance of e-DA4 peak at 14.3 minute concurrent with the appearance of several new major product peaks in the HPLC chromatogram with retention times (R_f in minute) being 3.7, 6.5, 7.8, 9.4, 15.4, 29.8 and 31.5.

The product with a retention time of 15.4 (Product-15.4) was isolated by preparative thin layer chromatography (TLC, silica, ethyl acetate-hexane 5:95 v:v), and both ^{1}H NMR and ^{13}C NMR were recorded and compared with the NMR spectra of e-DA4 (Figures 3-5, 3-6 and 3-7 and the structure diagram of e-DA4 shown below). For e-DA4 there are three protons in the region of 4 ~ 6 ppm of the ^{1}H NMR spectrum: the doublet at 5.48 ppm (J = 2.1 Hz) is assigned to H_c; the doublet of doublets at 4.84 ppm (J_1 = 5.7 Hz and J_2 = 2.1 Hz) is assigned to H_b; and the doublet at 3.50 ppm (J = 5.7 Hz) is assigned to H_a.
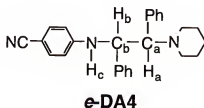
e-DA4

For the ^{1}H NMR of Product-15.4 there are two major differences from e-DA4: first, there are two protons in the region of 4 ~ 6 ppm, 4.61 ppm and 3.63 ppm, both are doublets and have the same coupling constant J = 10.5 Hz; the
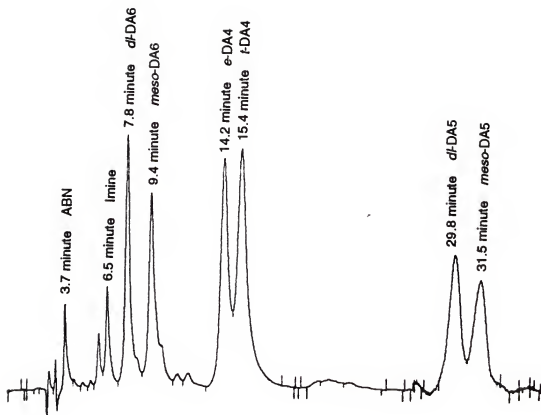
Figure 3-3

HPLC chromatogram of e-DA4 in argon-degassed acetonitrile. Conditions: reversed phase analytical column (Waterman ODS-3); THF- H_2O 50:50 v:v with 0.010 M 1-heptanesulfonic acid, sodium salt and 0.020 M triethylamine as mobile phase. 0-27 minute: λ_{det} = 290 nm; >27 minute: λ_{det} = 272 nm and signals were amplified by a factor of 32.
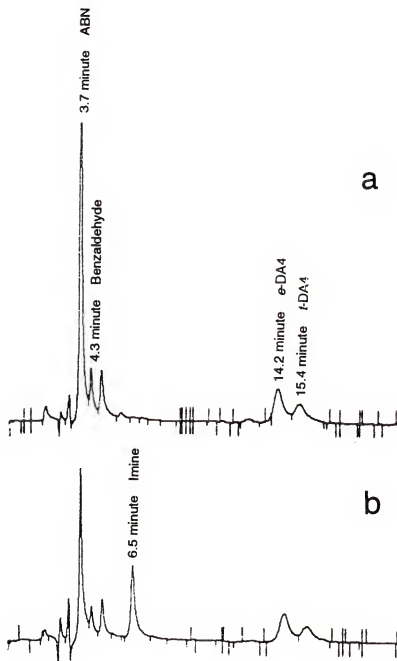
Figure 3-4

HPLC chromatogram of *e*-DA4 in air-saturated
acetonitrile (a) the original product solution + equal amount of H_2O with
pH=3; (b) the original product solution + equal amount of acetonitrile.
Conditions: The HPLC column and mobile phase are same as described in Figure 3-3;
λ_{det} = 280 nm; > 11 minute signals were amplified by a factor of 4.
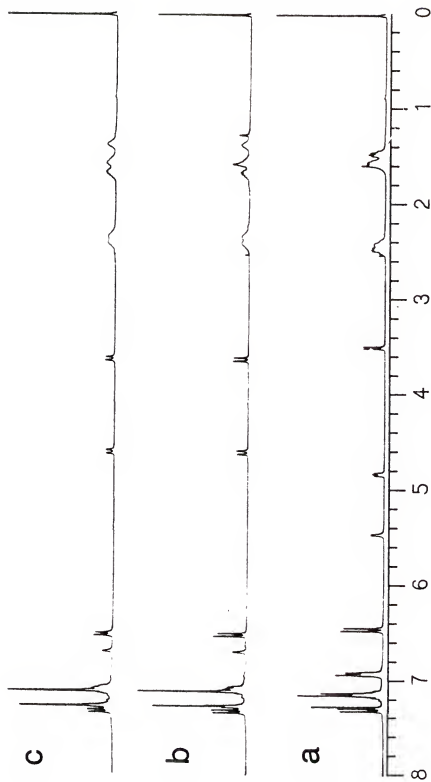
Figure 3-5 ^{1}H NMR (300 MHz, CDCl$_3$) of (a) *e*-DA4, (b) product-15.4, (c) *t*-DA4.
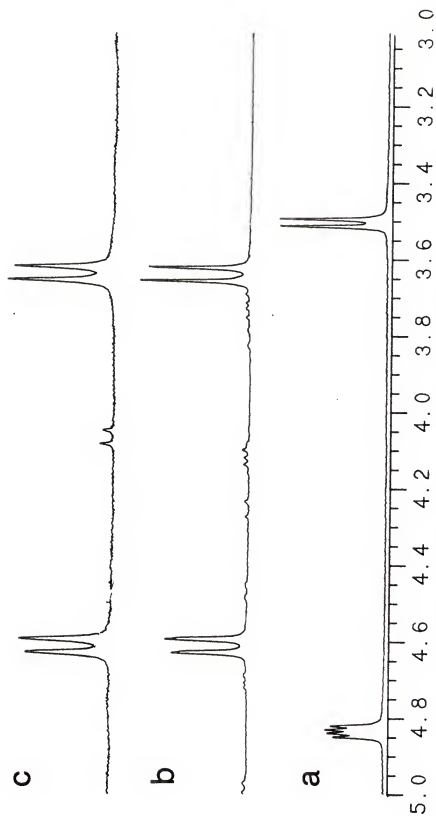
Figure 3-6   Extended ^{1}H NMR (300 MHz, CDCl$_3$) of (a) *e*-DA4, (b) product-15.4, (c) *t*-DA4.
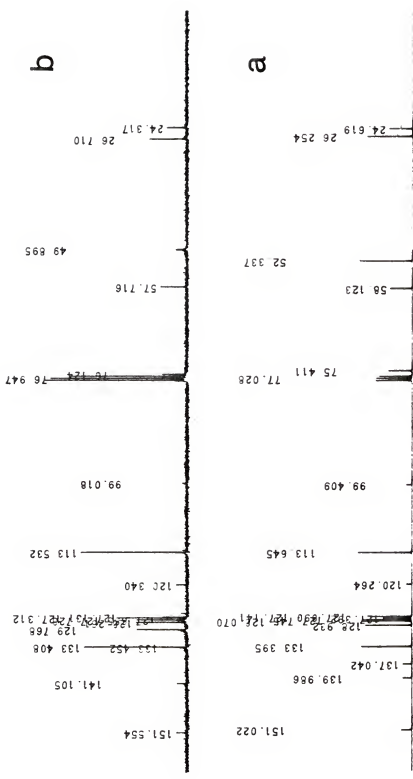
Figure 3-7   ¹³C NMR (75 MHz, CDCl₃) of (a) *e*-DA4, (b) product-15.4.

second, a singlet (1 proton) appears at 6.71 ppm. The number of piperidino-protons and protons in the aromatic region remains unchanged. e-DA4 has 18 magnetically inequivalent carbons. There are five carbons in the region of $0 \sim 80$ ppm: C_a, C_b and three piperidino-carbons. Specifically, the peak at 52.3 ppm is assigned to the piperidino-α-C. The ^{13}C NMR spectrum of Product-15.4 shows that there are also 18 carbons with two CH carbons and three CH_2 carbons in the saturated carbon region. The chemical shifts of all carbons change with small extent compared to e-DA4 except that the sharp peak of the piperidino-α-C of e-DA4 disappears and a broader peak which is CH_2 carbon indicated by APT spectrum appears at 49.9 ppm.

Product-15.4 is proposed to be the *threo* - isomer of DA4 based on the following observations and considerations: (1) the analyses of the NMR characteristics of e-DA4 and Product-15.4; (2) the similar polarity of e-DA4 and Product-15.4 exhibited on HPLC and TLC; (3) Product-15.4 has strong absorption at 290 nm in direct analogy to e-DA4; (4) Product-15.4 is photoreactive, the peak intensity attains a maximum and start to decrease during continuing photolysis; (5) the molecular weight found of e-DA4 is 382.2269 (M+1, HRMS), calc'd for $C_{26}H_{28}N_3$ is 382.2283; and the molecular weight found of Product-15.4 is 382.2320 (M+1, HRMS); (6) that 1,2-diamines undergo selective oxidative cleavage of the C-C bond between the two amino groups in both intermolecular and intramolecular photochemical reactions has been demonstrated by previous work. In order to confirm the proposed structure of Product-15.4, t-DA4, was synthesized starting from *cis* - stilbene oxide as shown in Scheme 3-2. The synthesis of e-DA is shown in Scheme 3-1 for comparison. t-DA4 was characterized by NMR (Figures 3-5 and 3-6). Both ^1H NMR and ^{13}C NMR of t-DA4 are identical with those of Product-15.4. The molecular weight found of t-DA4 is 382.2327 (M+1, HRMS). The retention time of t-DA4 on HPLC

Scheme 3-1

e-DA
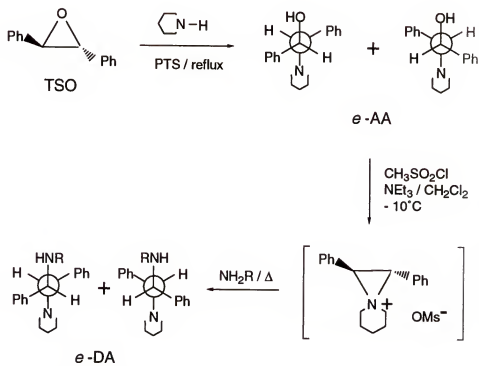
Scheme 3-2
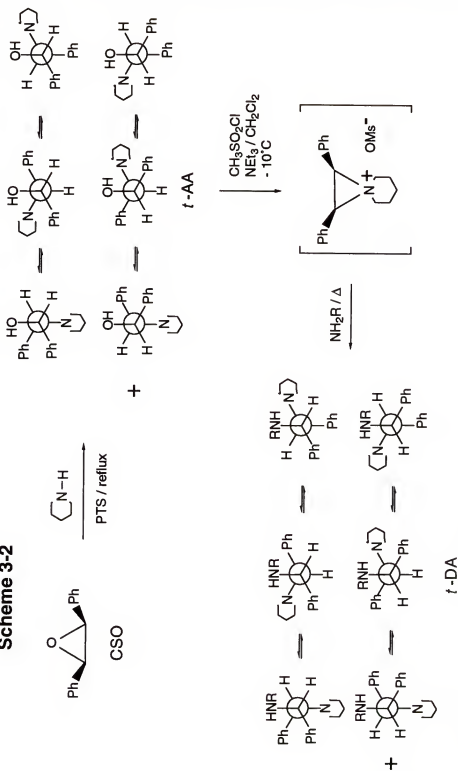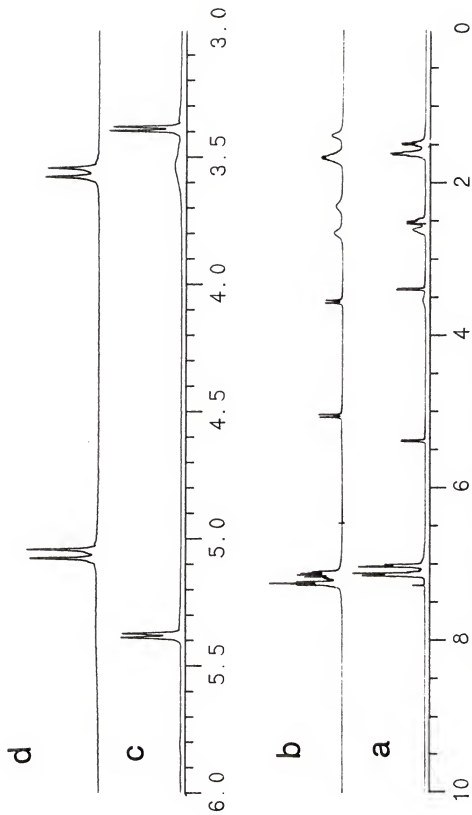
Figure 3-8 ^{1}H NMR (300 MHz, CDCl$_3$) of (a) *e*-AA, (b) *t*-AA, (c) extended spectrum of *e*-AA, (d) extended spectrum of *t*-AA.
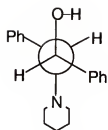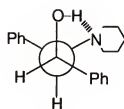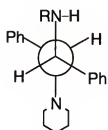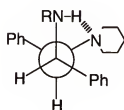
Figure 3-9   *Anti* - and *gauche* - conformers of
e -AA, *t* -AA, *e* -DA and *t* -DA.

chromatogram is the same as that of Product-15.4. The photolysis of t-DA4 in argon- degassed acetonitrile followed by HPLC analysis demonstrates formation of ABN and e-DA4. It is conclusive that Product-15.4 is t-DA4. The ^{1}H NMR spectra of e-DA4 and t-DA4 were also taken for DMSO solutions (Figure 3-10a and 3-10b).

e-AA and t-AA, were also characterized by ^{1}H NMR (Figure 3-8) which show the similar features described for e-DA4 and t-DA4. Figure 3-9 shows the anti and the gauche conformers of e AA, t-AA, e-DA and t-DA. For e-AA or e-DA, the anti conformer in which the two heteroatoms are anti with the two bulky phenyl groups as far as possible from each other, is lower in energy. For t-AA or t-DA, the gauche conformer in which the two heteroatoms are gauche, with the two bulky phenyl groups anti and the intramolecular hydrogen bonding, is lower in energy. These conformation assignments are supported by ^{1}H NMR data: (1) the strong intramolecular hydrogen bonding in t-DA4 decreases the electron density around the proton on the aniline nitrogen, and thus moves the proton absorption to lower field; (2) the entire spectrum of t-DA4 in CDCl$_3$ (Figure 3-5c) is similar to that in DMSO (Figure 3-10b) because the intramolecular hydrogen bonding is hardly affected by the polarity of solvents; (3) H$_c$, the proton on the aniline nitrogen in e-DA4 shifts its position from 5.48 ppm in CDCl$_3$ to 6.81 ppm in DMSO because of the intermolecular hydrogen bonding between H$_c$ and DMSO solvent.

The product with a retention time of 7.8 minute (Product-7.8 in Figure 3-3) was crystallized from concentrated product acetonitrile solution at room temperature. The acetonitrile mother liquor was concentrated to dryness and redissolved in chloroform, and the product with a retention time of 9.4 minute (Product-9.4 in Figure 3-3) was then crystallized from the cold concentrated chloroform. Both Product-7.8 and Product-9.4 were characterized by HRMS, ^{1}H

NMR and ^{13}C NMR. For Product-7.8 the NMR spectra were taken for DMSO solution only; the solubility of this compound was too low in CDCl$_3$ to allow the spectra to be obtained in this solvent. For Product-9.4 the NMR spectra were taken in both DMSO and CDCl$_3$ in order to obtain conformational information (Figures 3-10 and 3-11). Product-7.8 and Product-9.4 are identified as *dl*-DA6 and *meso*-DA6, respectively, based on the following facts: (1) the molecular weight found of Product-7.8 is 415.1909 (M+1, HRMS, POS, FAB), the molecular weight found of Product-9.4 is 415.1914 (M+1, HRMS, POS, FAB), calc'd for C$_{28}$H$_{23}$N$_4$ is 415.1923; (2) the NMR data are consistant with the assigned structures; (3) both compounds have strong absorption at 290 nm in direct analogy to ABN chromophore. It is likely that Product-9.4 is *meso*-DA6, since the ^1H NMR spectra of this compound show strong dependence on solvent polarity (see Figure 3-10d and 3-10e).

The peak with a retention time of 31.5 minute (Product-31.5) in Figure 3-3 was identified as *meso*-DA5 by HPLC analysis of independently synthesized *meso*-DA5. The peak with a retention time of 29.8 minute in Figure 3-3 remains unidentified; however, it is very likely *dl*-DA5. The peak shown at 3.7 minute in Figure 3-3 was identified as ABN by HPLC analysis of an ABN solution.

A qualitative photolysis survey was also performed on *e*-DA4 in air-saturated acetonitrile (Figure 3-4). Several features are significant: (1) The peaks with retention times of 3.7 minute and 4.3 minute in Figure 3-4 were readily identified as ABN and benzaldehyde. (2) The peak with a retention time of 6.5 minute is believed to be the corresponding imine (see Table 3-1 for structure), since it is the only stable photoproduct which hydrolyses rapidly and converts to ABN by addition of acidic H$_2$O to the original product solution. (3) There are not peaks at 7.8 minute and 9.4 minute indicating that there is no *meso*-DA6 and
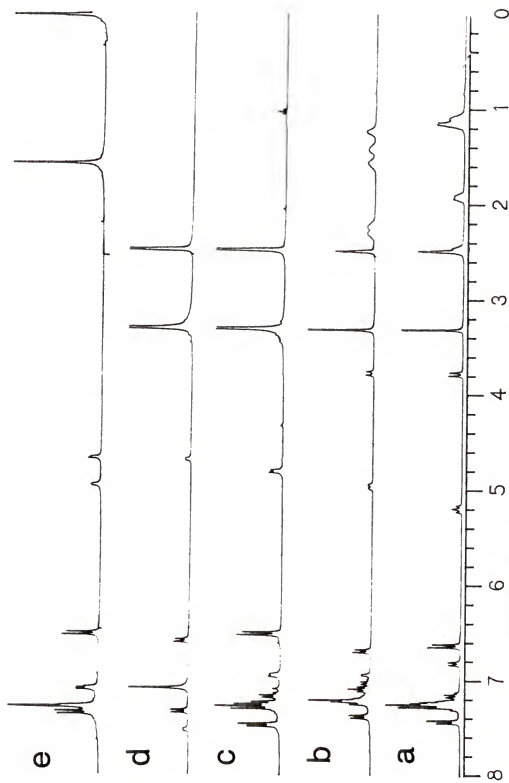
Figure 3-10 ^{1}H NMR (300 MHz) of (a) *e*-DA4, (b) *t*-DA4, (c) product-7.8, (d) product-9.4, (e) product-9.4. a,b,c,d were in DMSO; e was for CDCL$_3$.
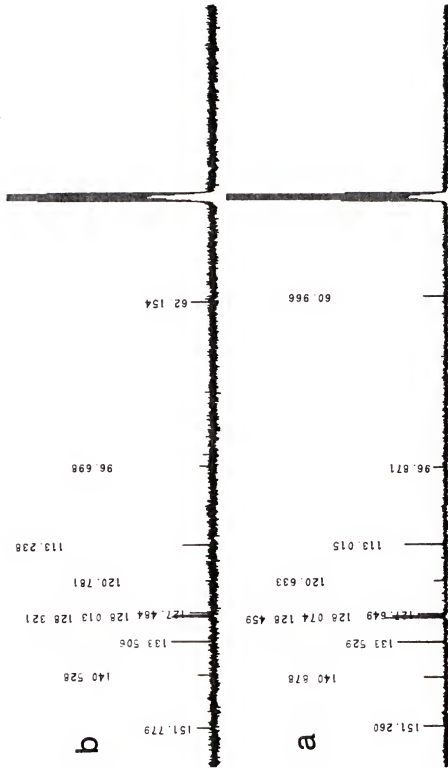
Figure 3-11 ^{13}C NMR (75 MHz, DMSO) of (a) product-7.8, (b) product-9.4.

dl-DA6 formed. (4) When the reaction reaches > 95% conversion both *e*-DA4 and *t*-DA4 are present in a ratio of 4:3 (estimated from the peak area). The significance of this last feature will be discussed in the discussion section.

Scheme 3-3 summarizes the overall photochemical reaction of *e*-DA4 under both argon-degassed and air-saturated conditions. The analogous reaction processes, the C-C BF and the photoisomerization, have also been observed for *t*-DA4 and *e*-DA3 (see Figures 3-12 and 3-14).

Quantitative photoreactions were performed for *e*-DA3, *e*-DA4 and *t*-DA4 in both air-saturated and argon-degassed acetonitrile solution. The quantum yields of the disappearance of starting DA ($\Phi^-_{starting\ DA}$), the appearance of isomer DA ($\Phi^+_{isomer\ DA}$), and the appearance of the corresponding free amine (Φ^+_{amine}) were determined by HPLC analysis, and the mobile phase for each of the 1,2-diamine molecules was adjusted so that the peaks corresponding to the starting DA and the isomer DA were very well resolved. Figures 3-12, 3-13 and 3-14 show the HPLC chromatograms of the photoproducts of *e*-DA3, *e*-DA4 and *t*-DA4, respectively. The photochemical quantum yield results (Table 3-3) demonstrate that for each DA: (1) $\Phi^+_{isomer\ DA}$ is larger in argon-degassed solution; (2) $\Phi^+_{isomer\ DA}$ is suppressed but not eliminated in the presence of O_2; (3) Φ^+_{amine} is significantly larger in the presence of O_2. In addition, *e*-DA4 is more reactive than *t*-DA4.

<u>Laser Flash Photolysis</u>

Laser flash photolysis experiments were conducted on *e*-DA3, *e*-DA4 and *t*-DA4 in order to gain spectroscopic and kinetic information on excited states and reactive intermediates of the photoreaction. Figure 3-15 shows the transient absorption spectra of BZABN, *e*-DA4 and *t*-DA4 in argon-degassed acetonitrile solutions (500 µs window). BZABN displays a weak absorption in the near UV

Scheme 3-3
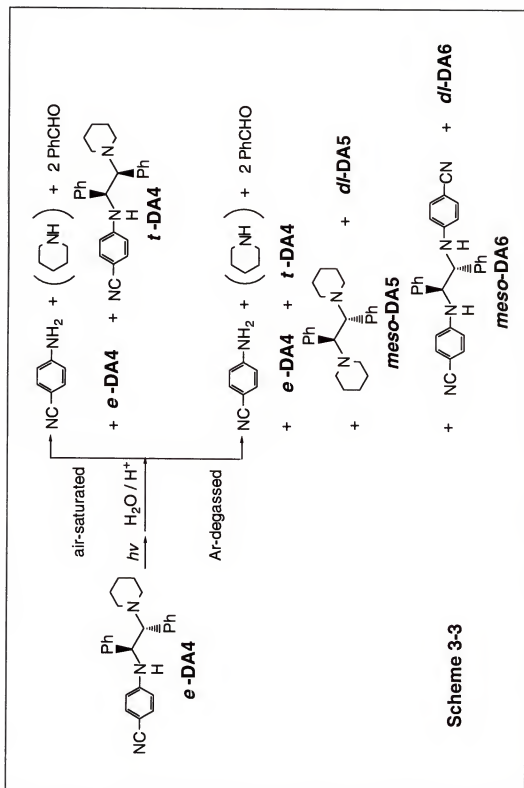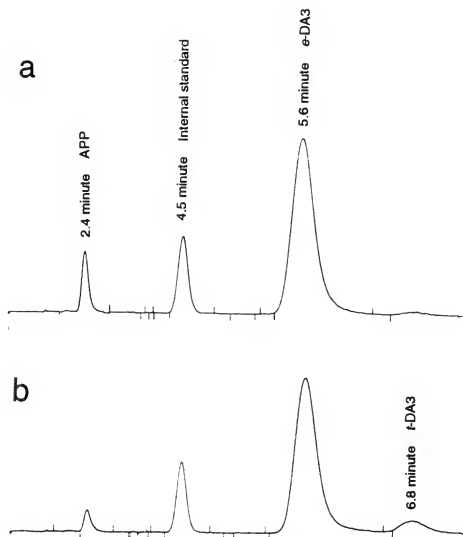
Figure 3-12

HPLC chromatogram of photoproducts of e-DA3 in (a) air-saturated acetonitrile, (b) argon-degassed acetonitrile. Conditions: reversed phase analytical column (Waterman ODS-3); CH_3CN- H_2O 40:60 v:v with 0.010 M 1-heptanesulfonic acid, sodium salt and 0.025 M triethylamine as mobile phase; λ_{det} = 320 nm; p-Nitroaniline as internal standard.
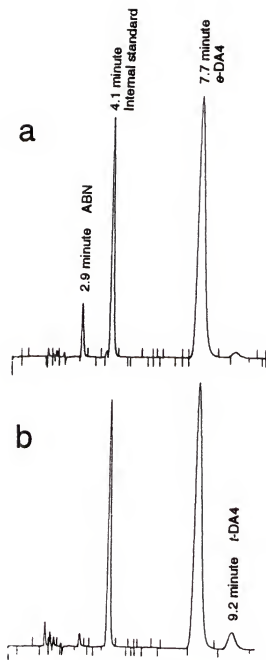
Figure 3-13

HPLC chromatogram of photoproducts of e-DA4 in (a) air-saturated acetonitrile, (b) argon-degassed acetonitrile. Conditions: reversed phase analytical column (Waterman ODS-3); THF-CH$_3$CN- H$_2$O 4:40:56 v:v:v with 0.010 M 1-heptanesulfonic acid, sodium salt and 0.025 M triethylamine as mobile phase; λ_{det} = 286 nm; Acetophenone as internal standard.
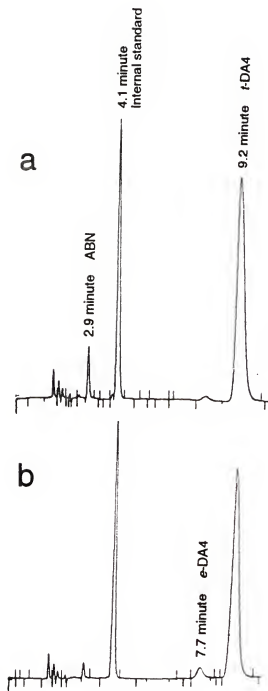
Figure 3-14

HPLC chromatogram of photoproducts of *t*-DA4 in (a) air-saturated acetonitrile, (b) argon-degassed acetonitrile. Conditions: reversed phase analytical column (Waterman ODS-3); THF-CH$_3$CN- H$_2$O 4:40:56 v:v:v with 0.010 M 1-heptanesulfonic acid, sodium salt and 0.025 M triethylamine as mobile phase; λ_{det} = 286 nm; Acetophenone as internal standard.

Table 3-3 Photochemical Quantum Yield of 1,2-Diamines[a]

Compound	$\Phi^-_{starting\text{-}DA}$	air-saturated $\Phi^+_{isomer\text{-}DA}$	Φ^+_{amine}
e-DA3	0.118 ± 0.01	0.016 ± 0.002	0.080 ± 0.004
e-DA4	0.155 ± 0.015	0.026 ± 0.002	0.089 ± 0.004
t-DA4	0.105 ± 0.007	0.018 ± 0.004	0.075 ± 0.004

Compound	$\Phi^-_{starting\text{-}DA}$	argon-degassed $\Phi^+_{isomer\text{-}DA}$	Φ^+_{amine}
e-DA3	0.065 ± 0.004	0.035 ± 0.01	0.011 ± 0.002
e-DA4	0.105 ± 0.003	0.062 ± 0.004	0.020 ± 0.003
t-DA4	0.065 ± 0.01	0.025 ± 0.003	0.020 ± 0.003

a: All the measurements were carried out in acetonitrile solutions.

due to the triplet charge-transfer state (^{3}CT).[87] The ^{3}CT decays by first-order single exponential kinetics, and the decay rate was determined to be 6 x 10^4 s^{-1} (see Figure 3-15 inset). The spectrum of e-DA4 shows two distinguishable absorption bands centered at 345 nm and 382 nm, respectively. These two bands partially overlap. Both 345 nm and 382 nm transients are long-lived, and decay by second-order kinetics. These two long-lived transients are quenched by Tempo, a radical quenching reagent, and also by O$_2$. The halftime of the 382 nm transient was found to be approximately 150 μs without quenching, 10 μs in the presence of Tempo, and 100 ns in the presence of O$_2$.

The lower energy band (λ_{max} = 382 nm) is assigned to the absorption of the corresponding α-aminobenzyl radical,[78] and the 345 nm band is likely due to absorption of the α-piperidinobenzyl radical. The latter assignment is supported by the ns-TA studies of a sensitized bimolecular reaction between Re-6 and $meso$-DA5. The reaction is expected to occur upon 355 nm laser excitation according to Scheme 3-4. Figure 3-16a shows the transient spectrum of this bimolecular photolysis in argon-degassed acetonitrile. The strong absorption band centered at 340 nm is clearly due to the α-piperidinobenzyl radical since it is the only possible intermediate which absorbs in this region. This radical is long-lived in argon-degassed acetonitrile and decays by second-order kinetics; it is also quenched by O$_2$. The halftime of the the α-piperidinobenzyl radical was found to be approximately 150 μs without quenching; and 100 ns in the presence of O$_2$.

The transient spectrum of t-DA4 (Figure 3-15) exhibits similar features to those described for e-DA4 except the absorption bands at 350 nm and 385 nm for t-DA4 are less intense compared to those for e-DA4.
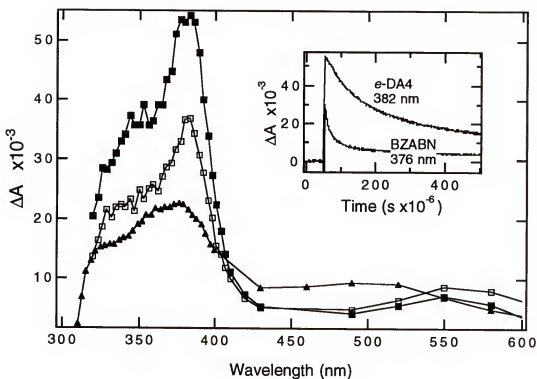
Figure 3-15

Transient absorption spectra of *e*-DA4 (full squares and lines);
t-DA4 (open squares and lines); BZABN (triangles and lines)
in argon-degassed acetonitrile solution, 5 μs delay from rising
edge of laser pulse. Conditions: λ_{exc}=266nm, laser power=5 mj/pulse.
INSET: Transient absorption kinetic traces.

Scheme 3-4

(bpy)Re^I(CO)$_3$(BP)$^+$ $\xrightarrow{\ h\nu\ }$ (b$\overline{\text{py}}$)Re^{II}(CO)$_3$(BP)$^+$
Re-6 **MLCT**

(b$\overline{\text{py}}$)Re^{II}(CO)$_3$(BP)$^+$ + *meso*-DA5
MLCT

ET $\downarrow$

(b$\overline{\text{py}}$)Re^I(CO)$_3$(BP) + *meso*-DA5$^{+\bullet}$
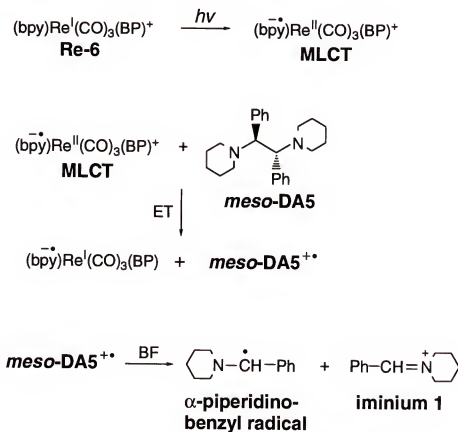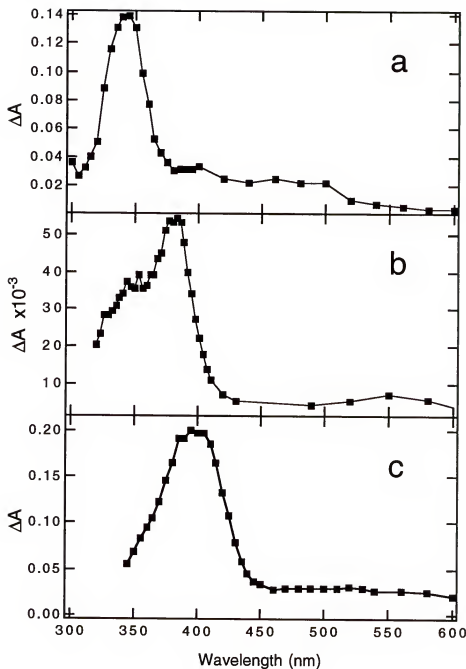
meso-DA5$^{+\bullet}$ $\xrightarrow{\ BF\ }$ $\langle$N–ĊH–Ph + Ph–CH=N$^+$$\rangle$
α-piperidino- **iminium 1**
benzyl radical

Figure 3-16

Transient absorption spectra of (a) Re-6 and *meso*-DA5,
λ_{exc}=355nm; (b) *e*-DA4, λ_{exc}=266nm; (c) *e*-DA3, λ_{exc}=
355nm. All spectra are for argon-degassed acetonitrile
solution, 5 µs delay from rising edge of laser pulse.
laser power=5 mj/pulse.

The spectrum of e-DA3 (Figure 3-16c) shows a broad absorption band centered at 390 nm. The 390 nm transient forms immediately after the laser pulse. It is long-lived in argon-degassed acetonitrile, and decays by second-order kinetics. The absorption centered at 390 nm is likely due to the corresponding α-aminobenzyl radical. The strong bleaching of ground state absorption of e-DA3 in the range of 300 to 350 nm inhibits the TA study in the higher energy region (<350 nm).

Electrochemistry

DA4 and DA3 contain of three kinds of amino groups: 4-aminobenzonitrile (2° aromatic amine) in DA4, 4-[p-(amino)phenyl]pyridine (2° aromatic amine) in DA3, and piperidino (3° aliphatic amine) in both DA3 and DA4. Cyclic voltammetry was carried out on compounds which contain only one amino group: N-substituted piperidines (PIP-N), N-substituted 4-aminobenzonitriles (ABN-N) and N-substituted 4-(4-aminophenyl)pyridines (APP-N) (Table 3-6). The $E_p^{+/0}$ values of PIP-N, ABN-N and APP-N are in the range of +0.8 to +1.0 V, +1.2 to +1.4 V and +0.9 to +1.0 V, respectively. The $E_p^{+/0}$ is somewhat concentration and sweep rate dependent, and it also varies with the substitutes. The $E_p^{+/0}$ of PIP-N is ~ 0.3 V less positive than that of ABN-N, which is comparable to that of APP-N. Cyclic voltammetry was also carried out on the following diamines: meso-DA5 (two PIP-N), DA6 (two ABN-N), DA4 (PIP-N and ABN-N) and DA3 (PIP-N and APP-N), and the results are shown in Table 3-4.

Discussion

A working mechanism for the interpretation of the results is shown in Scheme 3-5, and the kinetic model based on the proposed mechanism is established as shown in equations 3-1 to 3-4:

Table 3-4 Oxidation Potentials of 1,2-Diamines and Related Compounds[a]

compound	possible donor sites		$E^1_p{}^{+/0}$ (V)[b]
e-AA	PIP-N		+0.87
t-AA	PIP-N		+1.06
BZPIP	PIP-N		+0.96
ABN	ABN-N		+1.3
BZABN	ABN-N		+1.3
DMABN	ABN-N		+1.2
DBABN	ABN-N		+1.3
e-AA4	ABN-N		+1.2
meso-DA5	PIP-N	PIP-N	+0.8
e-DA4	PIP-N	ABN-N	+0.9
t-DA4	PIP-N	ABN-N	+1.0
meso-DA6	ABN-N	ABN-N	+1.2
dl-DA6	ABN-N	ABN-N	+1.2
APP	APP-N		+1.07
DMAPP	APP-N		+0.90
e-DA3	PIP-N	APP-N	+0.9

a: Experimental conditions: in 0.1 M tetrabutylammonium hexafluorophosphate acetonitrile solution; Pt disk working electrode; SCE reference; sweep rate = 200 mV / second. b: the first irreversible peak potential.

$$k_{FET} = 1 / \tau_{CT} - 1 / \tau°_{CT} \tag{3-1}$$

$$\Phi_{CS} = 1 - \tau_{CT} / \tau°_{CT} \tag{3-2}$$

$$\beta_{BF} = \Phi_{RXN} / \Phi_{CS} \tag{3-3}$$

$$\beta_{BF} = k_{BF} / (k_{BF} + k_{BET}) = k_{BF} \times \tau_{CS} \tag{3-4}$$

In these equations τ_{CT} and $\tau°_{CT}$ are the emission lifetimes of the 1,2-diamines and their corresponding models (APP as the model for e-DA3; ABN as the model for e-DA4 and t-DA4), respectively; τ_{CS} is the lifetime of the charge-separated state (CS); Φ_{CS} and Φ_{RXN} are the quantum efficiencies for FET and the overall BF the 1,2-diamines; β_{BF} is defined by equation 3-4; all other parameters are defined in Scheme 3-5.

The Primary Photochemical Reaction of the 1,2-Diamines

The absorption and emission spectra (in terms of energies and shapes) of DA4 compared to ABN, and of DA3 compared to APP show that the initial photoexcitation promotes DA4 to the same [1]CT excited state as that of ABN, and leads DA3 to the same [1]CT excited state as that of APP. The energy of the first [1]CT excited state is estimated to be ~ 3.8 eV for DA4 and ~ 3.4 eV for DA3 by using the emission data.[85,86] The emission lifetime of DA4 compared to ABN, and of DA3 compared to APP suggest that the first [1]CT excited states of DA4 and DA3 are quenched intramolecularly. Because of the existence of piperidino donor group in both DA3 and DA4 the [1]CT quenching is attributed to FET from the piperidino-nitrogen to the corresponding [1]CT excited state, and the primary photoreaction product is the charge-separated state (CS in Scheme 3-5). According to equations 3-1 and 3-2 k_{FET} and Φ_{CS} are 2×10^9 s^{-1} and 0.87 for DA4, 4×10^8 s^{-1} and 0.45 for DA3. The [1]CT emission quenching via ET mechanism for DA3 and DA4 is substantiated by the observation that

Scheme 3-5

Scheme 3-6

triethylamine quenches the fluorescence of ABN (and BZABN) with $k_q = 4 \times 10^9$ $s^{-1}M^{-1}$.

Since it is difficult to directly measure the reduction potentials ($E_{1/2}^{0/-}$) of DA4 and DA3, the free energy for FET, ΔG_{FET}, cannot be estimated according to equation 3-5:

$$\Delta G_{FET} = E_{1/2} (D^+ \cdot / D) - E_{1/2} (A / A^- \cdot) - E_{0,0} \qquad (3-5)$$

However, $E_{1/2}^{+/0}$ of PIP-N is ~ 0.3 V less positive than that of ABN-N, and if the interaction between PIP-N and ABN-N in DA4 is ignored, then ΔG_{FET} for DA4 can be qualitatively estimated as -0.3 eV based on the following arguments (see Scheme 3-6): (1) the transition to ^1CT state of DA4 is dominated by one electron photoexcitation from the low-lying π orbital of ABN chromophore occupied mainly by ABN-N lone pair in DA4 to the LUMO of the molecule; (2) the nature of the primary electrochemical reaction of DA4 is irreversible removal of one electron from the HOMO of the molecule which is likely the non-bonding orbital occupied by PIP-N lone pair in DA4; (3) the nature of the primary electrochemical reaction of molecules which contain only ABN-N is irreversible or reversible (depends on the structure of the substituent) removal of electron from the HOMO of the molecule which should be the low-lying π orbital occupied mainly by ABN-N lone pair; (4) the difference between the oxidation potential of PIP-N and ABN-N reflects qualitatively the relative energy difference between the HOMO and the low-lying π orbital of ABN chromophore in DA4. For DA3 ΔG_{FET} is estimated as ≈ -0.15 eV based on the difference between the oxidation potential of APP and PIP-N. The estimates of ΔG_{FET} for DA4 and DA3 are consistent with the fact that the ^1CT quenching in e-DA3 is substantially slower than that in e-DA4 (see Table 3-5).

According to this analysis, the $E_{1/2}{}^{0/-}$ values of e-DA4 and e-DA3 are estimated to be $\approx$ - 2.6 V and $\approx$ - 2.4 V, respectively. Literature values report -2.4 to -3.0 V for related compounds.[82]

The C-C Bond Fragmentation

The secondary reactions from the primary CS excited state include BET and C-C BF. The occurrence of the latter has been demonstrated by the characterization of the major stable photoproducts of e-DA4. A caged radical pair, the α-aminobenzyl radical and the α-piperidinobenzyl radical, is proposed as the initial C-C BF product (see Scheme 3-5) on the basis of the following observations and considerations: (1) Pulse excitation of all three 1,2-DA molecules rapidly produces long-lived transients that absorb in the near-UV and are quenched efficiently by O_2 and Tempo; (2) The anion radical group in the CS state is highly reducing ($E_{1/2} \approx$ - 2.5 V for both DA3 and DA4); (3) Under air-saturated conditions photoisomerization does occur for each of the starting 1,2-diamines (see Figures 3-12 to 3-14). (4) For starting e-DA4 all the possible radical recombination products, $meso$-DA6, dl-DA6, t-DA4, $meso$-DA5 and dl-DA5 have been identified under argon-degassed conditions; whereas under air-saturated conditions only photoisomerization product, t-DA4, has been identified together with the corresponding free amine, ABN (see Figure 3-4).

Under air-saturated conditions, O_2 in acetonitrile serves as a radical scavenger in the photolysis of DA molecules. In the ns-TA study on an air-saturated acetonitrile solution of e-DA4 it was observed that the half-life of the corresponding α-aminobenzyl radical is ~100 ns. In the ns-TA study on an air-saturated acetonitrile solution of Re-6 and DA5 bimolecular system (see Scheme 3-4) it was observed that the half-life of the α-piperidinobenzyl radical is also ~100 ns. In other words, the observed pseudo-first order rate constant for those

radicals being quenched by O_2 is ~10^7 s^{-1}. Since $[O_2]$ in air-saturated acetonitrile is $\approx$ 2 mM,[88] then the rate of bimolecular quenching of radicals by O_2 (k_{rq}) must be $\geq 10^{10}$ s^{-1}M^{-1}. Based on these parameters, it is reasonable to believe that in air-saturated solution O_2 will scavenge all radicals which diffuse away from the original solvent cage, converting them irreversibly to the corresponding iminium 1 and iminium 2 (see Table 3-1 for the structures). Because of the high k_{rq}, this quenching process will occur mainly within the solvent-separated radical pairs.[89,90] As a result, random recombination from free radicals is essentially eliminated and photoisomerization in air-saturated solution presumably occurs only within the original solvent cage; that is, the observed $\Phi^+_{isomer\ DA}$ under air-saturated conditions is attributed to the in-cage recombination only. In argon-degassed solution, if it is assumed that radical quenching by O_2 is entirely eliminated, geminate radical pairs then either recombine within the solvent cage or diffuse away from each other followed by random recombination to form DA6 (*meso*-DA6 and *dl*-DA6), DA4 (*e*-DA4 and *t*-DA4) and DA5 (*meso*-DA5 and *dl*-DA5) with the ratio of 1:2:1.[89,91]

Competition between BET and C-C BF can be quantitatively determined according equation 3-3 which requires values of Φ_{CS} as well as Φ_{RXN}. Φ_{CS} can be readily derived from the first ^1CT emission data. However, the occurence of photoisomerization suggests that the observed Φ_{RXN} must be less than the "true" value since starting DA is also expected to be a product of the isomerization under both air-saturated and argon-degassed conditions. (The quantum efficiency of formation of the isomer DA ($\Phi^+_{isomer\ DA}$) is measurable, whereas the quantum efficiency of formation of the starting DA ($\Phi^+_{starting\ DA}$) produced by the photoisomerization is not measurable.) As discussed above, the existence of O_2 changes the ultimate products distribution only, but not the overall quantum yield. A simple approach to determine the "true" Φ_{RXN} is to add $\Phi^+_{starting\ DA}$(air)

to $\Phi^-_{\text{starting DA}}$(air), and the sum of these two values can be used as the "true" Φ_{RXN}. To do so a question must be answered, that is, how much starting DA is produced as photoisomerization product from the photolysis of a starting DA under air-saturated conditions? The HPLC analysis of a photolysis product solution of e-DA4 at high % conversion in air-saturated acetonitrile revealed that no meso-DA6 and dl-DA6 were observed, however, both e-DA4 and t-DA4 were observed in a ratio of approximately 4:3 (see Figure 3-4). This result indicates that the in-cage recombination does occur, and the assumption, $\Phi^+_{\text{starting DA}}$(air) $\approx \Phi^+_{\text{isomer DA}}$(air), is approximately valid.[92,93] Based on this assumption, for each of the DA molecules the sum of $\Phi^-_{\text{starting DA}}$(air) and $\Phi^+_{\text{isomer DA}}$(air) is used as the "true" Φ_{RXN}.

<u>Kinetics of the CS State</u>

Table 3-5 summarizes the kinetics of the CS excited state. The k_{BF} values are estimated as $\geq 1 \times 10^8$ s^{-1} for both DA3 and DA4, since the corresponding CS excited state should absorb in the mid-visible region and no such band has been observed from ns-TA studies. This indicates that these CS excited states are short-lived, that is, $\tau_{\text{CS}} \leq 10$ ns which is the laser pulse lifetime. The C-C BF competes with BET characterized by β_{BF}. The driving force for BET, ΔG_{BET}, are estimated according to equation 3-6 by assuming the $E_{1/2}^{0/-}$ values for DA4 and DA3 obtained from the foregoing analysis.

$$\Delta G_{\text{BET}} = E_{1/2} (A / A^-) - E_{1/2} (D^+ / D) \tag{3-6}$$

The ΔG_{BET} is estimated as ≈ -3.5 V for DA4 and ≈ -3.3 V for DA3. These BET processes are probably in the Marcus inverted region.[34,35] The calculated values for BET in DA3 and DA4 may seem large in view of the large

exothermicity for these reactions; however, the rates are consistent with the large electronic coupling anticipated in these compounds.

Table 3-5 Kinetics of the Photofragmentation of 1,2-Diamines

Compound	e-DA3	e-DA4	t-DA4
ΔG°_{FET} (eV)	-0.15	-0.3	-0.3
k_{FET} (s^{-1})	4.0×10^8	2.0×10^9	2.0×10^9
Φ_{CS}	0.45	0.87	0.87
Φ_{RXN} (air)	0.134[a]	0.181[a]	0.123[a]
β_{BF}	0.31	0.21	0.13
ΔG°_{BET} (eV)	$\approx$ - 3.3	$\approx$ - 3.5	$\approx$ - 3.5
k_{BF} (s^{-1})	$\geq 1 \times 10^8$	$\geq 1 \times 10^8$	$\geq 1 \times 10^8$
k_{BET} (s^{-1})	$\geq 3 \times 10^8$	$\geq 4 \times 10^8$	$\geq 4 \times 10^8$

a: Calculated value with the correction discussed in text.

Conclusion

Several important results are obtained from this study: (1) the C-C BF in 1,2-diamines induced by intramolecular PET is very fast, and competes effectively with BET from the CS state; (2) the primary BF products are α-aminobenzyl radical and α-piperidinobenzyl radical pairs which undergo both in-cage and random recombination; (3) these radicals absorb strongly in the near-UV; (4) the reactivity toward C-C BF for e-DA is slightly higher than that for t-DA; (5) the study developed a novel approach using isomerization to monitor reactions of radicals.

CHAPTER 4

CHARGE TRANSFER PHOTOCHEMISTRY OF RE-DA COMPLEXES

The Re-DA complexes studied in this chapter are e-Re-DA1, e-Re-DA2 and e-Re-DA3 (see Figure 4-1 for structures). e-Re-DA4 was synthesized but found to undergo thermal dissociation in acetonitrile solution to release free DA4 ligand.

<u>Results</u>

<u>Absorption and Emission of Re-DA Complexes</u>

The absorption spectra of Re-DA1, Re-DA2 and Re-DA3 are shown in Figure 4-2. The assignments of the lowest absorption band for each complex are given in Table 4-1. For Re-DA1 and Re-DA2, the intraligand (π, π^*) absorption is negligible. For Re-DA3 the strong absorption band (λ_{max} = 370 nm, ε ~ 40,000 $M^{-1}cm^{-1}$) is mainly due to the intraligand (π, π^*) absorption of DA3 in the complex. The MLCT absorption of Re-DA3 is overlapped with the strong intraligand charge-transfer (ILCT) band.[68]

Steady-state emission studies were carried out on each of the Re-DA complexes in acetonitrile. The emission spectra of Re-DA1 and the non-donor substituted model complex, Re-6, are shown in Figure 4-3. Upon excitation at λ_{exc} = 350 nm both Re-DA1 and Re-6 display moderately intense luminescence at λ_{max} = 585 nm which is due to the $d\pi$(Re) -> π^*(bpy) MLCT excited state.[41,83]
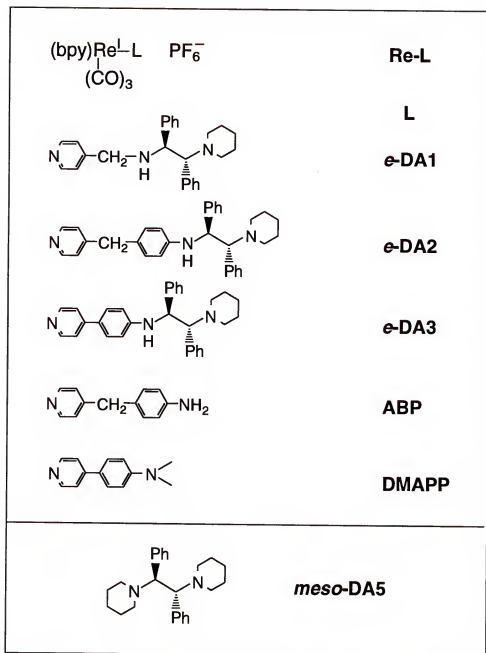
Figure 4-1

e-Re-DA complexes and related compounds in Chapter 4.
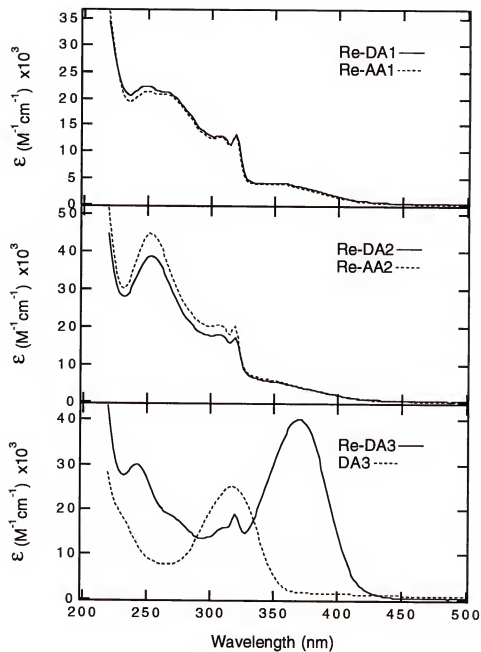
Figure 4-2
Absorption spectra of Re-DA and Re-AA complexes.
All the spectra were for acetonitrile solutons.
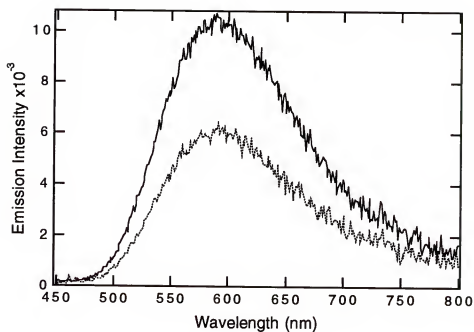
Figure 4-3

Emission spectra of Re-DA1 and Re-6 in air-saturated acetonitrile.
(dot line): Re-DA1; (solid line): Re-6.

Table 4-1   Absorption Data of Re-DA Complexes[a]

Compound	λ_{max}(nm)	ε(M^{-1}cm^{-1})	Assignment
Re-DA1	~350	4,000	MLCT
Re-DA2	~350	5,300	MLCT
Re-DA3	370	40,000	MLCT & ILCT

a: All the spectra were for acetonitrile solutions.

Table 4-2   Emission Lifetimes of Re-DA and Model Complexes[a]

Compound	argon-degassed τ(ns)	air-saturated τ(ns)
Re-6	209 ± 2	109 ± 1
Re-DA1	65 ± 2	53 ± 1
Re-DA2	0.5 ± 0.1	
Re-DA3	1.0 ± 0.1	

a: All the spectra and measurements were for acetonitrile solutions.

However, the MLCT emission from Re-DA1 is quenched compared to that of Re-6. The lifetime of the MLCT emission from Re-DA1 is substantially shorter than that of Re-6 under both argon-degassed and air-saturated conditions (Table 4-2). For Re-DA2 and Re-DA3, the MLCT emission is almost completely quenched. Virtually no steady-state emission is observed upon excitation of these two complexes at 350 nm; however, a short-lived emission is detected from Re-DA2 and Re-DA3 by using time-resolved single photon counting (Table 4-2).[83]

Steady-State Photochemistry

In order to examine similarities and differences of the reaction pathways of Re-DA complexes compared to DA ligands, photolysis of Re-DA2 resulting from excitation into the MLCT absorption was characterized in both argon-degassed and air-saturated acetonitrile. A semi-preparative photolysis of Re-DA2 in argon-degassed solution was carried out, and the reaction was monitored by HPLC (Figure 4-4). Irradiation of Re-DA2 (366 nm) leads to the disappearance of Re-DA2 peak at 9.6 minute concurrent with the appearance of benzaldehyde (R_f = 4.4 minute), Re-ABP (R_f = 5.5 minute) and a product with R_f of 10.8 minute (product-10.8). Product-10.8 was isolated and characterized by ^1H NMR, ^{13}C NMR and HRMS. In e-Re-DA2, H_b overlaps with H_c at ~ 4.85 ppm (see Figures 4-5 and 4-6); H_a appears as a doublet at 3.62 ppm (J = 8.1 Hz); and H_d appears as a singlet at 3.67 ppm. The ^1H NMR of product-10.8 shows two major

Figure 4-5 e-Re-DA2
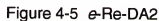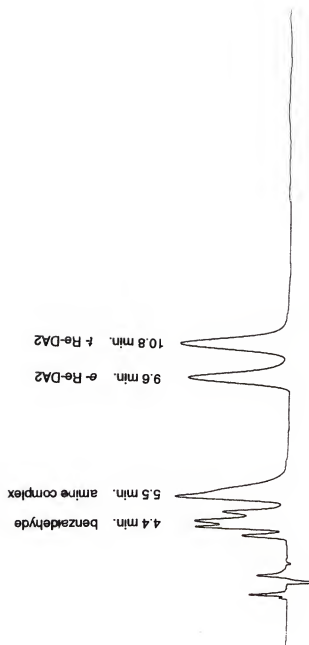
Figure 4-4

HPLC chromatogram of *e*-Re-DA2 in argon-degassed acetonitrile.
Conditions: reversed phase analytical column; 5% THF / 40% CH_3CN / 55% H_2O / 0.03 M 1-heptanesulfonic acid,
sodium salt / 0.03 M triethylamine / pH=4; λ_{det} = 250 nm.

differences: (1) there is a doublet (J ~ 10.5 Hz, 1H) at 4.62 ppm; (2) a broad peak appears at 6.07 ppm (1H). In the range of 3.6 to 3.7 ppm the spectrum is not well resolved, but it is clear that there is a singlet (2H) at 3.71 ppm and another proton at 3.66 ppm. As to the ^{13}C NMR, the sharp peak at 51.1 ppm corresponding to C_a in e-Re-DA2 disappears in product-10.8, and a new broad peak appears at 49.3 ppm (Figure 4-7). This feature has been observed in the ^{13}C NMR spectrum of t-DA4 studied in Chapter 3. The molecular weight found is 874.2730 for e-Re-DA2 (HRMS, POS, FAB), ca. 874.2769. The molecular weight found is 874.2835 for product-10.8 (HRMS, POS, FAB). All this evidence supports the hypothesis that product-10.8 is the $threo$ isomer of Re-DA2.

In addition to the aforementioned products, $meso$-DA5 (R_f = 13.8 minute) was also identified as a photoproduct by HPLC analysis. A peak (R_f = 13.4 minute) which partially overlaps with the peak for $meso$-DA5 also appeared on HPLC chromatogram; this peak is likely due to dl-DA5. The mobile phase for the identification of DA5 in the e-Re-DA2 reaction mixture contained THF-H_2O 64:36 v:v with 0.015 M 1-heptanesulfonic acid, sodium salt and 0.03 M triethylamine, and λ_{det} = 270 nm. The photoproduct solution was concentrated 5 times before injecting to the HPLC.

In air-saturated acetonitrile solution, Re-ABP (the corresponding free amine complex) and benzaldehyde are the only final photoproducts detected by HPLC. The overall reactions of e-Re-DA2 under argon-degassed and air-saturated conditions are summarized in Scheme 4-1. Scheme 4-1 is also applicable to Re-DA1 and Re-DA3 based on HPLC analysis of photoproduct solutions of these two complexes. The HPLC chromatograms of photoproducts of e-Re-DA1, e-Re-DA2 and e-Re-DA3 are shown in Figures 4-8, 4-9 and 4-10, respectively.
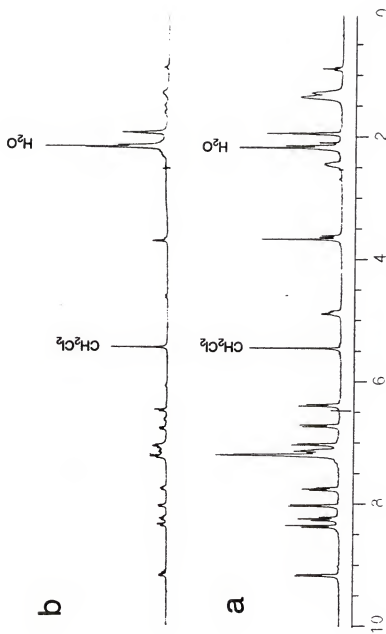
Figure 4-6

^{1}H NMR (300 MHz, CD$_3$CN) of (a) Re-DA2; (b) product-10.8 minute.
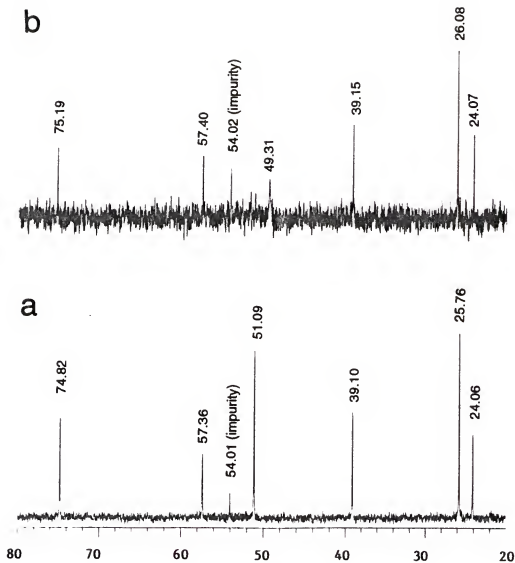
Figure 4-7

^{13}C NMR (75 MHz, CD$_3$CN) of (a) Re-DA2; (b) product-10.8 minute.
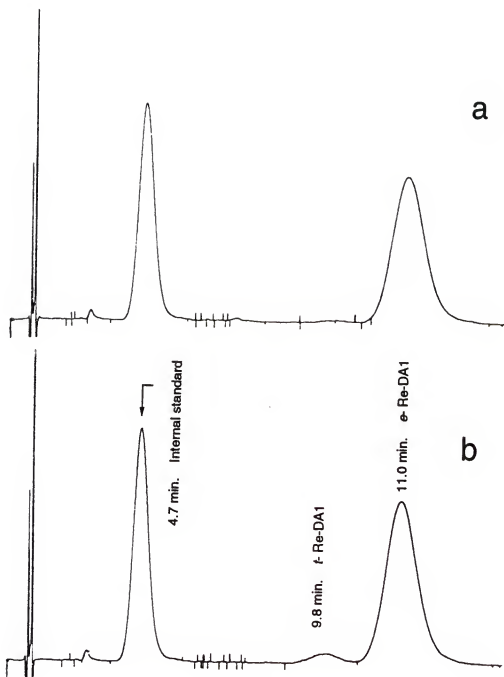
Figure 4-8
HPLC chromatogram of photoproduct of *e*-Re-DA1 in
(a) air-saturated acetonitrile; (b) argon-degassed acetonitrile.
Conditions: reversed phase analytical column (Waterman ODS-3);
THF-H$_2$O 68:32 v:v with 0.03 M 1-heptanesulfonic acid, sodium salt
and 0.03 M triethylamine; λ$_{det}$ = 250 nm.
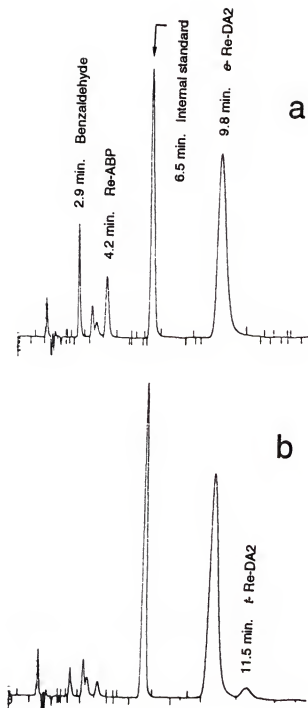
Figure 4-9
HPLC chromatogram of photoproduct of *e*-Re-DA2 in
(a) air-saturated acetonitrile; (b) argon-degassed acetonitrile.
Conditions: reversed phase analytical column (Waterman ODS-3);
THF-CH$_3$CN- H$_2$O 5:45:52 v:v:v with 0.04 M 1-heptane-sulfonic acid,
sodium salt and 0.05 M triethylamine; λ_{det} = 250 nm.
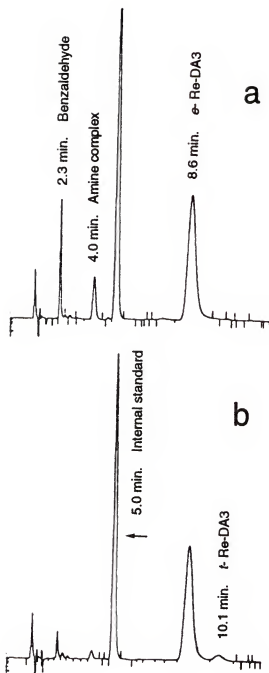
Figure 4-10
HPLC chromatogram of photoproduct of *e*-Re-DA3 in
(a) air-saturated acetonitrile; (b) argon-degassed acetonitrile.
Conditions: reversed phase analytical column (Waterman ODS-3);
THF-CH$_3$CN- H$_2$O 5:45:52 v:v:v with 0.04 M 1-heptane-sulfonic acid,
sodium salt and 0.05 M triethylamine; λ_{det} = 250 nm.

Scheme 4-1
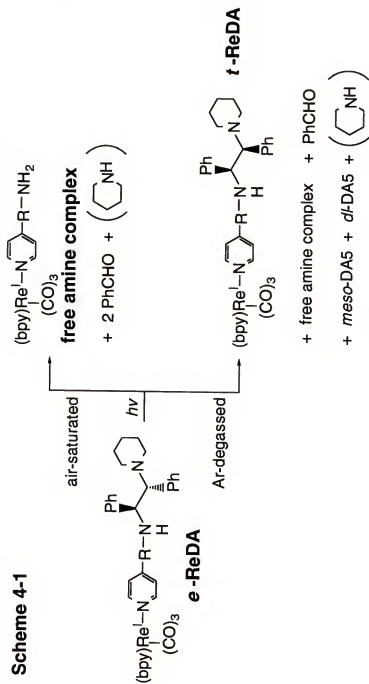
Table 4-3 Photochemical Quantum Yields of Re-DA Complexes[a]

Complex	air-saturated			
	$\Phi^-_{e\text{-Re-DA}}$	$\Phi^+_{t\text{-Re-DA}}$	Φ^+_{BA}	Φ^+_{amine}
Re-DA1	0.22 ± 0.03	0	0.35 ± 0.03	__
Re-DA2	0.54 ± 0.03	0	1.10 ± 0.05	0.48 ± 0.01
Re-DA3	0.43 ± 0.02	0	0.75 ± 0.04	__

Complex	argon-degassed			
	$\Phi^-_{e\text{-Re-DA}}$	$\Phi^+_{t\text{-Re-DA}}$	Φ^+_{BA}	Φ^+_{amine}
Re-DA1	0.14 ± 0.02	0.08 ± 0.01	0.09 ± 0.01	__
Re-DA2	0.29 ± 0.04	0.16 ± 0.01	0.19 ± 0.02	0.08 ± 0.01
Re-DA3	0.26 ± 0.03	0.09 ± 0.02	0.14 ± 0.02	__

a: All the measurements were carried out in acetonitrile solutions.

___The Φ values were not measured.

Quantitative photoreactions were performed on each of the *e*-Re-DA complexes in both air-saturated and argon-degassed acetonitrile solution. Irradiation (366 nm) was controlled so that the reactions were driven to < 15% conversion. The quantum yields for consumption of the starting *e*-Re-DA and for formation of the products were determined, and the results are summarized in Table 4-3. Several points are significant with respect to this data: for each of *e*-Re-DA complexes, (1) the photoisomerization is entirely eliminated in air-saturated acetonitrile solution-no *t*- Re-DA peak was observed on the HPLC chromatogram for the reactions; (2) the ratio between $\Phi^-_{e\text{-Re-DA}}$ (air) and Φ^+_{BA} (air) is nearly 1:2 in each case; (3) *e*-Re-DA -> *t*- Re-DA photoisomerization is significant in argon-degassed acetonitrile solution; (4) $\Phi^-_{e\text{-Re-DA}}$ (argon) is lower than $\Phi^-_{e\text{-Re-DA}}$ (air); (5) Φ^+_{BA} (argon) is significantly lower than Φ^+_{BA} (air) (see Figures 4-8, 4-9 and 4-10).

<u>Laser Flash Photolysis</u>

Nanosecond transient absorption (ns-TA) studies were carried out on each of the Re-DA complexes in order to gain spectroscopic and kinetic information on excited states and reactive intermediates involved in the photochemistry.

The results of ns-TA studies of Re-DA2 in argon-degassed acetonitrile are shown in Figure 4-11 (500 ns window) and Figure 4-12 (500 µs window). It can be seen clearly from Figure 4-11 that there is a strong absorption band in the range of 330 nm - 390 nm, and a weak band in the mid-visible (430 nm - 500 nm) immediately after laser excitation. The transient centered at 365 nm, which is long-lived, is attributed to the corresponding metal complex diradical that is produced directly by heterolytic C-C BF in the LLCT state (Scheme 4-2).[78] This assignment is based on the following facts: (1) previous studies indicate that α-amino benzyl radicals absorb strongly in the near-UV; (2) C-C BF of DA ligand is

Figure 4-11

Transient absorption spectra of Re-DA2 in argon-degassed
acetonitrile solution. Conditions: λ_{exc}=355nm, laser power=5 mj/pulse.
(lines and markers) Spectrum at 20 ns delay from rising edge of laser pulse;
(solid line) Spectrum at 100 ns delay from rising edge of laser pulse;
(dot line) Spectrum at 420 ns delay from rising edge of laser pulse.
INSET: Transient absorption kinetics at 460 nm.
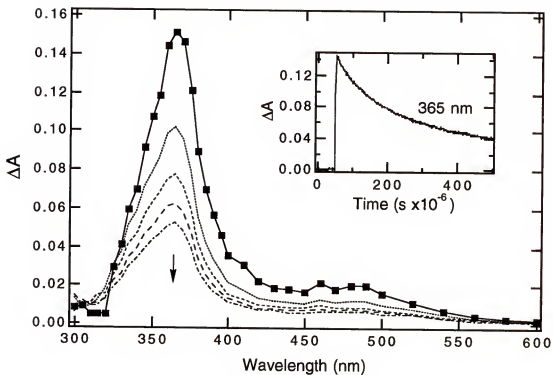
Figure 4-12

Transient absorption spectra of Re-DA2 in argon-degassed
acetonitrile solution. Conditions: λ_{exc}=355nm, laser power=5 mj/pulse.
(lines and markers) Spectrum at 5 μs delay from rising edge of laser pulse;
subsequent spectra at 85, 165, 245, 325 μs delay from rising edge of laser
pulse. INSET: Transient absorption kinetics at 365 nm.

a major photochemical pathway for Re-DA2; (3) the absorption band of α-piperidino benzyl radical is centered at 340 nm (see Figure 3-16a), which indicates that the heterolytic C-C BF in DA2 ligand occurs in the direction to produce the corresponding diradical metal complex. The intense 365 nm absorption is due to the α-amino benzyl radical chromophore, R-NH-CH(Ph)•[78]. This long-lived diradical decays by second-order kinetics (cal. $k \approx 4 \times 10^4$ $M^{-1}s^{-1}$) (see Figure 4-12 and the inset). The temporal profile at 460 nm (see Figure 4-11 inset) shows that immediatedly following the laser pulse the absorption reaches a maximum, decays rapidly at early time into a constant weak absorption. This behavior is observed in the range of 430 nm to 500 nm, which forms a weak but distinguishable absorption band in the mid-visible. This mid-visible band is assigned to the LLCT state of Re-DA2 based on the position and intensity after comparison with the TA spectra of Re-AA2 and the non-reactive donor model complex, Re-5.[83,76] The 460 nm kinetic trace implies that the lifetime of the LLCT state of Re-DA2 is ≤ 10 ns.

The results of ns-TA studies of Re-DA3 in argon-degassed acetonitrile are shown in Figure 4-13 (500 ns window) and Figure 4-14 (500 μs window). The shorter-time scale ns-TA displays several features immediately after laser excitation: (1) strong bleaching of the ground-state absorption in the range of 340 nm to 390 nm; (2) there is a broad, strong absorption band in the range of 400 nm to 480 nm, and the corresponding transient is long-lived (see Figure 4-13 inset); (3) there is moderately intense absorption in the range < 340 nm which is also long-lived. The strong absorption band centered at 425 nm is attributed to the corresponding metal complex diradical (see Scheme 4-2), which decays by second-order kinetics (ca. $k \approx 7 \times 10^4$ $M^{-1}s^{-1}$), and the ground state recovery follows the same kinetics as shown by the 370 nm temporal profile (see Figure 4-14 and the inset).

Figure 4-13

Transient absorption spectra of Re-DA3 in argon-degassed acetonitrile solution. Conditions: λ_{exc}=355nm, laser power=5 mj/pulse. (a) Transient absorption kinetics at 370 nm and 420 nm. (b) (lines and markers) Spectrum at 20 ns delay from rising edge of laser pulse; (dot line) Spectrum at 380 ns delay from rising edge of laser pulse.

Figure 4-14

Transient absorption spectra of Re-DA3 in argon-
degassed acetonitrile solution.

Conditions: λ_{exc}=355nm, laser power=5 mj/pulse.

(a) Transient absorption kinetics at 370 nm and 420 nm.

(b) (lines and markers) Spectrum at 5 μs delay from rising edge
of laser pulse; subsequent spectra at 85, 165, 245, 325 μs
delay from rising edge of laser pulse.

Figure 4-15
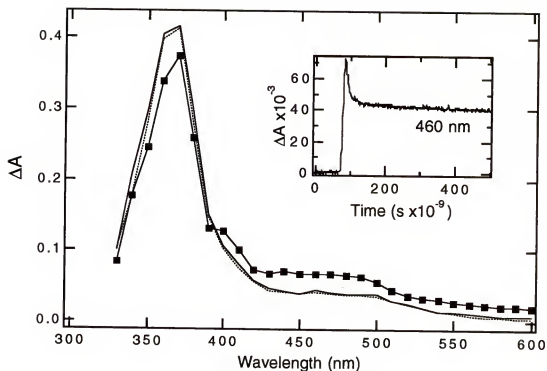
Transient absorption spectra of Re-DMAPP in argon-degassed acetonitrile solution. Conditions: λ_{exc}=355nm, laser power=5 mJ/pulse. For (a) and (b): (lines and markers) Spectrum at 20 ns delay from rising edge of laser pulse; (dot line) Spectrum at 60 ns delay from rising edge of laser pulse; (c) Transient absorption kinetics at 390 nm; (d) Transient absorption kinetics at 495 nm.

A ns-TA study was also carried out on the non-reactive donor model complex for Re-DA3, ReDMAPP, in order to probe the excited states of this complex. Figure 4-15 shows the TA spectra and kinetic traces at 390 nm and 495 nm of this complex in argon degassed acetonitrile (500 ns window). The concentration of ReDMAPP used for this experiment is comparable with that for the Re-DA3 TA experiment shown in Figure 4-13 and 4-14. Several significant features are revealed from the study. (1) Immediately after laser excitation, bleaching of the ground-state absorption in the range of 350 nm to 440 nm is obvious (see Figure 4-15a for TA spectrum and Figure 4-15c for the 390 nm trace). However, the signal is much weaker than that of Re-DA3 (compare Figure 4-15c with Figure 4-13 inset); (2) There is a broad, weak, but distinguishable absorption band in the range of 440 nm to 540 nm (Figure 4-15b), and the corresponding transient is very short-lived (see Figure 4-15d); (3) There is weak absorption in the range < 340 nm which is also very short-lived. The weak absorption band centered at 495 nm is likely due to the LLCT absorption of ReDMAPP.[68] The 495 nm kinetic trace implies that the lifetime of the LLCT state of ReDMAPP is << 10 ns.

The short timescale ns-TA study (500 ns window) of Re-DA1 in argon-degassed acetonitrile leads to interesting results illustrated in Figure 4-16. Immediately following the laser pulse a transient is observed that has a strong absorption with λ_{max} = 370 nm. Over the course of approximately 500 ns after excitation the 370 nm transient decays and a new transient grows-in that has λ_{max} = 315 nm and broad tailing absorption into the mid-visible. Studies carried out on longer timescale (500 μs window) reveal that in argon-degassed acetonitrile the 315 nm transient decays by second-order kinetics (cal. k $\approx$ 5 x 10^4 M^{-1}s^{-1}). Based on TA studies of a variety of (bpy)Re^I(CO)$_3$(L) complexes, the 370 nm transient can be unambiguously assigned to the dπ(Re) -> π*(bpy) MLCT

excited state.[69,83,84] The 315 nm transient is atrributed to the corresponding metal complex diradical for the same reasons discussed for Re-DA2 and Re-DA3. Kinetic analysis of the time-resolved TA data for Re-DA1 in argon-degassed acetonitrile indicates that the decay rate of the MLCT absorption at 370 nm is experimentally indistinguishable from the rate of increase in the absorption of the diradical at 315 nm (see Figure 4-16 inset). These two processes occur with a lifetime of τ = 63 ns, which is concordant with the lifetime of the MLCT excited state obtained by emission decay experiments (68 ns).

Figure 4-17 displays the temporal evolution of the TA spectrum of Re-DA1 in air-saturated acetonitrile. Immediately following laser excitation the MLCT state is again observed with λ_{max} = 370 nm. Concomitant to decay of the MLCT state, the absorption assigned to the corresponding metal complex diradical at 315 nm begins to grow-in; however, under air-saturated conditions, this species is quenched at a rate that is competitive with the rate at which it is formed (see Figure 4-17 inset). Kinetic analysis of the time-resolved TA data for Re-DA1 in air-saturated acetonitrile reveals that the decay rate of the MLCT absorption at 370 nm and the rate of increase in the absorption due to the diradical at 315 nm are experimentally indistinguishable and occur with a lifetime of τ = 47 ns, which is in good agreement with the MLCT emission decay lifetime of Re-DA1 in air-saturated condition. The transient at 315 nm decays according to a first-order kinetics with τ = 100 ns (k = 1 x 10^7 s^{-1}). Assuming that O_2 is the species responsible for quenching of the diradical and $[O_2] \approx 2$ mM[88] in air-saturated acetonitrile, the second-order rate constant for the reaction of the diradical with O_2 is ≈ 5 x 10^9 M^{-1} s^{-1}, which is very close to the diffusion-controlled limit.

In order to provide spectroscopic information concerning the α-piperidino-benzyl radical, a shorter timescale ns-TA experiment was performed on the bimolecular system comprised of *meso*-DA5 and Re-6 (see Scheme 3-4).
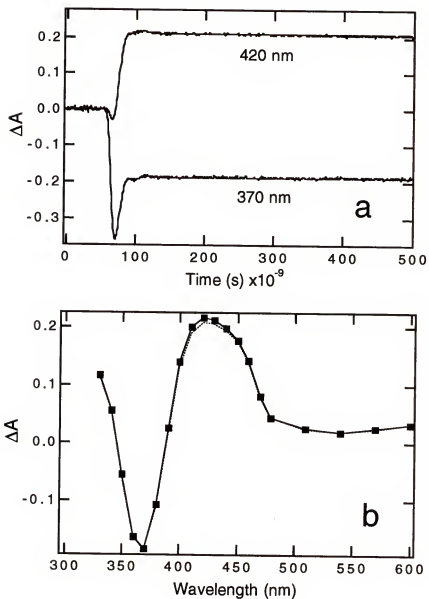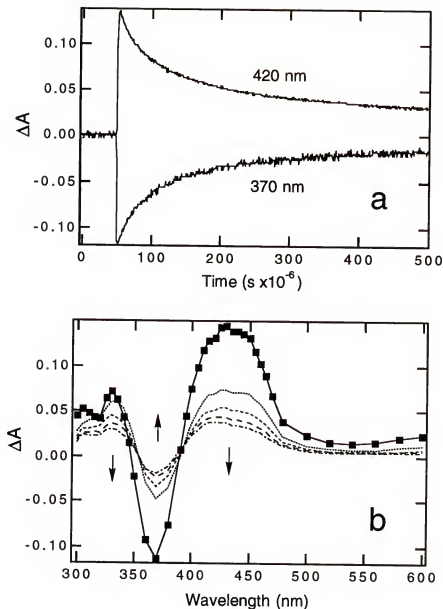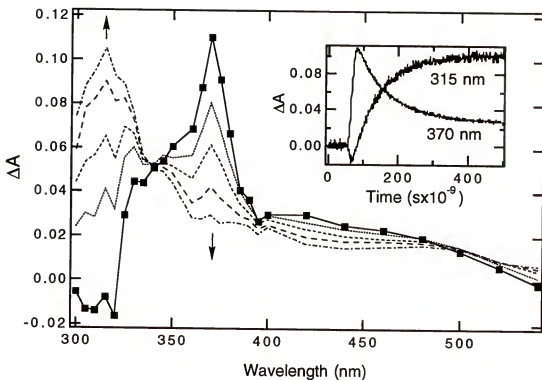
Figure 4-16

Transient absorption spectra of Re-DA1 in argon-degassed
acetonitrile solution. Conditions: λ_{exc}=355nm, laser power=5 mj/pulse.
(lines and markers) Spectrum at 30 ns delay from rising edge of laser pulse;
subsequent spectra at 70, 110, 190, 430 ns delay from rising edge of laser
pulse. INSET: Transient absorption kinetics at 315 nm and 370 nm.
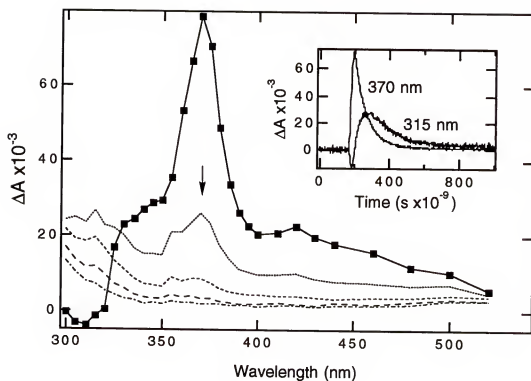
Figure 4-17

Transient absorption spectra of Re-DA1 in air-saturated acetonitrile solution. Conditions: λ_{exc}=355nm, laser power=5 mj/pulse. (lines and markers) Spectrum at 30 ns delay from rising edge of laser pulse; subsequent spectra at 110, 190, 270, 350 ns delay from rising edge of laser pulse. INSET: Transient absorption kinetics at 315 nm and 370 nm.
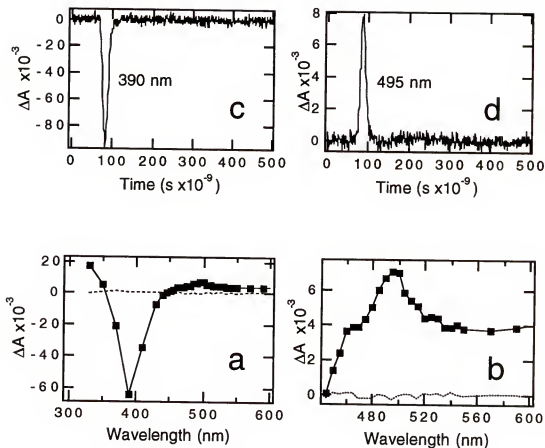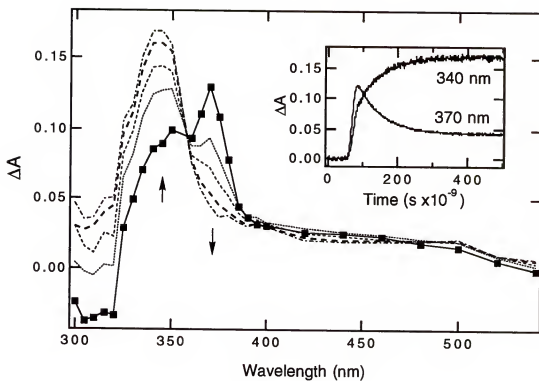
Figure 4-18

Transient absorption spectra of Re-6 and *meso*-DA5 in argon-degassed acetonitrile solution. Conditions: λ_{exc}=355nm, laser power= 5 mj/pulse. (lines and markers) Spectrum at 30 ns delay from rising edge of laser pulse; subsequent spectra at 70, 110, 190, 430 ns delay from rising edge of laser pulse. INSET: Transient absorption kinetics at 340 nm and 370 nm.
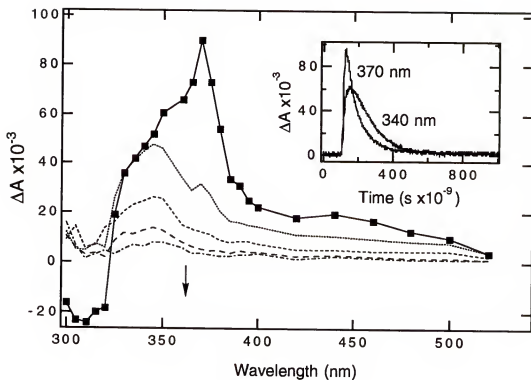
Figure 4-19

Transient absorption spectra of Re-6 and *meso*-DA5 in air-saturated
acetonitrile solution. Conditions: λ_{exc}=355nm, laser power=5 mj/pulse.
(lines and markers) Spectrum at 30 ns delay from rising edge of laser pulse;
subsequent spectra at 110, 190, 270, 350 ns delay from rising edge of laser pulse.
INSET: Transient absorption kinetics at 340 nm and 370 nm.

Figure 4-18 illustrates the temporal evolution of the TA spectrum following laser excitation of an argon-degassed acetonitrile solution of Re-6 (c = 70 μM) and *meso*-DA5 (c = 4 mM). The appearance and dynamics of this system are remarkably similar to that observed for Re-DA1 (see Figure 4-18 inset and Figure 4-16 inset), with the exception that the absorption band of α-piperidino-benzyl radical produced by C-C BF of *meso*-DA5 cation radical is centered at 340 nm. Figure 4-19 displays the temporal evolution of the TA spectrum of the same bimolecular system in air-saturated acetonitrile. Again, the appearance and dynamics of this system are remarkably similar to those observed for Re-DA1 in air-saturated acetonitrile (see Figure 4-19 inset and Figure 4-17 inset). The transient at 340 nm decays according to first-order kinetics with τ = 100 ns (k = 1×10^7 s^{-1}), which is exactly same as the decay rate of the 315 nm transient observed for Re-DA1.

Electrochemistry

The redox potentials of each of the Re-DA complexes were determined by cyclic voltammetry (see Figure 4-20 and Table 4-4). All of the Re-DA complexes display a reversible cathodic wave at $E_{1/2}$ = -1.17 V which is due to reduction of the coordinated bpy acceptor ligand.[40,41] On the other hand, all of the Re-DA complexes display an irreversible anodic wave with a peak potential of approximately + 0.9 V which is due to the oxidation of the DA ligand in the complex. Presumably the irreversibility of the anodic process is due to rapid C-C BF which occurs after anodic oxidation.[94] It is worthy to note that the peak potential of Re-DA1 is ≈ 0.9 V, which is at least 0.3 V less positive than that of Re-AA1. In addition the anodic peak of Re-DA1 is better-defined than that of Re-AA1 (see Figure 4-20).

Table 4-4   Electrochemical Potentials of Re-DA Complexes[a]

Compound	$E_{1/2}$ ($D^{+.}$ / D) / V[b]	$E_{1/2}$ (bpy / bpy$^{-.}$) / V[c]
Re-DA1	+ 0.89	-1.17
Re-DA2	+ 0.84	-1.17
Re-DA3	+ 0.85	-1.17

a: All measurements in acetonitrile/0.1 M [$(C_4H_9)_4N^+$][PF_6^-]
   relative to SCE reference electrode. Sweep rate = 200 mV/s.
b: E_p value for well-defined irreversible wave.
c: $E_{1/2}$ value for reversible wave.
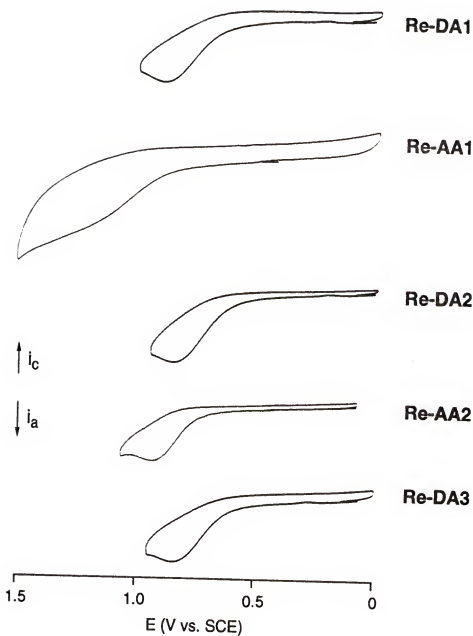
Figure 4-20
Oxidative cyclic voltammographs for DA molecules.
Conditions: in 0.1 M tetrabutylammonium hexafluorophosphate acetonitrile;
Pt disk working electrode; SCE reference, sweep rate = 200 mV / s.

<u>Discussion</u>

<u>Mechanism for the Photochemical Reactions in Re-DA Complexes</u>

Scheme 4-2 illustrates a mechanism that is consistent with the products observed in air-saturated and argon-degassed solutions, and with the spectroscopic characteristics of the intermediates observed in argon-degassed solutions by ns-TA. Briefly, photoexcitation of *e*-Re-DA produces the MLCT excited state. The MLCT state decays either by radiative or non-radiative paths to the ground state or via FET to form the LLCT state. In the LLCT state the DA ligand is oxidized and the odd electron is localized primarily on the bpy acceptor ligand. This charge-separated intermediate then either decays by BET, or via bond fragmentation (BF) across the 1,2 C-C bond in the oxidized DA ligand. The C-C BF produces an iminium ion and the corresponding metal complex diradical. Under air-saturated conditions the diradical is oxidized rapidly by O_2 to produce the corresponding imine metal complex. The imine and iminium ion hydrolyze under HPLC analysis conditions to form the corresponding free amine complex and benzaldehyde in a 1:2 ratio. By contrast, under argon-degassed conditions, the diradical is comparatively stable and decays predominantly via bimolecular ET from the diradical to the iminium ion and the following radical recombination to regenerate the starting complex with both *erythro*- and *threo*- stereochemistry at the DA donor ligand.

<u>Kinetic Model for the MLCT and LLCT States in Re-DA Complexes</u>

Equations 4-1 to 4-6 represent the kinetic model for the photochemical reactions in Re-DA complexes based on the proposed mechanism (Scheme 4-2).

Scheme 4-2
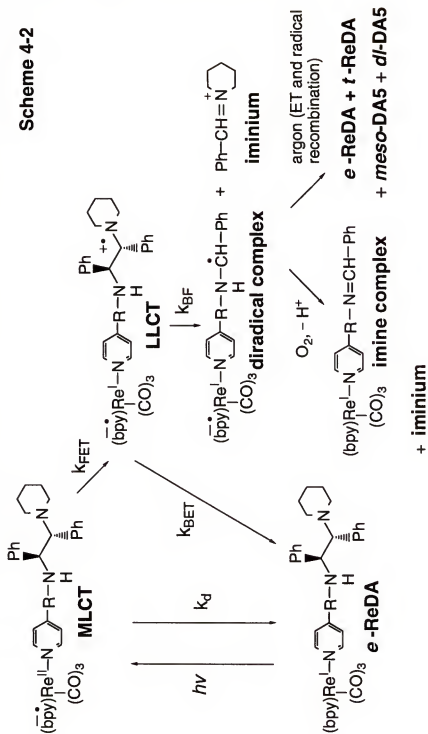
$$k_{FET} = 1/\tau_{MLCT} - 1/\tau^{\circ}_{MLCT} \qquad (4\text{-}1)$$

$$\Phi_{LLCT} = 1 - \tau_{MLCT} / \tau^{\circ}_{MLCT} \qquad (4\text{-}2)$$

$$\beta_{BF} = \Phi_{RXN} / \Phi_{LLCT} \qquad (4\text{-}3)$$

$$\beta_{BF} = k_{BF} / (k_{BF} + k_{BET}) = k_{BF} \times \tau_{LLCT} \qquad (4\text{-}4)$$

$$k_{BF} = \beta_{BF} / \tau_{LLCT} \qquad (4\text{-}5)$$

$$k_{BET} = 1/\tau_{LLCT} - k_{BF} \qquad (4\text{-}6)$$

In these equations τ_{MLCT} and τ°_{MLCT} are the emission lifetimes of the Re-DA complexes and the non-reactive donor complex, Re-6, respectively; τ_{LLCT} is the lifetime of the LLCT state of the Re-DA complexes; Φ_{LLCT} and Φ_{RXN} are the quantum efficiencies for FET and the overall BF in Re-DA complexes; β_{BF} is defined by equation 4-4; all other parameters are defined in Scheme 4-2. It is clear from this kinetic model that the experimental parameters needed to determine k_{FET}, k_{BET} and k_{BF} are τ_{MLCT}, τ°_{MLCT}, τ_{LLCT} and Φ_{RXN}. When these parameters are available, the kinetics of the MLCT and the LLCT states can be determined accurately.

An assumption that is implicit in the kinetic model is that BF is irreversible. The observation of t-Re-DA as a major photoproduct from photolysis in argon-degassed solution implies that it is possible for BF to be reversible under argon-degassed conditions. However, in air-saturated solution: (1) the only products produced by steady-state photolysis are consistent with BF being the sole photochemical pathway; (2) the TA studies of Re-DA1 indicate that the diradical complex is quenched rapidly and completely by reaction with O_2. On the basis of these results it is reasonable to believe that BF is irreversible under air-saturated

conditions. Therefore, the ensuing kinetic analysis is applicable using experimental data acquired under these conditions.

Kinetics of Photochemical Reactions in Re-DA Complexes

Based on experimental data and the kinetic model, rate constants for FET, BET and BF are determined for Re-DA2 and Re-DA3 as listed in Table 4-5. Rates of FET for these two complexes are easily calculated from the MLCT emission lifetime with Re-6 as the model complex. The key experimental parameter for calculating k_{BET} and k_{BF} for these two complexes is the corresponding τ_{LLCT}.

For Re-DA2, the LLCT state is indeed observed from ns-TA studies (Figure 4-11), but acurate lifetime determination is restricted by the temporal limit of the instrument. To the best estimation, the τ_{LLCT} of Re-DA2 is ≤ 10 ns, which implies that the sum of k_{BET} and k_{BF} for Re-DA2 is $\geq 1 \times 10^8$ s^{-1}. However, k_{BET} for Re-DA2 should be very close to k_{BET} for Re-AA2 because of the structural and driving force similarities of the two LLCT states.[83] k_{BET} for Re-AA2 has been determined accurately in Chapter 1 as 8.3×10^7 s^{-1}. Based on this value k_{BET} for Re-DA2 is estimated as $\approx 1 \times 10^8$ s^{-1}, and k_{BF} for Re-DA2 as $= 1 \times 10^8$ s^{-1} according to equation 4-4. Using these two rates the τ_{LLCT} of Re-DA2 is calculated as ~ 5 ns, which is consistent with the experimental value (≤ 10 ns).

For Re-DA3, the LLCT state is not observed from ns-TA studies (Figure 4-13). However, the kinetics for the LLCT state of Re-DA3 can still be estimated from the spectroscopic data for its non-reactive donor model (ReDMAPP), k_{BET} and k_{BF} of Re-DA2, and the overall quantum yield of the photochemical reaction for Re-DA3. The LLCT state of ReDMAPP is indeed observed from ns-TA studies (Figure 4-15b and 15d). Again, accurate lifetime determination is restricted by the temporal limit of the instrument. Kinetic analysis of the 495 nm trace of

Table 4-5   Kinetics of the Photofragmentation of Re-DA Complexes

Complex	Re-DA1	Re-DA2	Re-DA3
$\Delta G°_{FET}$ (eV)	-0.33	-0.38	-0.37
k_{FET} (s^{-1})	1.0×10^7	2.0×10^9	1.0×10^9
Φ_{LLCT} (air)	0.52	1.0	1.0
Φ_{RXN} (air)	0.21	0.54	0.43
$\Delta G°_{BET}$ (eV)	-2.06	-2.01	-2.02
k_{BET} (s^{-1})	$\geq 1.5 \times 10^8$	1.0×10^8	$2\sim3 \times 10^8$
k_{BF} (s^{-1})	$\geq 1.0 \times 10^8$	1.0×10^8	$1\sim2 \times 10^8$

Scheme 4-3
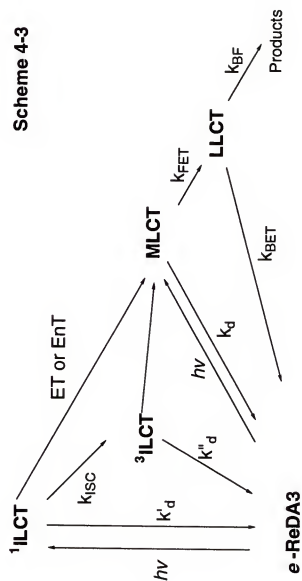
ReDMAPP indicates that τ_{LLCT} of ReDMAPP is much less than 10 ns. The driving force for BET from the LLCT state of Re-DA3 is similar to that of Re-DA2, but the electronic coupling between the two redox sites in Re-DA3 is expected to be larger than in Re-DA2. Therefore, k_{BET} in Re-DA3 is expected to be faster, but not much, than that of Re-DA2. On the other hand, k_{BF} of Re-DA3 is expected to be in the same order as that of Re-DA2 based on the thermodynamics of these two DA cation radicals which will be discussed below. Based on these arguments, we estimated that for Re-DA3, $k_{BET} \approx (2\sim3) \times 10^8$ s^{-1}, $k_{BF} \approx (1\sim2) \times 10^8$ s^{-1}, thus $\tau_{LLCT} \approx 2\sim3$ ns.[68]

Another issue to be addressed concerning Re-DA3 is that the MLCT band of this complex is overlapped by the strong ILCT band of the coordinated DA3 ligand (see Figure 4-2). According to the absorption spectrum, the extinction coefficient of the ILCT band is approximately 10 times greater than that of the MLCT band. Therefore at least 90% of the input 366 nm or 355 nm light which are used for steady-state photolysis and ns-TA studies, respectively, is absorbed by the DA3 ligand to produce the ^{1}ILCT state. However, the overall quantum yield of the photochemical reaction of Re-DA3 is comparable with that of Re-DA2 in which the ILCT absorption is negligible. A mechanism is proposed to address this issue as shown in Scheme 4-3. Briefly, initial photoexcitation generates 90% ^{1}ILCT state and 10% MLCT state; the major decay pathway for ^{1}ILCT state is via ET or energy transfer to produce ^{3}MLCT state. This mechanism is proposed based on the following arguments: (1) the overall quantum yield of the photochemical reaction of Re-DA3 is comparable with that of Re-DA2 in which the ILCT absorption is negligible; (2) the overall quantum yield of the photochemical reaction of Re-DA3 is 4 times higher than that of DA3 ligand which indicates that at least 75% of the BF of Re-DA3 occurs from some other excited state than the ^{1}ILCT state. A reasonable assumption is that the other

excited state is the triplet LLCT state which is produced via FET from the MLCT state; (3) the quantum efficiency for intersystem crossing from ^{1}ILCT to ^{3}ILCT is expected to be low for DA3.[87]

For Re-DA1, k_{FET} in argon-degassed solution is calculated to be 1.6×10^7 s^{-1} using the MLCT emission data with Re-6 as the model complex. This value is 70 times higher than that of Re-AA1 (2.2×10^5 s^{-1} from Chapter 1), which can be explained by the fact that the FET process in Re-DA1 is exothermic by ~ 0.3 eV, whereas ΔG_{FET} for Re-AA1 is ~ 0, or even positive. On the other hand, k_{FET} for Re-DA1 is 120 and 60 times lower than that for Re-DA2 and Re-DA3, respectively, although ΔG_{FET} for these three complexes are very close, ≈ -0.35 eV. For Re-DA2 and Re-DA3 it is reasonable to believe that the donor is the aniline nitrogen lone pair within the corresponding DA ligand because of the shorter distance and larger electronic coupling between the orbital occupied by the aniline nitrogen lone pair and the half-vacant dπ orbital of Re^{II} within the MLCT state. The experimental data support this argument: τ_{MLCT} of Re-AA2 and τ_{MLCT} of Re-DA2 are same (≈ 0.5 ns), which indicates that they have the same k_{FET}. The big differences in ΔG_{FET} and k_{FET} for Re-DA1 and Re-AA1 suggests that for Re-DA1 the donor is actually the piperidino nitrogen lone pair. If this argument is true, it is then reasonable to believe that for Re-DA1 the electronic coupling between the orbital occupied by the piperidino nitrogen lone pair and the half-vacant dπ orbital of Re^{II} within the MLCT state is weaker compared with the cases of Re-DA2 and Re-DA3. This may explain why k_{FET} is much slower for Re-DA1 than that for Re-DA2 and Re-DA3, even though ΔG_{FET} values of these three complexes are comparable.

The ns-TA studies of Re-DA1 reveal that within the limits of experimental error the decay rate of the MLCT excited state corresponds exactly to the appearance rate of the diradical complex (see Figure 4-16 inset). This implies

that the rate determining step for both MLCT decay and the diradical complex appearance is the same: formation of the LLCT state by FET. While it is clear that this situation arises because $k_{BF} \gg k_{FET}$, it is of interest to know just how much larger k_{BF} is than k_{FET} in order for the MLCT decay and the diradical complex appearance rates to be indistinguishable. In order to explore this question a kinetic simulation was carried out for the following sequential reaction:

$$\text{MLCT} \xrightarrow{k_{FET}} \text{LLCT} \xrightarrow{k_{BF}} \text{diradical complex} \qquad (4\text{-}7)$$
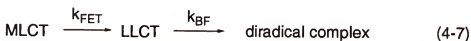
The simulation reveals that when $k_{BF} \geq 10 \times k_{FET}$, the rise time of the diradical complex would be experimentally indistinguishable from the MLCT decay. Based on this analysis a reasonable lower limit for k_{BF} of Re-DA1 is $\geq 1.0 \times 10^8$ s^{-1} ($k_{FET} = 1.0 \times 10^7$ s^{-1} in air-saturated solution is used here) , and a lower limit for k_{BET} of Re-DA1 is $\geq 1.5 \times 10^8$ s^{-1}. Interestingly, the estimated lower limit for k_{BET} in Re-DA1 is comparable to k_{BET} in Re-DA2. Note that BET is exothermic by ~ 2.0 eV in both complexes. This implies that the estimated limits for both k_{BET} and k_{BF} in Re-DA1 are, in fact, close to the actual values. Another kinetic simulation on Re-DA1 using the rates for FET, BET and BF listed in Table 4-5 reveals that under these conditions the concentration of the LLCT state in Re-DA1 never exceeds 2 % of the initial concentration of the MLCT state. As a result it would be impossible to directly detect the LLCT by TA spectroscopy in this system.

The diradical complex produced via BF from the LLCT state of Re-DA1 has an exceedingly strong absorption in the near-UV with $\lambda_{max} \approx 315$ nm. The α-amino benzyl radical, R-NH-CH(Ph)$\cdot$, which is present in the diradical complex, is the chromophore responsible for this strong absorption. By using the available quantitative photophysical and photochemical yield information the molar absorptivity of this chromophore is estimated to be $\approx 40,000$ M^{-1}cm^{-1} at 315

nm.[95] This extinction coefficient is much greater than that of the unsubstituted benzyl radical ($\varepsilon_{320 \text{ nm}} \approx 8{,}800$ M^{-1}cm^{-1}).[96] The enhanced absorptivity of the R-NH-CH(Ph)• chromophore may be attributed to a substantial auxochromic effect of the α-alkyl amine substitute.

Thermodynamics and Rates of BF in Re-AA and Re-DA Complexes

With the BF rates in Re-AA and Re-DA complexes available, it is of interest to correlate the BF rates with the C-C bond strengths in the 1,2-AA and 1,2-DA cation radicals. As discussed in Chapter 1, the bond dissociation energy (BDE) of a donor cation radical is defined by equation 4-8 (see Figure 1-7).[97,98,99]

$$\text{BDE (AB}^{+\bullet}) = \text{BDE (AB)} + F\,[E^\circ\,(B^+/\,B\bullet) - E^\circ\,(AB^{+\bullet}/\,AB)] \qquad (4\text{-}8)$$

The manner of the C-C BF within the donor cation radicals studied in this work, which has been unambiguously determined from ns-TA studies on those systems and on other related systems,[78] is summarized in equation 4-9 (for Re-AA complexes studied in Chapter 2), equation 4-10 (for Re-DA complexes studied in Chapter 4).

$$(4\text{-}9)$$

$$(4\text{-}10)$$

Figure 4-21

Bond dissociation energy of 1,2-AA and 1,2-DA cation radicals.
a: Estimates by the method descibed in text.

In order to estimate the BDE for AA and DA cation radicals according to equation 4-8, the BDE of the corresponding neutral compounds and related redox potentials are required. The redox potentials needed for these estimates are available from experimental data and from the literature, and in some cases the BDE of the corresponding neutral compounds can be estimated as shown in Figure 4-21. For example, compounds 5 and 6 in Figure 4-21 serve as good models for AA1 and DA1, respectively, while compounds 3 and 4 are the analogous of 5 and 6, but without vicinal phenyl substituents. The BDE for 4 is reported to be 11 kcal/mole lower than that of 3.[105] The steric and resonance effects of 1,2 diphenyl substitution reduce the center C-C BDE by ~ 22 kcal/mole in 2 compared with 1.[103,104] Under the assumption that the steric and resonance effects of the 1,2-diphenyl substitution on the BDE of 1,2-AA and 1,2-DA molecules are additive, the BDE for 5 and 6 are estimated as 49 and 38 kcal/mole, respectively. The BDE for $5^{+\cdot}$ and $6^{+\cdot}$ are estimated as +2 and -5 kcal/mole, respectively. This estimation unequivocally establishes that the BF for 1,2-DA cation radical $6^{+\cdot}$ will be thermodynamically favored over that 1,2-AA cation radical $5^{+\cdot}$. The BF rates for Re-AA1 and Re-DA1 are determined as $\approx 4 \times 10^6$ s^{-1} and $\geq 1 \times 10^8$ s^{-1} from this study, which is qualitatively consistent with the estimations of BDE for $5^{+\cdot}$ and $6^{+\cdot}$.

The BDE of AA2 and DA2 or analogous compounds cannot be estimated because of lack of a key piece of information, the heat of formation (ΔH_f°) of $\cdot CH_2$-NH-Ph, or for that matter for any $\cdot CR_1R_2$-NH-Ph. Note that the oxidation potential of Re-AA2 is much less positive (≥ 0.3 V) than Re-AA1. The fact that the BF rate of Re-AA2 is approximately 10 times slower than Re-AA1 may reflect that the BDE for AA2$^{+\cdot}$ is greater than for AA1$^{+\cdot}$. On the other hand, the oxidation potential of neutral Re-DA2 is comparable to that of Re-AA2. Assuming that the anilino group has the same effects on the BDE of DA2 and AA2, then the BDE of

$DA2^{+\cdot}$ will be expected to be much smaller than that of $AA2^{+\cdot}$, the difference could be similar to the difference between the BDE for $5^{+\cdot}$ and $6^{+\cdot}$ (11 kcal/mole). The BF rates for Re-DA2 and Re-AA2 are determined as 1×10^8 s^{-1} and 5×10^5 s^{-1} from this study, which strongly supports this estimation. The BF rate for Re-DA3 is comparable to that for Re-DA2, which may indicate a comparable BDE for $DA3^{+\cdot}$ in Re-DA3.

BF in 1,2-DA Ligands and Re-DA Complexes

The BF rates for organic ligands themselves (e-DA3, e-DA4 and t-DA4) are estimated to be in the order of $\geq 10^8$ s^{-1} in Chapter 3 without any further speculation. The fact that the overall quantum efficiency of the photochemical reaction for e-DA3 is approximately 3 times lower than that for Re-DA3 can be explained by the faster BET from the singlet CS state in e-DA3 than BET from the triplet LLCT in Re-DA3.

For Re-DA complexes there are no isomerization products observed in air-saturated acetonitrile solutions, whereas for DA ligands the isomerization does occur in air-saturated acetonitrile solutions. A possible explaination is that for Re-DA complexes the ET from reduced bpy to the iminium ion (see Scheme 4-2) is only exothermic by ~ 0.2 eV, as a result the rate for ET might be lower than the rate for the cage-escape. For DA ligands the initial BF products are caged radical pairs. The rate for recombination of the caged radical pairs might be comparable to the rate for cage-escape.[92,93]

Conclusion

The study in this chapter demonstrates that 1,2-diamines can effectively quench the luminescence of Re-based MLCT excited state via intramolecular PET, and the subsequent rapid C-C BF ($\geq 10^8$ s^{-1}) in all of the three 1,2-DA

cation radicals can effectively probe BET from the corresponding LLCT states. For every Re-DA complex studied the kinetics of the corresponding LLCT state has been well-characterized.

The studies on Re-DA1 demonstrate that by using a donor which undergoes a very rapid reaction triggered by FET, it is possible to obtain information concerning the dynamics of the charge-separated state, even when it would not be possible to directly interrogate the intermediate charge-separated state (such as the LLCT state) by TA spectroscopy. Owing to the occurrence of the rapid BF reaction, the fact that PET indeed occurs is clearly evident by the prompt appearance of the BF product, the corresponding diradical complex.

CHAPTER 5

EXPERIMENTAL

Materials and General Synthetic

Solvents and chemicals used for synthesis were of reagent grade and used without purification unless noted. Silica gel (Merck, 230 - 400 mesh) and neutral alumina (Fisher, Brockman grade III) were used for chromatography. NMR spectra were run on either GE QE-300 MHz or Varian VXR-300 MHz spectrophotometers. The metal complexes $(bpy)Re^I(CO)_3Cl$ and $[(bpy)Re^I(CO)_3(4\text{-}benzylpyridine)][PF_6]$ (Re-6) were synthesized as previously described.[40,106] All Re(I) complexes were isolated as PF_6^- salts.

Synthesis of Compounds Studied in Chapter 2

erythro-2-[N-4-(Pyridyl)methyl]amino-1,2-diphenylethanol (AA1)

4-(Aminomethyl)pyridine (4.1 ml, 4.37 g, 40 mmol) and *trans*-stilbene oxide (1.57 g, 8 mmol) were heated at 100° C under a blanket of Argon . The reaction was monitored by TLC (silica, MeOH-CHCl₃ 5:95 v:v); heating was discontinued after 6.5 hours when the high R_f *trans*-stilbene spot had disappeared completely. The crude product was purified by repeated chromatography (silica, CH₃CN-CH₂Cl₂ 40:60 v:v). Pure AA1 was obtained as white crystals, yield 600 mg (25%). Analytical Data: TLC (silica, CH₃CN-CH₂Cl₂ 40:60 v:v) R_f = 0.35. ¹H NMR (300 MHz, CDCl₃) δ 3.51 (d, 1H, diastereotopic CH₂), 3.69 (d, 1H, diastereotopic CH₂), 3.87 (d, 1H, benzylic), 4.83 (d, 1H,

benzylic), 7.07 (d, 2H, pyridyl), 7.18-7.37 (m, 10 H, phenyls), 8.43 (d, 2H, pyridyl). ^{13}C NMR (75 MHz, CDCl$_3$) δ 49.8 (adjacent to pyridyl), 68.1 (benzylic), 77.3 (benzylic), 122.8, 126.9, 127.9, 127.9, 128.2, 128.4 (2C), 139.0, 140.6, 149.1, 149.6 (all aromatic). The molecular weight found: 305.1739 (M+H, HRMS); calc'd for C$_{20}$H$_{21}$N$_2$O is 305.1654.

4-(N-Benzyl)aminomethylpyridine (1)

4-(Aminomethyl)pyridine (5 ml, 5.32 g, 49 mmol) was placed into a 50 ml round-bottom flask which was then purged with argon. The flask was heated to 70° C and then α-bromotoluene (1 ml, 1.44 g, 8.4 mmol) was added dropwise over a period of 5 minutes. The resulting mixture was stirred and heated for 2 hours. The crude product was purified by repeated chromatography (silica, MeOH-CHCl$_3$ 7:93 v:v) Analytica Data: TLC (silica, MeOH-CHCl$_3$ 7:93 v:v) R$_f$ = 0.30. ^{1}H NMR (300 MHz, CDCl$_3$) δ 2.05 (broad, NH), 3.81 (s, 2H, CH$_2$), 3.83 (s, 2H, CH$_2$), 7.28 (d, 2H, pyridyl), 7.35 (m, 5H, phenyl), 8.57 (d, 2H, pyridyl). The molecular weight found: 198.115 (HRMS); calc'd for C$_{13}$H$_{14}$N$_2$ is 198.1155.

erythro-1,2-Diphenyl-3-(4-pyridyl)-1-propanol (2)

A solution of phenyl lithium in cyclohexane (1.44 M, 7 ml, 10 mmol) was added to a solution of 4-picoline (1.0 g, 10 mmol) in 10 ml of ether that was contained in an argon-purged schlenk bottle. The resulting solution was stirred at room temperature for 1.5 hours and then it was cooled to -70° C in a dry ice/isopropanol bath. Then *trans*-stilbene oxide (1.5 g, 7.7 mmol) in 15 ml of ether was added to the cold solution. After stirring for 30 min the reaction mixture was warmed to 20° C and then gently refluxed for an additional 30 min. The reaction mixture was poured into 20 ml of 1 M HCl and then the mixture was made basic by addition of sufficient Na$_2$CO$_3$. The mixture was extracted 3 times

with 30 ml portions of ether, the ether layers were combined, dried, and the solvent was evaporated. The crude product was obtained as 3.5 g of a yellow oil which was purified by repeated chromatography (silica, MeOH-CHCl$_3$ 5:95 v:v) Pure 2 was obtained as a white crystalline solid, yield 700 mg (32%). Analytical Data: TLC (silica, MeOH-CHCl$_3$ 5:95 v:v) R$_f$ = 0.30. ^{1}H NMR (300 MHz, CDCl$_3$) δ 2.12 (broad, 1H, OH), 2.78-2.93 (m, 2H, diastereotopic CH$_2$), 3.18 (m, 1H, benzylic), 4.87 (d, 1H, benzylic), 6.79 (d, 2H, pyridyl), 7.12 (m, 2H, phenyls), 7.20-7.40 (m, 8H, phenyls), 8.29 (d, 2H, pyridyl). ^{13}C NMR (75 MHz, CDCl$_3$) δ 38.0 (benzylic), 55.3 (benzylic), 77.6 (benzylic), 124.3, 126.8, 127.2, 128.0, 128, 128.5, 128.9, 139.3, 142.1, 149.1, 149.3 (all aromatic). The molecular weight found: 290.1544 (M+H, HRMS); calc'd for C$_{20}$H$_{20}$NO is 290.1544.

erythro-N-(1,2-Diphenyl-2-hydroxyethyl)-p-[4-(pyridyl)methyl]aniline (AA2)

(a) p-[4-(Pyridyl)methyl]aniline [4-(Pyridyl)methyl]nitrobenzene (6.3 g, 30 mmol), and Fe powder (18.5 g, 33 mmol), were added to a mixture of 24 ml of absolute ethanol, 6 ml of H$_2$O and 0.3 ml of concentrated HCl. The mixture was heated at reflux for 2 hrs under a stream of N$_2$. The reaction mixture was cooled, the Fe powder was filtered out, and the residue was washed with excess hot ethanol. The combined filtrate was evaporated leaving 5.1 g of a light tan product. The product was purified by chromatography on silica gel using 30 CH$_3$CN/CH$_2$Cl$_2$ as eluant.

(b) AA2 This compound was prepared by a variation of a literature method for preparation of α-amino alcohols.[107] p-[4-(Pyridyl)methyl]aniline (370 mg, 2.0 mmol) was dissolved in 15 ml of CH$_2$Cl$_2$ in a 100 ml round bottom flask. The solution was purged with Ar and cooled to 0° C. Then a solution of AlMe$_3$ in CH$_2$Cl$_2$ (1.4 ml, 2.5 mmol) was added slowly via a syringe. The resulting mixture was kept cold and stirred for 30 min. At this time a solution of *trans*-stilbene

oxide (328 mg, 1.67 mmol) dissolved in 3 ml of CH_2Cl_2 was added via a syringe. The reaction mixture was allowed to come to room temperature and was stirred for 4 hours. After this time 6 ml of a 6 M $NaOH_{(aq)}$ solution was added and the mixture was stirred for 1 hour. An additional 40 ml of CH_2Cl_2 was added and the organic layer was separated and dried over Na_2SO_4. The CH_2Cl_2 was evaporated and the crude product was purified by repeated chromatography: first on silica (CH_3CN-CH_2Cl_2 35:65 v:v), and then on alumina (CH_3CN-cyclohexane-CH_2Cl_2 5:5:90 v:v:v). Pure AA2 was obtained as an off-white powder, yield 260 mg (41%). Analytical Data: TLC (silica gel, 35 CH_3CN/CH_2Cl_2 eluant) R_f = 0.35. ^1H NMR (300 MHz, $CDCl_3$) δ 3.70 (s, 2H, benzylic CH_2), 4.55 (d, 1H, CH), 4.98 (d, 1H, CH), 6.39 (d, 2H, aniline), 6.77 (d, 2H, aniline), 6.95 (d, 2H, pyridyl), 7.00 - 7.10 (m, 4H, phenyl), 7.13 - 7.22 (m 6H, phenyl), 8.30 (d, 2H, pyridyl). ^{13}C NMR ($CDCl_3$, 75 MHz) δ 40.2 (benzylic), 63.8 (CH), 77.0 (CH), 114.1, 124.1 (2C), 126.6, 127.4, 127.7, 127.8, 128.0, 128.1 (2C), 129.6, 138.7, 140.4, 145.7, 149.3, 151.2 (all aromatic). The molecular weight found: 381.2015 (M+H, HRMS); calc'd for $C_{26}H_{25}N_2O$ is 381.1967.

p-[4-(Pyridyl)methyl]-N,N-dimethylaniline (5)

p-[4-(Pyridyl)methyl]aniline (see above for synthesis) (1.5 g, 8.1 mmol), formaldehyde (1.9 ml, 37% aqueous), and formic acid (1.9 g, 97% solution) were combined and heated over a steam bath for 1 hour. After this time the reaction was cooled whereupon 1.4 ml of concentrated HCl was added. The solution was concentrated under vacuum and the remaining viscous liquid was added to 20 ml of H_2O. The liquid was basified by addition of 25% $NaOH_{(aq)}$ at which point a sticky solid separated. The solid was isolated by extracting the aqueous suspension with several portions of $CHCl_3$. The $CHCl_3$ layer was dried and concentrated under reduced pressure. The crude product was purified by

chromatography (silica, $CH_3CN-CH_2Cl_2$ 15:85 v:v). Pure 5 was obtained as a yellow crystalline solid, yield after purification: 150 mg (10%). Analytical Data: TLC (silica, $CH_3CN-CH_2Cl_2$ 15:85 v:v) R_f = 0.25. ^{1}H NMR ($CDCl_3$, 300 MHz), δ 2.91 (s, 6H, 2 x CH_3), 3.85 (s, 2H, benzylic), 6.68 (d, 2H, aniline), 7.03 (d, 2H, aniline), 7.10 (d, 2H, pyridyl), 8.48 (d, 2H, pyridyl).

<u>General Procedure for Preparation of Re Complexes</u>

In a typical preparation, (bpy)Re^I(CO)$_3$Cl (0.25 mmol), AgPF$_6$ (0.5 mmol), and the substituted pyridine ligand (AA1, AA2, 1, 2, and 5, 0.5 mmol) were dissolved in 3 ml of DMF. The solution was purged with argon and then heated to 75° C. The reactions were monitored by TLC (silica, MeOH-CHCl$_3$ 5:95 v:v) and heating was discontinued when the yellow fluorescent spot due to the product was not increasing any longer; typical time required was 2 - 3 hours. After cooling, the solution was filtered through a medium porosity fritted filter and the DMF was evaporated under reduced pressure. The products were purified by chromatography (alumina, $CH_3CN-CH_2Cl_2$ 10:90 v:v to $CH_3CN-CH_2Cl_2$ 50:50 v:v). Typical yield after purification was 40 - 50%.

<u>Re-AA1</u> Analytical Data: ^{1}H NMR (300 MHz, CD$_3$CN) δ 3.32 (broad, 1H, NH), 3.41 (d, 1H, diastereotopic CH$_2$), 3.47 (d, 1H, diastereotopic CH$_2$), 3.62 (d, 1H, benzylic), 4.72 (d, 1H, benzylic), 7.01 (d, 2H, pyridyl), 7.05-7.28 (m, 10H, phenyls), 7.80 (m, 2H, bpy), 8.00 (d, 2H, pyridyl), 8.28 (tt, 2H, bpy), 8.39 (d, 2H, bpy), 9.21 (d, 2H, bpy). ^{13}C NMR (75 MHz, CD$_3$CN) δ 48.6 (adjacent to pyridyl), 67.7 (benzylic), 76.3 (benzylic), 124.3, 125.1, 126.6, 126.9, 127.0, 127.5 (2C), 128.3, 128.5, 139.8, 140.8, 142.0, 150.8, 153.5, 155.2, 155.4 (all aromatic).

<u>Re-1</u> Analytical Data: ^{1}H NMR (300 MHz, CD$_3$CN) δ 3.70 (s, 2H, CH$_2$), 3.80 (s, 2H, CH$_2$), 7.33 (m, 7H, phenyl and pyridyl), 7.90 (t, 2H, bpy), 8.22 (d, 2H, pyridyl), 8.38 (t, 2H, bpy), 8.49 (d, 2H, bpy), 9.32 (d, 2H, bpy).

<u>Re-2</u> Analytical Data: ^{1}H NMR (300 MHz, CD$_3$CN) δ 2.83 (m, 2H, diastereotopic CH$_2$), 3.08 (m, 1H, benzylic), 3.25 (d, 1H, OH), 4.80 (dd, 1H, benzylic), 6.83 (d, 2H, pyridyl), 6.95 (m, 2H, phenyls), 7.05-7.25 (m, 8H, phenyls), 7.75 (m, 2H, bpy), 7.85 (d, 2H, pyridyl), 8.20-8.35 (m, 4H, bpy), 9.15 (dd, 2H, bpy). ^{13}C NMR (75 MHz, CD$_3$CN) δ 37.5 (adjacent to pyridyl), 53.4 (benzylic), 76.2 (benzylic), 124.2, 126.2, 126.3, 126.8, 127.0, 127.4, 127.6, 128.4, 128.7, 139.6, 140.8, 143.0, 150.5, 153.4, 154.6, 155.2 (all aromatic).

<u>Re-AA2</u> Analytical Data: ^{1}H NMR (CD$_3$CN, 300 MHz), δ 4.54 (dd, 1H, CH), 4.96 (broad d, 1H, NH), 5.22 (d, 1H, CH), 6.42 (d, 2H, aniline), 6.70 (d, 2H, aniline), 6.99 (d, 2H, pyridyl), 7.15 - 7.25 (m, 10 H, phenyls), 7.74 (t, 2H, bpy), 8.01 (d, 2H, pyridyl), 8.23 (t, 2H, bpy), 8.34 (d, 2H, bpy), 9.15 (d, 2H, bpy). ^{13}C NMR (CD$_3$CN, 75 MHz), δ 39.0 (benzylic), 62.8 (benzylic), 75.8 (benzylic), 113.3, 117.0, 124.4, 125.6, 126.2, 126.4, 126.6, 126.9, 127.3, 127.4, 128.1, 128.4, 129.2, 139.9, 140.8, 142.0, 146.0, 151.1, 153.4, 155.4, 156.0 (all aromatic).

<u>Re-5</u> Analytical Data: ^{1}H NMR (CD$_3$CN, 300 MHz), δ 2.81 (s, 6H, 2 x CH$_3$), 3.76 (s, 2H, benzylic), 6.62 (d, 2H, aniline), 6.92 (d, 2H, aniline), 7.10 (d, 2H, pyridyl), 7.78 (t, 2H, bpy), 8.09 (d, 2H, bpy), 8.27 (t, 2H, bpy), 8.37 (d, 2H, pyridyl), 9.19 (d, 2H, bpy). ^{13}C NMR (CD$_3$CN, 75 MHz) δ 40.3 (aliphatic), 40.7 (aliphatic), 113.8, 118.3, 125.6, 126.3, 127.4, 129.8, 130.6, 142.1, 152.5, 154.7, 156.7, 157.4 (all aromatic).

Synthesis of Compounds Studied in Chapter 3

erythro-2-Piperidino-1,2-diphenylethanol (*e*-AA)

A mixture of *trans*-stilbene oxide (2.94 g, 15 mmole), piperidine (12 ml, 10.3 g, 120 mmole) and *p*-Toluene sulfonic acid (0.2 g, 1 mmole, as catalyst) was heated to reflux under a blanket of nitrogen. The reaction was monitored by TLC (silica, ethyl acetate-hexane 20:80 v:v). The reaction was stopped after 11 h refluxing when the *trans*-stilbene oxide spot (R_f =0.8) had disappeared completely. The unreacted piperidine was removed by vacuum roto-vap, and a white solid was obtained. The solid was dissolved in 50 ml ethyl acetate and washed with NaOH solution (1 M) and then with H_2O. After drying with $MgSO_4$, the solvent was removed. Pure *erythro* AA was obtained as an off-white crystalline solid without further purification, yield 3.87 g (92%). Analytical data: TLC (silica, ethyl acetate-hexane 20:80 v:v) R_f = 0.3 - 0.4. ^{1}H NMR (300 MHz, CDCl₃) δ 1.5 (m, 2H, pip CH₂), 1.6 (m, 4H, pip CH₂), 2.5 (m, 2H, pip CH₂), 2.6 (m, 2H, pip CH₂), 3.39 (d, J = 4.8 Hz, 1H, benzylic), 3.53 (br,1H, OH), 5.38 (d, J = 4.8 Hz, 1H, benzylic), 7.0 - 7.2 (m, 10H, phenyl); ^{13}C NMR (75 MHz, CDCl₃) δ 24.6, 26.3, 52.5 (all pip), 71.6 (benzylic), 76.5 (benzylic), 126.2, 126.6, 127.0, 127.4 (2C), 129.5, 136.7, 141.4 (all phenyls).

threo-2-Piperidino-1,2-diphenylethanol (*t*-AA)

The synthesis of this compound followed the same procedure as that of *erythro*-AA in 90% yield except that *cis*-stilbene oxide was used as the starting epoxide. Analytical data: TLC (silica, ethyl acetate-hexane 10:90 v:v) R_f = 0.3 - 0.5. ^{1}H NMR (300 MHz, CDCl₃) δ 1.4 (m, 2H, pip CH₂), 1.7 (m, 4H, pip CH₂), 2.3 (m, 2H, pip CH₂), 2.7 (m, 2H, pip CH₂), 3.568 (d, J = 10.5 Hz, 1H, benzylic), 5.074 (d, J = 10.5 Hz, 1H, benzylic), 5.4 (br,1H, OH), 7.1 - 7.3 (m, 10H, phenyl);

^{13}C NMR (75 MHz, CDCl$_3$) δ 24.3 (pip), 26.6 (pip), 50.3 (broad, pip), 70.4 (benzylic), 77.2 (benzylic), 127.3 (2C), 127.6, 127.7, 127.9, 129.9, 133.5, 141.8 (all phenyls).

4-(p-Aminophenyl)-pyridine (APP)

(a) 4-(p-Nitrophenyl)-pyridine[108] A mixture of 4-Phenylpyridine (3.1 g, 20 mmole), 10 ml concentrated H$_2$SO$_4$ and 1 ml HNO$_3$ (fuming, red) was heated to 100°C under a blanket of nitrogen for 2 h. After cooling to room temperature, the resulting mixture was poured into 100 g ice to yield a yellow transparant solution. NH$_4$OH (5 M) was added to the solution and at pH=6, a copious amount of yellow precipitate formed. ^{1}H NMR (300 MHz, DMSO) spectrum of this solid shows that it is a mixture of 4-(p-, m-, o- Nitrophenyl)-pyridine. The mixture of isomers was dissolved in 25 ml of boiling HCl (5 M) in an erlenmeyer flask, and the solution was cooled to room temperature. The solution was then placed on an ice bath, and a white-yellowish crystalline solid formed quickly. This recrystalization procedure was repeated an additional two times. A white crystalline solid was obtained. After the solid was dissolved in HCl (5M) and upon heating, NH$_4$OH (5 M) was added to produce a yellow crystalline solid, yield 1.36 g of 4-(p-Nitrophenyl)-pyridine (34%). Analytical data: ^{1}H NMR (300 MHz, DMSO) δ 7.80 (d, J = 6.0 Hz, 2H, pyridyl), 8.07 (d, J = 8.7 Hz, 2H, phenyl), 8.34 (d, J = 8.7 Hz, 2H, phenyl), 8.70 (d, J = 6.0 Hz, 2H, pyridyl); ^{13}C NMR (75 MHz, DMSO) δ 122.0, 124.5, 128.6, 143.9, 145.1, 148.2, 150.9.

(b) APP A mixture of 4-(p-Nitrophenyl)-pyridine (435 mg, 2.1 mmole), iron powder (hydrogen reduced, 325 mesh, 2.4 g, 42 mmole), 0.2 ml HCl (5 M), 40 ml EtOH and 2 ml H$_2$O was heated to reflux under a blanket of nitrogen for 2 h. The resulting mixture was filtered through a large diameter short column (silica, CH$_3$CN-CH$_2$Cl$_2$ 50:50 v:v). The collection was monitored by TLC. After removing

the solvent, a yellowish crystalline solid was obtained, yield 330 mg (92%). Analytical data: ^{1}H NMR (300 MHz, DMSO) δ 5.52 (br, 2H, NH$_2$), 6.68 (d, J = 8.7 Hz, 2H, phenyl), 7.54 (d, J = 8.7 Hz, 2H, phenyl), 7.56 (d, J = 6.0 Hz, 2H, pyridyl), 8.49 (d, J = 6.0 Hz, 2H, pyridyl); ^{13}C NMR (75 MHz, DMSO) δ 114.5, 119.8, 121.5, 127.8, 147.6, 150.3, 150.6.

<u>General Procedure for Preparation of 1,2-Diamine Ligands</u>

erythro-1-N-(4-Cyanophenyl)amino-2-piperidino-1,2-diphenylethane (*e*-DA4)[55] A mixture of *e*-AA (562 mg, 2.0 mmole), 10 ml of freshly distilled CH$_2$Cl$_2$ and triethylamine (0.8 ml, 6.0 mmole) was placed in a 100 ml three-necked round bottom flask, and purged with nitrogen for 30 minutes. At the same time the temperature was adjusted to -20°C with a dry ice-isopropanol bath. A solution of methanesulfonyl chloride (0.155 ml, 2.0 mmole) dissoved in 2 ml of freshly distilled CH$_2$Cl$_2$ was added dropwise by using a syringe. The resulting mixture was kept stirring at low temperature (<10°C) for 1 h. ABN (4-aminobenzonitrile, 236 mg, 2.0 mmole) was dissoved in 3 ml of freshly distilled CH$_2$Cl$_2$ and added dropwise by using a syringe at low temperature. After the temperature increased to room temperature, the solution was heated to reflux. The reaction was monitored by TLC (silica, ethyl acetate-hexane 30:70 v:v, R$_f$ of the product=0.6). The reaction was discontinued after 16 h refluxing when the spot of ABN (R$_f$ =0.2) had disappeared. The solvent was removed, and the crude product was purified by chromatography (silica, ethyl acetate-hexane 15:85 v:v). Pure *e*-DA4 was obtained as an off-white crystalline solid, yield 500 mg (66%). Analytical data: TLC (silica, ethyl acetate-hexane 5:95 v:v) R$_f$ = 0.2. ^{1}H NMR (300 MHz, CDCl$_3$) δ 1.4-1.65 (m, 6H, pip), 2.35- 2.55 (m, 4H, pip), 3.50 (d, J = 5.7 Hz, 1H, benzylic), 4.84 (d of d, J$_1$ = 5.7 Hz, J$_2$ = 2.7 Hz, 1H, benzylic, adjacent to NH), 5.48 (d, J = 2.7 Hz, 1H NH), 6.47 (d, J = 9.0 Hz, 2H, benzonitrile), 6.9-7.0 (m, 4H,

phenyl), 7.1-7.2 (m, 6H, phenyl), 7.31 (d, J = 9.0 Hz, 2H, benzonitrile); ^{13}C NMR (75 MHz, CDCl$_3$) δ 24.6, 26.2, 52.3 (all pip) 58.0 (benzylic), 75.3 (benzylic), 99.1, 113.6, 120.4, 127.0 (2C), 127.3, 127.7, 128.0, 128.9, 133.4, 137.0, 139.9, 151.0 (all aromatic); ^{1}H NMR (300 MHz, DMSO) δ 1.0-1.4 (m, 6H, pip), 1.91 (m, 2H, pip), ~2.45 (m, 2H, pip), 3.773 (d, J = 10.5 Hz, 1H, benzylic), 5.189 (d of d, J$_1$ = 10.5 Hz, J$_2$ = 8.7 Hz, 1H, benzylic, adjacent to NH), 6.626 (d, J = 8.4 Hz, 2H, benzonitrile), 6.814 (d, J = 8.7 Hz, 1H NH), 7.1-7.3 (m, 10H, phenyl), 7.432 (d, J = 8.4 Hz, 2H, benzonitrile); the molecular weight found: 382.2269 (M+H, HRMS); calc'd for C$_{26}$H$_{28}$N$_3$ is 382.2283.

erythro-1-[N-4-(Pyridyl)methyl]amino-2-piperidino)-1,2-diphenylethane (e-DA1)

The synthesis of this compound followed the same procedure as described for e-DA4 to the point that after adding 4-(Aminomethyl)-pyridine the temperature increased to room temperature. The reaction mixture was stirred at room temperature overnight. The crude product was purified by chromatography (silica, ethyl acetate-hexane 25:75 v:v). Pure e-DA1 was obtained as a yellow oil in 60% yield after purification. Analytical data: TLC (silica, ethyl acetate-hexane 35:65 v:v) R$_f$ = 0.3. ^{1}H NMR (300 MHz, CDCl$_3$) δ 1.32 (m, 2H, pip), 1.42 (m, 4H, pip), 2.24 (m, 2H, pip), 2.37 (m, 2H, pip), 3.39 (d, J = 6.6 Hz, 1H, benzylic), 3.47 (d, J = 14.7 Hz, 1H, diastereotopic CH$_2$), 3.69 (d, J = 14.7 Hz, 1H, diastereotopic CH$_2$), 4.25 (d, J = 6.6 Hz, 1H, benzylic), 7.0-7.3 (m, 12H, pyridyls and phenyls), 8.52 (d, J = 5.7 Hz, pyridyl); ^{13}C NMR (75 MHz, CDCl$_3$) δ 24.5, 26.1 (pip), 50.1 (methylene), 52.0 (pip), 61.7 (benzylic), 76.3 (benzylic), 123.2, 126.8, 127.0, 127.4, 127.7, 128.2, 129.6, 136.9, 141.3, 149.6, 149.7 (all aromatic).

erythro-1-N-[p-[4-(Pyridyl)methyl]anilino-2-piperidino)-1,2-diphenylethane (e-DA2)

The synthesis of this compound followed the general procedure described above for *e*-DA4. The crude product was purified by chromatography (silica, ethyl acetate-hexane 40:60 v:v). Pure *e*-DA2 was obtained as a yellow solid in 35% yield after purification. Analytical data: TLC (silica, ethyl acetate-hexane 40:60 v:v) R_f = 0.4. ^{1}H NMR (300 MHz, CDCl$_3$) δ 1.45 (m, 2H, pip), 1.56 (m, 4H, pip), 2.45 (br, 4H, pip), 3.45 (d, J = 5.7 Hz, 1H, benzylic), 3.80 (s, 2H, methylene), 4.76 (d, J = 5.7 Hz, 1H, benzylic), 5.0 (br,1H, NH), 6.45 (d, J = 8.1 Hz, 2H), 6.86 (d, J = 8.1 Hz), 6.9-7.25 (m, 12H, pyridyls and phenyls), 8.45 (d, J = 6.0 Hz, pyridyl); ^{13}C NMR (75 MHz, CDCl$_3$) δ 24.6, 26.2 (pip), 40.4 (methylene), 52.3 (pip), 58.9 (benzylic), 75.9 (benzylic), 114.4, 124.1, 126.5, 127.0, 127.3, 127.4, 127.5, 127.7, 129.1, 129.4, 137.6, 141.5, 146.7, 149.6, 150.8 (all aromatic).

erythro-1-N-[4-(Pyridyl)]anilino-2-piperidino-1,2-diphenylethane (*e*-DA3)

The synthesis of this compound followed the general procedure described above for *e*-DA4. The crude product was purified by chromatography (silica, ethyl acetate-hexane 50:50 v:v). Pure *e*-DA3 was obtained as a yellow solid in 31% yield after purification. Analytical data: TLC (silica, ethyl acetate-hexane 50:50 v:v) R_f = 0.4. ^{1}H NMR (300 MHz, CDCl$_3$) δ 1.36 (m, 2H, pip), 1.47 (m, 4H, pip), 2.36 (br, 4H, pip), 3.40 (d, J = 5.4 Hz, 1H, benzylic), 4.75 (d, not well resolved, 1H, benzylic), 5.16 (s,1H, NH), 6.48 (d, J = 8.1 Hz, 2H), 6.8-7.1 (m, 12H), 7.29 (d, not well resolved, 2H, pyridyl), 8.42 (d, J = 4.8 Hz, 2H, pyridyl).

threo-1-N-(4-Cyanophenyl)amino-2-piperidino-1,2-diphenylethane (*t*-DA4)

A mixture of *t*-AA (281 mg, 1.0 mmole), 5 ml of freshly distilled CH$_2$Cl$_2$ and triethylamine (0.4 ml, 3.0 mmole) was placed in a 100 ml three-necked round bottom flask, and purged with nitrogen for 30 minutes. At the same time the temperature was adjusted to -20°C by using a dry ice-isopropanol bath. A

solution of methanesulfonyl chloride (0.08 ml, 1.0 mmole) dissoved in 1 ml of freshly distilled CH_2Cl_2 was added dropwise by using a syringe. The resulting mixture was kept stirring at low temperature (<10°C) for 1 h. 4-Aminobenzonitrile (118 mg, 1.0 mmole) was dissoved in 2 ml of freshly distilled CH_2Cl_2 and added dropwise to the reaction mixture which was at low temperature. After the temperature increased to room temperature, the solution was heated to reflux. The reaction was monitored by TLC (silica, ethyl acetate-hexane 30:70 v:v, R_f of the product = 0.7). The reaction occured very slowly under these conditions. The CH_2Cl_2 solvent was removed by bubbling N_2 and 5 ml of 1,2-dichloroethane was added to the flask, and the resulting solution was heated to reflux for 18 hours. The solvent was removed, and the crude product was purified by chromatography (silica, ethyl acetate-hexane 15:85 v:v). Pure t-DA4 was obtained as an off-white crystalline solid, yield 180 mg (47%). Analytical data: TLC (silica, ethyl acetate-hexane 30:70 v:v) R_f = 0.7. ^{1}H NMR (300 MHz, CDCl$_3$) δ 1.39 (m, 2H, pip), 1.59 (m, 2H, pip), 1.68 (m, 2H, pip), 2.38 (m, 4H, pip), 3.64 (d, J = 10.5 Hz, 1H, benzylic), 4.63 (d, J = 10.5 Hz, 1H, benzylic), 6.53 (d, J = 8.7 Hz, 2H, benzonitrile), 6.72 (s, 1H, NH), 7.0-7.3 (m, 10H, phenyl), 7.34 (d, J = 8.7 Hz, 2H, benzonitrile); ^{13}C NMR (75 MHz, CDCl$_3$) δ 24.3, 26.7, 49.9 (br) (all pip), 57.7 (benzylic), 76.1 (benzylic), 99.0, 113.5, 120.4, 127.1, 127.3, 127.7, 127.7, 128.3, 129.8, 133.4, 141.1, 151.6 (all aromatic); ^{1}H NMR (300 MHz, DMSO) δ 1.23 (m, 2H, pip), 1.42 (m, 2H, pip), 1.56 (m, 2H, pip), 2.22 (m, 2H, pip), 2.29 (m, 2H, pip), 3.761 (d, J = 10.8 Hz, 1H, benzylic), 4.948 (d of d, J_1 = 10.8 Hz, J_2 = 3.0 Hz, 1H, benzylic, adjacent to NH), 6.672 (d, J = 8.4 Hz, 2H, benzonitrile), 6.92 (d, J = 3.0 Hz, 1H NH), 7.0-7.3 (m, 10H, phenyl), 7.367 (d, J = 8.4 Hz, 2H, benzonitrile); the molecular weight found: 382.2327 (M+H, HRMS); calc'd for $C_{26}H_{28}N_3$ is 382.2283.

meso-1,2-Dipiperidino-1,2-diphenylethane (_meso_-DA5)

A mixture of _e_-AA (1 g, 3.56 mmole), 15 ml freshly distilled CH_2Cl_2 and triethylamine (1.5 ml, 11 mmole) was placed in a 100 ml three-necked round bottom flask, and purged with nitrogen for 30 minutes. At the same time the temperature was adjusted to -20˚C by a dry ice-isopropanol bath. A solution of methanesulfonyl chloride (0.28 ml, 3.56 mmole) dissoved in 2 ml of freshly distilled CH_2Cl_2 was added dropwise by using a syringe. The resulting mixture was kept stirring at low temperature (<10˚C) for 1 h whereupon 0.35 ml of piperidine (3.56 mmole) dissoved in 2 ml of freshly distilled CH_2Cl_2 was added dropwise. The reaction was discontinued after 1 hour stirring at low temperature. The product solution was washed twice with H_2O, and the organic layer was dried with Na_2SO_4. After removing the solvent pure _meso_-DA5 was obtained as an off-white crystalline solid, yield 1.19 g (93%). Analytical data: TLC (silica, ethyl acetate-hexane 10:90 v:v) $R_f = 0.6$. ^1H NMR (300 MHz, $CDCl_3$) δ 1.10 (m, 4H, pip), 1.24 (m, 2H, pip), 2.16 (m, 2H, pip), 2.35 (m, 2H, pip), 4.15 (s, 1H, benzylic), 7.2-7.4 (m, 5H, phenyl); ^{13}C NMR (75 MHz, $CDCl_3$) δ 24.6, 26.4, 50.5 (all pip), 69.8 (benzylic), 126.1, 127.0, 129.2, 137.4 (all aromatic).

Synthesis of Compounds Studied in Chapter 4

General Procedure A for preparation of Re-DA Complexes

_e_-Re-DA2 The reaction was carried out with minimal exposure to room light. In a typical preparation, (bpy)Re(CO₃)Cl (138 mg, 0.3 mmole), $AgPF_6$ (250 mg, 10 mmole), and _e_-DA2 (268 mg, 0.6 mmole) were dissolved in 5 ml of DMF. The solution was purged with nitrogen and then heated to 75˚C. The reactions were monitored by TLC (silica, MeOH-$CHCl_3$ 4:96 v:v), and the heating was discontinued when the orange fluorescent spot due to the starting

(bpy)Re(CO$_3$)Cl disappeared almost completely. After cooling, the solution was filtered through a medium-porosity fritted filter, and the DMF was removed under reduced pressure. The products were purified by chromatography (alumina, MeOH-CHCl$_3$ 4:96 v:v) using 4 MeOH/CHCl$_3$ as eluant. After removal of the solvent, the residue was dissolved in a minimal amount of CH$_2$Cl$_2$ and precipitated from n-pentane to give a dark-yellow powder, yield 330 mg after purification (46%). Analytical data: TLC (silica, MeOH-CHCl$_3$ 4:96 v:v) R$_f$ = 0.2-0.3. ^{1}H NMR (300 MHz, CD$_3$CN) δ 1.28 (b, 2H, pip),1.36 (b, 4H, pip), 2.15 (b, 2H, pip), 2.43 (b, 2H, pip), 3.62 (d, J = 8.1 Hz, 1H, benzylic), 3.67 (s, 2H, methylene), 4.8-4.9 (m, 2H, NH overlapped with a benzylic), 6.38 (d, J = 8.1 Hz, 2H), 6.72 (d, J = 8.1 Hz, 2H), 7.02 (d, J = 6.3 Hz, 2H),   7.1-7.3 (m, 10H, phenyls), 7.75 (t, J = 5.1 Hz, 2H, bpy), 8.02 (d, J = 6.3 Hz, 2H, pyridyl), 8.24 (t, J = 8.1 Hz, 2H), 8.36 (d, J = 8.1 Hz, 2H), 9.16 (d, J = 5.1 Hz 2H) (all bpy); ^{13}C NMR (75 MHz, CD$_3$CN) δ 24.1, 25.8 (pip), 39.1 (methylene), 51.1 (pip), 57.4 (benzylic), 74.8 (benzylic), 124.4, 125.8, 126.2 (2C), 126.7, 127.1, 127.2, 127.4, 128.5, 128.9, 129.2, 136.8, 140.8, 142.6, 146.5, 151.2, 153.5, 155.5, 156.0 (all aromatic); the molecular weight found: 874.2730 (HRMS, POS, FAB), calc'd for C$_{44}$H$_{41}$N$_5$O$_3$Re is 874.2769.

General Procedure B for Preparation of Re-DA Complexes

(a) (bpy)Re(CO$_3$)CF$_3$SO$_3$ (Re-TFMS) A mixture of (bpy)Re(CO$_3$)Cl (0.6 g, 1.3 mmole) and 35 ml of freshly distilled CH$_2$Cl$_2$ was purged with nitrogen for 10 minutes. The suspension dissolved gradually as triflic acid (0.8 ml, 9 mmole) was added slowly. The resulting yellow transparant solution was stirred for 1 h. 25 ml of diethyl ether (anhydrous) then was added to give a bright yellow precipitate which was filtered through a medium-porosity fritted filter to give 577

mg product (77.2%). ^{1}H NMR (300 MHz, CD$_3$CN) δ 7.73 (t, J = 5.7 Hz, 2H), 8.30 (t, J = 7.8 Hz, 2H), 8.51 (d, J = 7.8 Hz, 2H), 9.03 (d, J = 5.7 Hz, 2H) (all bpy).

(b) e-Re-DA1. A mixture of Re-TFMS (115 mg, 0.2 mmole), e-DA1 (112 mg, 0.3 mmole), NH$_4$PF$_6$ (326 mg, 2 mmole) and 5 ml of freshly distilled THF was stirred at room temperature under a blanket of nitrogen for 4h. The reaction was carried out with minimal exposure to room light. The crude product was purified by chromatography (alumina, CH$_3$CN-CH$_2$Cl$_2$ 5:95 v:v). After removal of the solvent, the residue was dissolved in a minimal amount of CH$_2$Cl$_2$ and precipitated from n-pentane to produce a yellow powder, yield 114 mg after purification (61%). Analytical data: TLC (silica, CH$_3$CN-CH$_2$Cl$_2$ 10:90 v:v) R$_f$ = 0.3. ^{1}H NMR (300 MHz, CD$_3$CN) δ 1.22 (b, 6H, pip), 2.0-2.35 (m, 4H, pip), 3.43 (s, 2H, methylene), 3.45 (partially overlapped with methylene peak, 1H), 4.08 (d, J = 8.1 Hz, 1H, benzylic), 7.0-7.3 (m, 12H, pyridyls and phenyls), 7.80 (t, J = 5.1 Hz, 2H, bpy), 8.03 (d, J = 6.6 Hz, 2H, pyridyl), 8.28 (t, J = 8.1 Hz, 2H), 8.38 (d, J = 8.1 Hz, 2H), 9.21 (d, J = 5.1 Hz 2H) (all bpy); ^{13}C NMR (75 MHz, CD$_3$CN) δ 24.0, 25.8 (pip), 49.0 (methylene), 51.0 (pip), 61.8 (benzylic), 75.2 (benzylic), 124.4, 125.5, 126.4, 126.7, 127.1, 127.3, 127.9, 128.6, 129.3, 136.8, 140.9, 141.8, 150.9, 153.6, 155.2, 155.5 (all aromatic).

e-Re-DA3 The synthesis of this compound followed the general procedure B except that the crude product was purified by chromatography (alumina, CH$_3$CN-CH$_2$Cl$_2$ 10:90 v:v). Analytical data: TLC (silica, CH$_3$CN-CH$_2$Cl$_2$ 20:80 v:v) R$_f$ = 0.3-0.6. ^{1}H NMR (300 MHz, CD$_3$CN) δ 1.25 (b, 2H, pip),1.33 (b, 4H, pip), 2.15 (b, 2H, pip), 2.46 (b, 2H, pip), 3.70 (d, J = 8.7 Hz, benzylic), 5.00 (m, 1H, benzylic), 5.43 (br, 1H, NH), 6.54 (d, J = 8.7 Hz, 2H), 7.1-7.4 (m, 14H), 7.77 (t, J = 5.1 Hz, 2H, bpy), 8.01 (d, J = 6.3 Hz, 2H, pyridyl), 8.24 (t, J = 7.5 Hz, 2H), 8.34 (d, J = 7.5 Hz, 2H), 9.20 (d, J = 5.1 Hz 2H) (all bpy); ^{13}C NMR (75 MHz,

CD$_3$CN) δ 24.2, 25.9, 51.2 (pip), 57.3 (benzylic), 74.8 (benzylic), 113.5, 121.5, 122.2, 124.5, 126.6, 127.0, 127.4 (2C), 127.6, 127.9, 128.6, 129.0, 136.5, 141.0, 142.1, 150.2, 150.6, 151.3, 153.6, 155.6 (all aromatic).

e-Re-DA4 The synthesis of this compound followed the general procedure B except that the crude product was purified by chromatography (alumina, CH$_3$CN-CH$_2$Cl$_2$ 10:90 v:v). Analytical data: TLC (silica, CH$_3$CN-CH$_2$Cl$_2$ 20:80 v:v) R$_f$ = 0.7-0.8. ^{1}H NMR (300 MHz, CD$_3$CN) δ 1.23 (b, 2H, pip), 1.30 (b, 4H, pip), 2.1 (b, 2H, pip), 2.45 (b, 2H, pip), 3.71 (d, J = 9.0 Hz, benzylic), 5.00 (m, 1H, benzylic), 5.85 (d, J = 6.3 Hz, 1H, NH), 6.44 (d, J = 8.1 Hz, 2H, benzonitrile), 7.03 (d, J = 8.1 Hz, 2H, benzonitrile), 7.1-7.3 (m, 10H, phenyls), 7.69 (t, J = 5.1 Hz, 2H, bpy), 8.26 (t, J = 8.1 Hz, 2H), 8.44 (d, J = 8.1 Hz, 2H), 9.04 (d, J = 5.1 Hz 2H) (all bpy); ^{13}C NMR (75 MHz, CDCL$_3$) δ 24.4, 26.0, 52.2 (pip), 57.5 (benzylic), 74.9 (benzylic), 92.3, 113.9, 124.7 (nitrile C), 125.3, 127.0, 127.2, 127.5, 127.9, 128.1, 128.2, 128.7, 134.8, 136.2, 139.0, 141.5, 152.8, 153.0, 155.7 (all aromatic).

ReDMAPP The synthesis of this compound followed the general procedure B except that the crude product was purified by chromatography (alumina, CH$_3$CN-CH$_2$Cl$_2$ 10:90 v:v) followed by chromatography (silica, CH$_3$CN-CH$_2$Cl$_2$ 10:90 v:v) Analytical data: TLC (silica, CH$_3$CN-CH$_2$Cl$_2$ 10:90 v:v) R$_f$ = 0.6-0.8. ^{1}H NMR (300 MHz, CD$_3$CN) δ 2.97 (s, 6H, methyls), 6.72 (d, J = 8.7 Hz, 2H, phenyl), 7.42 (d, J = 6.3 Hz, 2H, pyridyl), 7.55 (d, J = 8.7 Hz, 2H, phenyl), 7.79 (t, J = 5.1 Hz, 2H, bpy), 8.05 (d, J = 6.3 Hz, 2H, pyridyl), 8.26 (t, J = 8.1 Hz, 2H, bpy), 8.37 (d, J = 8.1 Hz, 2H, bpy), 9.23 (d, J = 5.1 Hz 2H, bpy); ^{13}C NMR (75 MHz, CDCL$_3$) δ 39.2 (methyl), 112.2, 120.8, 121.4, 124.6, 127.9, 128.7, 141.0, 150.7, 151.4, 152.4, 153.7, 155.7 (all aromatic).

Preparative Scale Photolyses

General Procedures for Preparative Scale Photolyses

For Re-AA1 and *e*-Re-DA2, preparative scale photolyses were carried out using a 450 W Hanovia medium pressure Hg arc lamp which was contained in a pyrex cooling well. The 366 nm Hg line was isolated using Corning 7-54 and Schott LG-350 nm filters. For *e*-DA4, preparative scale photolyses were carried out using a 450 W Hanovia medium pressure Hg arc lamp which was contained in a quartz cooling well without optical filter being used.

Preparative Photolysis of Re-AA1 and Isolation of Re-4

A stock solution of Re-AA1 (0.0001 M) was prepared by dissolving 30.5 mg of Re-AA1 into 350 ml of acetonitrile. 10 ml of the stock solution was placed in a pyrex test tube and degassed with argon for 20 minutes. The argon-degassed solution was irradiated (366 nm, 450 W Hanovia lamp) for 20 minutes. The photolysis procedure was repeated 35 times until all of the stock solution was photolyzed. The product solution was then concentrated, and the residue was chromatographed (alumina, MeOH-CH$_3$CN 10:90 v:v). The major component solution was concentrated to dryness which was then dissolved in a minimal amount of CH$_2$Cl$_2$ and precipitated from dry ether to yield a few mg of yellow powder. Analytical Data: ^{1}H NMR (300 MHz, CD$_3$CN) δ 3.76 (s, 2H, CH$_2$), 7.27 (d, 2H, pyridyl), 7.79 (t, 2H, bpy), 8.12 (d, 2H, pyridyl), 8.27 (t, 2H, bpy), 8.38 (d, 2H, bpy), 9.21 (d, 2H, bpy). ^{13}C NMR (75 MHz, CD$_3$CN) δ 44.0 (CH$_2$) ~124.3 (2C), 128, 141, 151, 153.5 (2C), 155.5 (all aromatic). The molecular weight found: 536 (M+H, LRMS, POS, FAB), calc'd for C$_{19}$H$_{17}$N$_4$O$_3$Re 536.0862. The analytical data are consistant with the expected structure of Re-4.

Preparative Photolysis of Re-AA1 and Isolation of Re-1

A stock solution of Re-AA1 (0.0001 M) was prepared by dissolving 13.5 mg Re-AA1 into 150 ml acetonitrile. 10 ml of the stock solution was placed in a pyrex test tube and degassed with argon for 20 minutes. The argon-degassed solution was irradiated (366 nm, 450 W Hanovia lamp) for 20 minutes. The photolysis procedure was repeated 15 times until all the stock solution was photolyzed. To the combined product solution was added 30 mg of Na(CN)BH$_3$, the resulting mixture was placed in the refregerator for overnight. The solid was removed by filtration, and the solution was concentrated. The residue was chromatographed (alumina, CH$_3$CN-CH$_2$Cl$_2$ 10:90 v:v to CH$_3$CN-CH$_2$Cl$_2$ 50:50 v:v), and the separation process was monitored by HPLC. The HPLC analysis was carried out by using a C$_{18}$ reversed phase column (Whatman ODS-3). The mobile phase was THF-MeOH-H$_2$O 30:30:40 v:v:v with 0.005 M 1-heptanesulfonic acid, sodium salt. The major component solution was concentrated to dryness which was then placed in vacuo for a few hours. Analytical Data: ^{1}H NMR (300 MHz, CD$_3$CN) δ 3.70 (s, 2H, CH$_2$), 3.80 (s, 2H, CH$_2$), 7.33 (m, 7H, phenyl and pyridyl), 7.90 (t, 2H, bpy), 8.22 (d, 2H, pyridyl), 8.38 (t, 2H, bpy), 8.49 (d, 2H, bpy), 9.32 (d, 2H, bpy). The ^{1}H NMR data of this isolated product is identical with that of independently synthesized Re-1. (see above)

Preparative Photolysis of e-DA4 and Major Products Isolation

A stock solution of e-DA4 (0.003 M) was prepared by dissolving 160 mg e-DA4 into 140 ml acetonitrile. 70 ml of the stock solution was placed in a quartz test tube and degassed with argon for 2 hours. The argon-degassed solution was irradiated (254 nm, 450 W Hanovia lamp) for 30 minutes. The procedure was

repeated twice until all the stock solution was photolyzed. The HPLC chromatogram of the product solution is shown in Figure 3-3. The product with 7.8 min. retention time was crystallized from concentrated product acetonitrile solution at room temperature. The acetonitrile mother liquor was concentrated to dryness and redissolved in chloroform, and the product with 9.4 min. retention time was then crystallized from the cold concentrated chloroform solution. The chloroform mother liquor was concentrated to dryness and redissolved in a minimal amount of ethyl acetate, and was chromatographed by preparative-scale TLC (silica, ethyl acetate-hexane 5:95 v:v). The TLC separation was carried-out overnight. The strip of TLC which was adjacent to and with slightly higher R_f than that of *e*-DA4 was scrached, the silica powder was then collected and suspended in chloroform. HPLC analysis of the chloroform solution confirmed that this component is the product with 15.4 min. retention time. The suspended silica powder was removed from the solvent by filtration, and pure product-15.4 was obtained as a white crystal after evapration of the solvent.

Product-7.8 minute This compound was found to be very polar, and was soluble only in DMSO. Analytical data: ^{1}H NMR (300 MHz, DMSO) δ 4.81 (d, J = 6.6 Hz, 1H, benzylic), 6.51 (d, J = 8.7 Hz, 2H, benzonitrile), 6.94 (d, J = 6.6 Hz, 1H NH), 7.15 (t, 1H, phenyl), 7.24 (d, J = 7.5 Hz, 2H, phenyl), 7.29 (d, J = 8.7 Hz, benzonitrile), 7.47 (d, J = 7.5 Hz, 2H, phenyl); ^{13}C NMR (75 MHz, DMSO) δ 60.9 (benzylic), 96.8, 113.0, 120.6, 127.6, 128.0, 128.4, 133.5, 140.8, 151.2 (all aromatic); the molecular weight found: 415.1909 (M+H, HRMS, FAB); calc'd for $C_{28}H_{23}N_4$ is 415.1923. The analytical data are consistant with the structure of proposed product *dl*-DA6.

Product-9.4 minute Analytical data: ^{1}H NMR (300 MHz, DMSO) δ 4.68 (d, not very well resolved, 1H, benzylic), 6.59 (d, J = 8.7 Hz, 2H, benzonitrile), 7.08 (s, 5H, phenyl), 7.34 (d, J = 8.7 Hz, benzonitrile), 7.53 (d, not very well resolved,

1H NH); ^{13}C NMR (75 MHz, DMSO) δ 62.1 (benzylic), 96.6, 113.2, 120.7, 127.4, 128.0, 128.3, 133.5, 140.5, 151.7 (all aromatic); ^{1}H NMR (300 MHz, CDCl$_3$) δ 4.66 (d, not very well resolved, 1H, benzylic), 4.95 (d, not very well resolved, 1H NH), 6.51 (d, J = 8.7 Hz, 2H, benzonitrile), 7.08 (m, 2H, phenyl), ~7.3 (m, phenyl, the number of the protons cannot be counted correctly because of existence of the solvent peak), 7.34 (d, J = 8.7 Hz, benzonitrile); the molecular weight found: 415.1914 (M+H, HRMS, FAB); calc'd for C$_{28}$H$_{23}$N$_4$ is 415.1923. The analytical data are consistant with the structure of proposed product *meso*-DA6.

Product-15.4 minute Analytical data: Both ^{1}H NMR and ^{13}C NMR data of this isolated product are identical with that of independently synthesized *t*-DA4; the molecular weight found: 382.2320 (M+H, HRMS); calc'd for C$_{26}$H$_{28}$N$_3$ is 382.2283. The analytical data are consistant with the structure of *t*-DA4.

Preparative Photolysis of *e*-Re-DA2 and Isolation of *t*-Re-DA2

A solution of Re-DA2 (0.0007 M) was prepared by dissolving 50 mg of Re-DA2 into 70 ml of acetonitrile. The solution was placed in a pyrex test tube and degassed with argon for 2 hours. This argon-degassed solution was irradiated (366 nm, 450 W Hanovia lamp) for 80 minutes. The product solution was then concentrated, and the residue was chromatographed (alumina, CH$_3$CN-CH$_2$Cl$_2$ 5:95 v:v). The component solution (silica, CH$_3$CN-CH$_2$Cl$_2$ 5:95 v:v, R$_f$ =0.7-0.8) was concentrated to dryness, and the residue was dissolved in a minimal amount of CH$_2$Cl$_2$ and precipitated from n-pentane to obtain a few mg of yellow powder. Analytical Data: ^{1}H NMR (300 MHz, CD$_3$CN) δ 1.30 (m, 2H, pip), 1.50 (m, 2H, pip), 1.60 (m, 2H, pip), ~2.3 (m, pip, the number of the protons cannot be counted correctly because of the existence of the H$_2$O peak), 3.66 (1H, benzylic), 3.71 (s, 2H, methylene), 4.62 (d, J ≈ 10.5 Hz, 1H, benzylic), 6.07 (1H, possibly NH), 6.48 (d, 2H), 6.77 (d, J = 8.1 Hz, 2H), 7.0-7.3 (m, 12H, phenyls and pyridyl), 7.74 (t,

2H, bpy), 8.03 (d, J = 5.1 Hz, 2H, pyridyl), 8.24 (t, 2H), 8.35 (d, J = 8.1 Hz, 2H), 9.17 (d, 2H) (all bpy); ^{13}C NMR (75 MHz, CD_3CN) δ 24.0, 26.0 (pip), 39.1 (methylene), 49.3 (broad, pip), 57.4 (benzylic), 75.1 (benzylic), 124.3, 126.2 (2C), 126.4, 127.1, 127.2 (2C), 127.6, 127.8, 128.4, 129.2, 129.6, 133.4, 140.7, 142.8, 147.4, 151.2, 153.5, 155.5, 156.0 (all aromatic); the molecular weight found: 874.2835 (HRMS, POS, FAB); calc'd for $C_{44}H_{41}N_5O_3Re$ is 874.2769. The analytical data are consistant with the structure of the proposed product t-Re-DA2.

Quantitative Photolyses

General Procedures for Quantitative Photolyses

Quantum yield studies were carried out using a 75 W high pressure Hg lamp housed in an elliptical reflector housing (PTI ALH-1000). The output from the 75 W lamp was passed through a grating monochromator and focused into a small compartment which contained the sample cell. The light intensity was determined twice each working day by using the Aberchrome 540 actinometer.[109] HPLC was carried out on a system that was comprised of a Waters isocratic pump, a Valco injector, an ABI variable wavelength absorption detector, and a Hewlett-Packard integrating recorder. The HPLC columns used were either a DuPont analytical column (Zorbax C_{18}) or a Whatman semi-preparative column (ODS-3). The mobile phase used for each measurement will be provided individually.[110] Peak identifications were established using standard solutions which contain the known starting materials and expected photoproducts when available. Standard solutions were also used to determine the calibration factors for components in the photoproduct mixture. Every calibration factor and each reported Φ value is an average of ≥ 4 individual measurements. For

quantum yield determinations in argon-degassed solution, prior to irradiation the sample was bubbled gently with argon which was passed through an argon-saturated acetonitrile solution for 30 minutes and then sealed by wax and parafilm. Before irradiation the absorption spectrum of the sample solution must be taken and the absorption at irradiation wavelength must be recorded. Quantum yields were calculated from moles produced (or consumed) vs. irradiation time. An example for a typical Quantum yield experiment and subsequent calculations will be provided in detail in the section of "Quantum Yield measurements of *e*-Re-DA2".

Comments on Adjusting the Mobile Phases for the HPLC Analyses Conducted in This Work

The mobile phases used in this work are generally a mixture of THF-CH_3CN-H_2O with 1-heptanesulfonic acid, sodium salt and triethylamine. Usually the volumn ratio of CH_3CN is fixed, and the volumn ratio between THF and H_2O are adjusted. THF is very sensitive to retention times of both organic compounds and Re-based complexes. The more THF the mixture contains, the shorter retention times of samples are. However, in some cases such as analysing stereoisomers which possess very similar polarity toward solvents, both shorter retention time and good resolution are desired, whereas the good resolution is the most important for quantifying reactions. H_2O has the tendency to prolong retension times of both organic compounds and Re-based complexes and to improve resolutions. On the other hand, the longer the retention times of samples are, the broader the peak shapes are. It is worthy to note that accuracy of integrated peak areas for broad peaks is usually low. 1-heptanesulfonic acid, sodium salt and triethylamine have the tendency to reduce retention times, to compress the distribution of compounds (especially for Re-based complexes

which usually possess a long tail) in the separation process, and therefore to narrow peak shapes.

Quantum Yield Measurements of Re-AA complexes

Photochemical quantum yields were determined by irradiation (366 nm, 75 W Hg lamp) of 3 ml aliquots of a solution containing the reactive Re-AA1 for various time increments. Following irradiation, a benzophenone internal standard was added to each aliquot and the samples were analyzed by triplicate injections into the HPLC. HPLC analysis of Re-AA complexes was carried out by using MeOH-THF-H$_2$O 35:35:30 v:v:v with 0.005 M 1-heptanesulfonic acid, sodium salt, and λ_{det} = 250 nm. HPLC analysis of organic products (e.g. benzaldehyde) was carried out by using MeOH-H$_2$O 80:20 v:v, and λ_{det} = 250 nm. The flow rates were usually in the range of 0.5 ml/min to 2 ml/min. Quantum yields were determined from the slope of a plot of moles produced (or consumed) vs. irradiation time.

N,N-dimethylaniline (DMA) Quenching Re-AA1 Photochemical Reaction Experiment

Four measurements were conducted, each measurement started with 3 ml of Re-AA1 (0.00051 M) and the concentration of DMA and irradiation (366 nm, 75 W Hg lamp) times were: (1) [DMA]=0, t=60 minute; (2) [DMA]=0.001 M, t=120 minute; (3) [DMA]=0.002 M, t=180 minute; (4) [DMA]=0.003 M, t=240 minute. Following irradiation, a benzophenone internal standard was added to each aliquot and the samples were analyzed by triplicate injections into the HPLC. HPLC analysis of benzaldehyde was carried out by using MeOH-H$_2$O 80:20 v:v, and λ_{det} = 250 nm. Quantum yields were determined from the moles of benzaldehyde produced vs. irradiation time.

<u>Quantum Yield Measurements of *e*-DA3</u>

3 ml of an acetonitrile solution of *e*-DA3 (0.0005 M) was irradiated (313 nm, 75 W Hg lamp) for 9 and 18 minutes for air-saturated and argon-degassed solutions, respectively. 2 ml of the photoproduct solution was concentrated to dryness by bubbling N_2, and 0.5 ml of an internal standard solution (*p*-Nitroaniline 0.0005 M in H_2O-CH_3CN 10:90 v:v pH=3) was then added. The mixture was analyzed by triplicate injections into the HPLC. The mobile phase contained CH_3CN-H_2O 40:60 v:v with 0.01 M 1-heptanesulfonic acid, sodium salt and 0.025 M triethylamine, and λ_{det} = 320 nm for determination of all Φ values. For $\Phi^+{}_{t\text{-DA3}}$ (argon) the calculation assumed that *t*-DA3 and *e*-DA3 have the same absorptivity at 320 nm (The calibration factor was determined only for *e*-DA3/*p*-Nitroaniline).

<u>Quantum Yield Measurements of *e*-DA4 and *t*-DA4)</u>

3 ml of an acetonitrile solution of *e*-DA4 (0.0005 M) was irradiated (313 nm, 75 W Hg lamp) for 7 and 10 minutes for air-saturated and argon-degassed solutions, respectively. 0.5 ml of an internal standard solution (acetophenone 0.015 M in H_2O-CH_3CN 10:90 v:v pH=3) was added to 2 ml of the photoproduct solution, and the mixture was analyzed by triplicate injections into the HPLC. The mobile phase contained THF-CH_3CN-H_2O 4:40:56 v:v:v with 0.01 M 1-heptanesulfonic acid, sodium salt and 0.025 M triethylamine, and λ_{det} = 286 nm for determination of all Φ values.

<u>Quantum Yield Measurements of *e*-Re-DA1</u>

3 ml of an acetonitrile solution of *e*-Re-DA1 (0.0005 M) was irradiated (366nm, 75 W Hg lamp) for 2.5 minutes for both air-saturated and argon-

degassed solutions. 0.5 ml of an internal standard solution (Re-ABP 0.0015 M in H_2O-CH_3CN 10:90 v:v pH=3) was added to 2 ml of the photoproduct solution, and the mixture was analyzed by triplicate injections into the HPLC. The mobile phase contained THF-H_2O 68:32 v:v with 0.01 M 1-heptanesulfonic acid, sodium salt and 0.02 M triethylamine, and λ_{det} = 320 nm for determinations of $\Phi^-_{e\text{-Re-}DA1}$(air), $\Phi^-_{e\text{-Re-}DA1}$(argon) and $\Phi^+_{t\text{-Re-}DA1}$(argon); the mobile phase contained THF-CH_3CN-H_2O 3:45:50 v:v:v with 0.02 M 1-heptanesulfonic acid, sodium salt and 0.04 M triethylamine, and λ_{det} = 250 nm for determinations of $\Phi^+_{benzaldehyde}$(air) and $\Phi^+_{benzaldehyde}$(argon). For $\Phi^+_{t\text{-Re-}DA1}$(argon) the calculation assumed that t-Re-DA1 and e-Re-DA1 have the same absorptivity at 320 nm. (Re-ABP stands for (bpy)Re(CO)$_3$-(4-(p-aminobenzyl)-pyridine)).

Quantum Yield Measurements of e-Re-DA2

3 ml of an acetonitrile solution of e-Re-DA2 (0.0005 M) was irradiated (366nm, 75 W Hg lamp) for 2 and 3 minutes for air-saturated and argon-degassed solutions, respectively (note that before irradiation the absorption spectrum of the sample solution must be taken and the absorption at irradiation wavelength must be recorded). 0.5 ml of an internal standard solution (benzophenone 0.002 M H_2O-CH_3CN 10:90 v:v pH=3) was added to 2 ml of the photoproduct solution, and the mixture was analyzed by triplicate injections into the HPLC. The mobile phase contained THF-CH_3CN-H_2O 5:45:52 v:v:v with 0.04 M 1-heptanesulfonic acid, sodium salt and 0.05 M triethylamine, and λ_{det} = 250 nm for determination of all Φ values. For $\Phi^+_{t\text{-Re-}DA2}$(argon) the calculation assumed that t-Re-DA2 and e-Re-DA2 have the same absorptivity at 250 nm.

An example for a typical Quantum yield determination is provided in detail as several steps shown below.

Step 1. Determination of the lamp intensity (Int). The intensity of the lamp was determined by using Aberchrome 540 (AC540). 3 ml of AC540 (0.005 M in toluene) was placed in a UV cuvette. UV-Vis spectrum was taken before irradiation, and the absorption at 494 nm was recorded ($Abs_0^{494nm} = 0.00004$). The solution was then irradiated (366nm, 75 W Hg lamp) for 5 minutes, and UV-Vis spectrum was taken after irradiation, and the absorption at 494 nm was recorded again ($Abs_t^{494nm} = 0.52043$). The intensity of the lamp was calculated according to equation 5-1:

$$Int = (Abs_t^{494nm} - Abs_0^{494nm}) \times vol \,/\, (irr.\ time \times 8200 \times 0.2) \qquad (5\text{-}1)$$
$$= (0.52043 - 0.00004) \times 0.003 \,/\, (300 \times 8200 \times 0.2)$$
$$= 3.17 \times 10^{-9}\ Einstein\,/\,second$$

where 8200 is the extinction coefficient of the photoproduct of AC540 at 494 nm, 0.2 is the quantum qield of the corresponding photochemical reaction. This procedure should be performed twice, at the beginning and at the end of each working day, and an average should be taken for the quantum yield calculations.

Step 2. Determination of calibration factors for the starting material and products. In this experiment the starting material was *e*-Re-DA2, and, under air-saturated condition, products were benzaldehyde (BA) and Re-ABP. The internal standard used was benzophenone (BP). Standard solutions were prepared and analyzed as the following (Note that in reality, at least three parallel solutions should be prepared and analyzed for each kind of standard).

solution 1 = [BA] = 0.00032 M in acetonitrile.

solution 2 = [Re-ABP] = 0.0002 M in acetonitrile.

solution 3 = [Re-DA2] = 0.0005 M in acetonitrile.

solution 4 = [BP] = 0.002 M in H_2O-CH_3CN 10:90 v:v pH=3.

standard solution for BA (S_{BA}) = 2 ml of solution 1 + 0.5 ml of solution 4

standard solution for Re-ABP (S_{Re-ABP})

$\qquad$ = 2 ml of solution 2 + 0.5 ml of solution 4

standard solution for Re-DA2 (S_{Re-DA2})

$\qquad$ = 2 ml of solution 3 + 0.5 ml of solution 4

Each of the standard solutions was analyzed by triplicate injections into the HPLC (see above for the HPLC conditions). The concentration and peak area (A) for each component in the above three standard solutions are listed in Table 5-1 (note that for each component only one area value is listed in the table as an example for the calculations). The calibration factors are calculated according to equations 5-2 to 5-4.

Table 5-1 Concentration and Area for Each Component in Standard Solutions

	[BA]	[Re-ABP]	[Re-DA2]	[BP]
S_{BA}	0.000256			0.0004
S_{Re-ABP}		0.00016		0.0004
S_{Re-DA2}			0.0004	0.0004
	A_{BA}	A_{Re-ABP}	A_{Re-DA2}	A_{BP}
S_{BA}	427160			834960
S_{Re-ABP}		682210		1047700
S_{Re-DA2}			1976200	1017100

$$k_{BA} \quad = ([BA] / A_{BA}) / ([BP] / A_{BP}) \qquad (5\text{-}2)$$

$$= (0.000256 / 427160) / (0.0004 / 834960) = 1.251$$

$$k_{Re-ABP} = ([Re-ABP] / A_{Re-ABP}) / ([BP] / A_{BP}) \qquad (5\text{-}3)$$

$$= (0.00016 / 682210) / (0.0004 / 1047700) = 0.614$$

$$k_{Re-DA2} = ([Re-DA2] / A_{Re-DA2}) / ([BP] / A_{BP}) \qquad (5-4)$$

$$= (0.0004 / 1976200) / (0.0004 / 1017100) = 0.515$$

Step 3. Irradiation of a sample solution and collection of data for quantum yield calculations. 3 ml of an air-saturated acetonitrile solution of e-Re-DA2 (0.0005 M) was irradiated (366nm, 75 W Hg lamp) for 2 minutes (note that before irradiation the absorption spectrum of the sample solution must be taken and the absorption at 366 nm must be recorded). 0.5 ml of solution 4 was added to 2 ml of the photoproduct solution, and the mixture was analyzed by triplicate injections into the HPLC. The mobile phase contained THF-CH_3CN-H_2O 5:45:52 v:v:v with 0.04 M 1-heptanesulfonic acid, sodium salt and 0.05 M triethylamine, and $\lambda_{det} = 250$ nm for determination of all Φ values. The areas (A) for each component in the sample solution are listed in Table 5-2 (note that for each component only one area value is listed in the table as an example for the calculations). The concentration of each component is calculated according to equations 5-5 to 5-8.

Table 5-2 Areas for Each Component in the Sample Solution

	A_{BA}	A_{Re-ABP}	A_{Re-DA2}	A_{BP}
sample	300980	284550	2498500	1456700

$$[BA] = ([BP] \times k_{BA} \times A_{BA} / A_{BP}) \times (0.0025 / 0.002) \qquad (5-5)$$

$$= (0.0004 \times 1.251 \times 300980 / 1456700) \times (0.0025 / 0.002)$$

$$= 1.29 \times 10^{-4} \text{ M}$$

$$[Re-ABP] = ([BP] \times k_{Re-ABP} \times A_{Re-ABP} / A_{BP}) \times (0.0025 / 0.002) \qquad (5-6)$$

$$= (0.0004 \times 0.614 \times 284550 / 1456700) \times (0.0025 / 0.002)$$

$$= 5.92 \times 10^{-5} \text{ M}$$

$$[Re-DA2] = ([BP] \times k_{Re-DA2} \times A_{Re-DA2} / A_{BP}) \times (0.0025 / 0.002) \qquad (5-7)$$

$$= (0.0004 \times 0.515 \times 2498500 / 1456700) \times (0.0025 / 0.002)$$

$$= 4.35 \times 10^{-4} \text{ M}$$

$$[\text{Re-DA2}]_{\text{consumed}} = 0.0005 - 4.35 \times 10^{-4} = 6.5 \times 10^{-5} \text{ M} \qquad (5\text{-}8)$$

Step 4. Quantum yield calculations. To calculate the quantum yields the fraction of the light absorbed by the sample solution (F) has to be calculated according to equation 5-9. The quantum yield of the photochemical reaction then can be calculated in terms of formation of the products and/or consumption of the starting material according to equations 5-10 to 5-12.

Abs (366 nm) = 1.8098

$$F (366 \text{ nm}) = 1 - 10^{-\text{Abs}(366 \text{ nm})} = 1 - 10^{-1.8098} = 0.9845 \qquad (5\text{-}9)$$

$$\Phi^+{}_{BA} = [BA] \times \text{vol} / (\text{irr. time} \times \text{Int} \times F)$$

$$= 1.29 \times 10^{-4} \times 0.003 / (120 \times 3.2 \times 10^{-9} \times 0.9845) = 1.02 \qquad (5\text{-}10)$$

$$\Phi^+{}_{\text{Re-ABP}} = [\text{Re-ABP}] \times \text{vol} / (\text{irr. time} \times \text{Int} \times F)$$

$$= 5.92 \times 10^{-5} \times 0.003 / (120 \times 3.2 \times 10^{-9} \times 0.9845) = 0.47 \qquad (5\text{-}11)$$

$$\Phi^-{}_{\text{Re-DA2}} = [\text{Re-DA2}]_{\text{consumed}} \times \text{vol} / (\text{irr. time} \times \text{Int} \times F)$$

$$= 6.5 \times 10^{-5} \times 0.003 / (120 \times 3.2 \times 10^{-9} \times 0.9845) = 0.52 \qquad (5\text{-}12)$$

Quantum Yield Measurements of e-Re-DA3

3 ml of an acetonitrile solution of e-Re-DA3 (0.00042 M) was irradiated (366nm, 75 W Hg lamp) for 2.5 and 4 minutes for air-saturated and argon-degassed solutions, respectively. 0.5 ml of an internal standard solution (benzophenone 0.002 M H_2O-CH_3CN 10:90 v:v pH=3) was added to 2 ml of the photoproduct solution, and the mixture was analyzed by triplicate injections into the HPLC. The mobile phase contained THF-CH_3CN-H_2O 5:45:52 v:v:v with 0.04 M 1-heptanesulfonic acid, sodium salt and 0.05 M triethylamine, and $\lambda_{\text{det}} = 250$

nm for determination of all Φ values. For $\Phi^+_{t\text{-Re-DA3}}$(argon) the calculation assumed that t-Re-DA3 and e-Re-DA3 have the same absorptivity at 250 nm.

Other Experiments

Cyclic Voltammetry

Cyclic voltammetry measurements were carried out using a BAS CV-2 voltammograph with Pt disk working and Pt wire auxilliary electrodes, and a saturated sodium chloride calomel (SSCE) reference electrode. Tetrabutylammonium hexafluorophosphate (TBAH) was used as the supporting electrolyte at a concentration of 0.1 M in freshly distilled acetonitrile.

UV-Visible Spectra

Absorption spectra were obtained on a Hewlett-Packard Model 8452A Diode-Array spectrophotometer.

Steady-State Emission Spectra

Emission spectra were obtained on a Spex Industries F-112A spectrophotometer. Emission spectra were corrected for instrument response with correction factors that were generated using a tungsten filament primary standard lamp. Emission quantum yields for (bpy)Re^I-L complexes were measured relative to [Ru(bpy)$_3$]Cl$_2$ in argon-degassed water (Φ = 0.055).[111]

Emission Lifetimes

Emission lifetime measurements were measured on a Photochemical Research Associates time-correlated single photon counting spectrophotometer.

Emission lifetimes were computed using the DECAN deconvolution package which was provided by Prof. F.C. DeSchryver.

Nano-Second Transient Absorption Spectroscopy

Nano-second transient absorption experiments were carried out using equipment and techniques that have been previously described.[112,113]

LIST OF REFERENCES

1. "A. Weller Festschrift", J. Phys. Chem. 1991, 95, 1867-2097.

2. Marcus, R. A. Angew. Chem. Int. Ed. Engl. 1993, 32, 1111.

3. "Photoinduced Electron Transfer", Parts A-D, Fox, M. A.; Chanon, M. (Eds.), Elsevier, Amsterdam, 1988.

4. Kavarnos, G. J.; and Turro, N. J., Chem. Rev. 1986, 86, 401.

5. "Photochemical Conversion and Storage of Solar Energy", Connolly, J. S. (Eds.), Academic, New York, 1981.

6. Willner, I.; and Willner, B., Top. Curr. Chem. 1991, 159, 153.

7. Gust, D.; and Moore, T. A., Top. Curr. Chem. 1991, 159, 103.

8. "Supramolecular Photochemistry", Balzani V.; and Scandola, F. (Eds.), Ellis Horwood, New York, 1991.

9. Bowler, B. E.; Raphael, A. L.; and Gray, H. B., in "Progress in Inorganic Chemistry: Bioinorganic Chemistry", Lippard, S. J. (Eds.), 1990, 38, 259.

10. Rehm, D.; Weller, A., Isr. J. Chem. 1970, 8, 259.

11. Weller, A., Pure Appl. Chem. 1968, 16, 115.

12. Leonhardt, H.; Weller, A., Z. Phys. Chem. 1961, 29 277.

13. Marcus, R. A. J. Chem. Phys. 1956, 24, 966.

14. Marcus, R. A. J. Chem. Phys. 1956, 24, 979.

15. Marcus, R. A. J. Chem. Phys. 1957, 26, 867.

16. Marcus, R. A. J. Chem. Soc. 1957, 26, 872.

17. Marcus, R. A. Faraday Discuss. Chem. Soc. 1960, 29, 21.

18. Marcus, R. A. J. Chem. Phys. 1965, 43, 679.

19. Hush, N. S. J. Chem. Phys. 1958, 28, 962.

20. Marcus, R. A.; Sutin, N. Biochim. Biophys. Acta 1985, 811, 265.

21. Marcus, R. A. Annu. Rev. Phys. Chem. 1964, 15, 155.

22. Sutin, N. Acc. Chem. Res. 1982, 15, 275.

23. Sutin, N. Prog. Inorg. Chem. 1983, 30, 441.

24. Newton, M. D., Sutin, N. Annu. Rev. Phys. Chem. 1984, 35, 437.

25. Sutin, N. In Bioinorganic Chem. Eichorn, g. L. (ed), Elsevier: New York, 1973, 2, 611.

26. Sutin, N.; Brunschwig, B. S. ACS Symp. Ser. 198 1982, 105.

27. Ballardini, R.; Varani, G.; Indelli, M. T.; Sandola, F.; and Balzani, V., J. Am. Chem. Soc. 1978, 100, 7219.

28. Indelli, M. T.; Ballardini, R.; and Sandola, F.; J. Phys. Chem. 1984, 88, 2547.

29. Mattay, J,; and Vondenhof, M., Top. Curr. Chem. 1991, 159, 219.

30. McConnell, H. M., J. Chem. Phys. 1961, 35, 508.

31. Gould, I. R.; Ege, D.; Mattes, S. L.; and Farid, S., J. Am. Chem. Soc. 1987, 109, 3794.

32. Gould, I. R.; Moser, J. E.; Ege, D.; and Farid, S., J. Am. Chem. Soc. 1988, 110, 1991.

33. Gould, I. R.; Moody, R.; and Farid, S., J. Am. Chem. Soc. 1988, 110, 7242.

34. Gould, I. R.; Ege, D.; Moser, J. E.; and Farid, S., J. Am. Chem. Soc. 1990, 112, 4290.

35. (a) Gould, I. R.; Young, R. H.; Moody, R.; and Farid, S., J. Phys. Chem. 1991, 95, 2068. (b) Mattes, S. L.; and Farid, S., J. Chem. Soc., Chem. Commun. 1980, 126. (c) Mattes, S. L.; and Farid, S., J. Am. Chem. Soc. 1983, 105, 1386. (c) Mattes, S. L.; and Farid, S., J. Am. Chem. Soc. 1986, 108, 7356.

36. Ohno, T.; Yoshimura, A.; and Mataga, N., J. Phys. Chem. 1990, 94, 4871.

37. Schmidt, J. A.; McIntosh, A. R.; Weedon, A. C.; Bolton, J. R.; Connolly, J. S.; Hurley, J. K.; and Wasielewski, M. R., <u>J. Am. Chem. Soc.</u> 1988, 110, 1733.

38. Schmidt, J. A.; Liu, J.; Bolton, J. R.; Archer, M. D.; and Gadzekpo, V. P. Y., <u>J. Chem. Soc., Faraday Trans. 1</u> 1989, 85(5), 1027.

39. Wasielewski, M. R., <u>Chem. Rev.</u> 1992, 92, 435.

40. MacQueen, D. B.; and Schanze, K. S., <u>J. Am. Chem. Soc.</u> 1991, 113, 7470.

41. Schanze, K. S., MacQueen, D. B.; Perkins, T. A.; and Cabana, L. A., <u>Coordination Chemistry Reviews</u> 1993, 122, 63.

42. Saeva, F. D., <u>Top. Curr. Chem.</u> 1990, 156, 60.

43. Ci, X.; and Whitten, D. G., in "Photoinduced Electron Transfer", Parts C, 533, Fox, M. A.; Chanon, M. (Eds.), Elsevier: Amsterdam, 1988.

44. Mariano, P. S., in "Photoinduced Electron Transfer", Parts C, 372, Fox, M. A.; Chanon, M. (Eds.), Elsevier: Amsterdam, 1988.

45. Chatterjee, S.; Gottschalk, P.; Davis, P. D.; and Schuster, G. B., <u>J. Am. Chem. Soc.</u> 1988, 110, 2326.

46. Maslak, P., <u>Top. Curr. Chem.</u> 1993, 168, 1.

47. Wayner, D. D. M.; and Parker, V. D., <u>Acc. Chem. Res.</u> 1993, 26, 287.

48. Popielarz, R.; and Arnold, D. R., <u>J. Am. Chem. Soc.</u> 1990, 112, 3068.

49. Ci, X.; Lee, L. Y. C.; and Whitten, D. G., <u>J. Am. Chem. Soc.</u> 1987, 109, 2536.

50. Ci, X.; and Whitten, D. G., <u>J. Am. Chem. Soc.</u> 1987, 109, 7215.

51. Ci, X.; and Whitten, D. G., <u>J. Am. Chem. Soc.</u> 1989, 111, 3459.

52. Ci, X.; and Whitten, D. G., <u>J. Phys. Chem.</u> 1991, 95, 1988.

53. Ci, X.; Kellett, M. A.; and Whitten, D. G., <u>J. Am. Chem. Soc.</u> 1991, 113, 3893.

54. Kellett, M. A.; and Whitten, D. G., <u>J. Am. Chem. Soc.</u> 1989, 111, 2314.

55. Leon, J. W.; and Whitten, D. G., <u>J. Am. Chem. Soc.</u> 1993, 115, 8038.

56. Chatterjee, S.; Davis, P. D.; Gottschalk, P.; Kurz, M. E.; Sauerwein, B.; Yang, X.; and Schuster, G. B., J. Am. Chem. Soc. 1990, 112, 6329.

57. Schuster, G. B., Pure Appl. Chem. 1990, 62(8), 1565.

58. Eaton, D. F., J. Am. Chem. Soc. 1981, 103, 7235.

59. Gardner, H. C.; and Kochi, J. K., J. Am. Chem. Soc. 1976, 98, 2460.

60. Ohga, K.; and Mariano, P. S., J. Am. Chem. Soc. 1982, 104, 617.

61. Dinnocenzo, J. P.; Farid, S.; Goodman, J. L.; Gould, I. R.; Todd, W. P.; and Mattes, S. L., J. Am. Chem. Soc. 1989, 111, 8973.

62. Dinnocenzo, J. P.; Farid, S.; Goodman, J. L.; Gould, I. R.; and Todd, W. P., Mol. Cryst. Liq. Cryst. 1991, 194, 151.

63. Todd, W. P.; Dinnocenzo, J. P.; Farid, S.; Goodman, J. L.; and Gould, I. R., J. Am. Chem. Soc. 1991, 113, 3601.

64. Todd, W. P.; Dinnocenzo, J. P.; Farid, S.; Goodman, J. L.; and Gould, I. R., Tetrahedron Lett. 1993, 34(18) 2863.

65. Chen, P.; Westmoreland, T. D.; Danielson, E.; Schanze, K. S.; Anthon, D.; Neveaux, P. P.; Meyer, T. J. Inorg. Chem. 1987, 26, 1116.

66. Danielson, E.; Elliott, C. M.; Merkert, J. W.; Meyer, T. J. J. Am. Chem. Soc. 1987, 109, 2519.

67. Meyer, T. J. Acc. Chem. Res. 1989, 22, 163.

68. Perkins, T. A.; Pourreau, D. B.; Netzel, T. L.; Schanze, K. S. J. Phys. Chem. 1989, 93, 4511.

69. Perkins, T. A.; Humer, W.; Netzel, T. L.; Schanze, K. S. J. Phys. Chem., 1990, 94, 2229.

70. Perkins, T. A.; Hauser, B. T.; Eyler, J. R.; Schanze, K. S. J. Phys. Chem. 1990, 94, 8745.

71. MacQueen, D. B.; Schanze, K. S. J. Am. Chem. Soc. 1991, 113, 6108.

72. Wrighton, M. S.; Morse, D. L. J. Am. Chem. Soc. 1974, 96, 998.

73. Giordano, P. J.; Wrighton, M. S. J. Am. Chem. Soc. 1979, 101, 2888.

74. Worl, L. A.; Duesing, R.; Chen, P.; Della Ciana, L.; Meyer, T. J. J. Chem. Soc. Dalton Trans. 1991, 849.

75.   Tapolsky, G.; Duesing, R.; Meyer, T. J. J. Phys. Chem. 1989, 93, 3885.

76.   Shida, T. "Electronic Absorption of Spectra of Radical Ions", Elsevier: Amsterdam, 1988.

77.   Lane, C. F. Synthesis 1975, 135.

78.   Lucia, L. A.; Burton, R. D.; and Schanze, K. S. J. Phys. Chem. 1993, 97, 9078.

79.   Grammp, G.; Jaenicke, W. Ber. Bunsenges Phys. Chem. 1984, 88, 325.

80.   Grammp, G.; Jaenicke, W. Ber. Bunsenges Phys. Chem. 1984, 88, 335.

81.   Grammp, G.; Jaenicke, W. J. Chem. Soc., Faraday Trans. 2 1985, 81, 1035.

82.   Rieger, P. H.; Bernal, I.; Reinmuth, W. H.; and Fraenkel, B. K., J. Am. Chem. Soc. 1963, 85, 683.

83.   Wang, Y.; Hauser, B. T.; Roony, M. M.; Burton, R. D.; and Schanze, K. S., J. Am. Chem. Soc. 1993, 115, 5675.

84.   Lucia, L. A.; Burton, R. D.; and Schanze, K. S. Inorg. Chim. Acta 1993, 208, 103.

85.   Rettig, W., Angew. Chem. Int. Ed. Engl. 1986, 25, 971.

86.   Rotkiewicz, K; Grellmann, K. H.; and Grabowski, Z. R., Chem. Phys. Lett. 1973, 19, 315.

87.   Wang, Y., J. Chem. Soc., Faraday Trans. 2 1988, 84, 1809.

88.   Murov, S. L.; Carmichael, I.; and Hug, G. L., Handbook of Photochemistry Marcel Dekker: New York, 1993.

89.   "Free radicals", Volumn I, Kochi, J. K. (Eds), Wiley: New York, 1973, 157.

90.   Turro, N. J.; and Weed, G. C., J. Am. Chem. Soc. 1983, 105, 1861.

91.   Turro, N. J., Tetrahedron 1982, 38, 809.

92.   Greene, F. D.; Berwick, M. A.; and Stowell, J. C., J. Am. Chem. Soc. 1970, 92, 867.

93.   Kopecky, K. R.; and Gillan, T., Can. J. Chem. 1969, 47, 2371.

94.   Andrieux, C. P.; and Saveant, J. M., J. Electroanal. Chem. 1970, 26, 223.

95. Lucia, L. A.; Schanze, K. S., _Inorg. Chim. Acta_ submitted.

96. Claridge, R. F. C.; Fischer, H., _J. Phys. Chem._ 1983, 87, 1960.

97. Wayner, D. D. M.; and Parker, V. D., _Acc. Chem. Res._ 1993, 26, 287.

98. Popielarz, R.; and Arnold, D. R., _J. Am. Chem. Soc._ 1990, 112, 3068.

99. Griller, D.; Simoes, J. A. M.; Sim, B. A.; and Wayner, D. D. M., _J. Am. Chem. Soc._ 1989, 111, 7872.

100. Coulson, D. M.; Crowell, W. R.; and Tendick, S. K., _J. Am. Chem. Soc._ 1957, 79, 1354.

101. Crowell, W. R.; and Coulson, D. M., _J. Phys. Chem._ 1963, 67, 734.

102. Andrieux, C. P.; and Saveant, J. M., _Bull. Soc. Chim. Fr._ 1968, 4671.

103. Ruchardt, C.; and Beckhaus, H.-D., _Top. Curr. Chem._ 1985, 130, 1.

104. Birkhofer, H.; Beckhaus, H.-D.; and Ruchardt, C., _Tetrahedron Lett._ 1983, 24, 185.

105. McMillen, D. F.; and Golden, D. M., _Annu. Rev. Phys. Chem._ 1982, 33, 493.

106. MacQueen, D. B.; and Schanze, K. S., _J. Am. Chem. Soc._ 1992, 114, 1897.

107. Overman, L. E.; and Flippin, L. A., _Tetrahedron Lett._ 1981, 22, 195.

108. Katritzky, A. R.; and Simmons, P., _J. Chem. Soc._ 1960, 1511.

109. Heller, H. G.; Langan, J. R. _J. Chem. Soc., Perkin Trans. 1_, 1981, 341.

110. "Practical HPLC Method Development", Snyder, L. R.; Glajch, J. L.; and Kirkland, J. J., Wiley: New York, 1988.

111. Harriman, A., _J. Chem. Soc., Chem. Commun._ 1977, 777.

112. Wang, Y.; and Schanze, K. S., _Chem. Phys._ 1993, 176, 305.

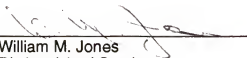113. Schanze, K. S., _I-APS Newsletter_ 1993.

BIOGRAPHICAL SKETCH

Yingsheng Wang was born on April 21, 1953, in Beijing, China, to Jinyu Wang and Jingyun Zhang as the fourth child in a family of eight. As a youth her student and social life was very active and fun-filled. Unfortunately, her education was interrupted in 1966 for a period of twelve years. During the long span of time she was absent from school, she worked as a factory machinist. After this period, she was among an elect group of students to matriculate to the Qinghua University in 1978. Here she majored in chemistry and finished her degree in four years. She then secured a position as an analytical chemist for five years. At the age of thirty-five, she departed to the United States of America to study chemistry under Professor Winston Lloyd at the University of Texas at El Paso for two and half years. She received her M.S. in chemistry in 1991 and proceeded to the University of Florida where she eventually studied photochemistry under Dr. Kirk Schanze and finished her research in 1994. Upon completing her studies, she plans to continue her career as a postdoctoral research associate at the University of Rochester.

I certify that I have read this study and that in my opinion it conforms to acceptable standards of scholarly presentation and is fully adequate, in scope and quality, as a dissertation for the degree of Doctor of Philosophy.

Kirk S. Schanze, Chairman
Associate Professor of Chemistry

I certify that I have read this study and that in my opinion it conforms to acceptable standards of scholarly presentation and is fully adequate, in scope and quality, as a dissertation for the degree of Doctor of Philosophy.
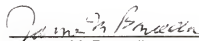
William M. Jones
Distinguished Service
Professor of Chemistry

I certify that I have read this study and that in my opinion it conforms to acceptable standards of scholarly presentation and is fully adequate, in scope and quality, as a dissertation for the degree of Doctor of Philosophy.
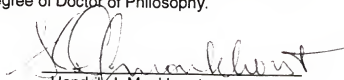
William R. Dolbier
Professor of Chemistry

I certify that I have read this study and that in my opinion it conforms to acceptable standards of scholarly presentation and is fully adequate, in scope and quality, as a dissertation for the degree of Doctor of Philosophy.

James M. Boncella
Associate Professor of Chemistry

I certify that I have read this study and that in my opinion it conforms to acceptable standards of scholarly presentation and is fully adequate, in scope and quality, as a dissertation for the degree of Doctor of Philosophy.

Hendrik J. Monkhorst
Professor of Physics

This dissertation was submitted to the Graduate Faculty of the Department of Chemistry in the College of Liberal Arts and Sciences and to the Graduate School and was accepted as partial fulfillment of the requirements for the degree of Doctor of Philosophy.

August, 1994

Dean, Graduate School